A doctoral dissertation

Energy-resolved density of electron traps as a novel structural index for identification and characterization of metal-oxide powders

金属酸化物粉末の同定と評価のための新規構造指標としての電子トラップ密度のエネルギー分布解析に関する研究

Akio Nitta

Division of Environmental Materials Science
Graduate School of Environmental Science
Hokkaido University

2018

Table of Contents

Chapter 1

General Introduction

1.1 Metal-oxide Powders

1.1.1 Use of Metal Oxides

Metal oxides, one of the solid materials, have been widely used in large quantities not only as structural materials but also as chemical functional materials such as photocatalysts [Lazar 2012], catalysts [Harriman 1988], sensors [Niu 2004], electrodes [Zhong 2010], and luminescent material [Katelnikovas 2012]. For example, although nitrides and sulfides are generally unstable and readily become deactivated through photocorrosion or self-oxidation [Matsumura 1983/Hitoki 2002], metal oxides are generally highly stable against photocorrosion, thereby metal oxides have been extensively used for heterogeneous photocatalysis such as water splitting [Sato 1980]. Durability against poisonous gases and sever ambient conditions is one of the reasons for metal oxides to have been used in sensors. Many electrodes used in electrochemical studies are composed of metal oxides, for example, dye-sensitized solar cells have porous layers containing titania or another metal oxide as electrodes [Ito 2007/McCune 2012], and it is well known that the surfaces of metal electrodes are more or less covered with oxides unless those oxide layers are removed intentionally.

1.1.2 Composition and Size of Metal-oxide Powders

In most cases, powders are used as a raw material of metal oxides, and their performances as functional materials are governed by the structural characteristics of the powders. Well then, how metal-oxide powders have been evaluated?

Most metal oxides have an electronic energy structure, called as a band structure, classified as semiconductors or insulators. As shown in **Fig. 1-1** left, band structure consists of electron-filled valence band and electron-vacant conduction band, and there is an energy gap which separates valence band and conduction band from each other [Ohtani 2014]. Difference in potential between valence-band top (VBT) and conduction-band bottom (CBB) is called as a band gap, and band gaps of metal-oxide powders depend on crystalline composition. Thus, band gap is one of the structural parameters of metal-oxide powders. For metal-oxide powders, diffuse reflectance spectroscopy (DRS) has been often used for estimation of the band gaps. It was

demonstrated that titania, zinc oxide, and lead oxide absorb UV light, by DR spectra for the first time [Goodeve 1937]. Since metal-oxide powders are strong scattering substances, light was introduced through an aperture into a prism for spectrum recording by light irradiation to the flat surface of a powder sample applied onto a flat sample holder. Value obtained by subtracting reflectance from 100 corresponds to DR spectrum and Kubelka-Munk (KM) function have been used as for band-gap energy estimation. Band gap estimated from *x*-intercept of linear line can be different depending on *y*-axis, %absorption or values included KM with assumption of indirect and direct transition, but DRS has been often used for determination of the band gap. However, a given metal-oxide powders cannot be determined by information on the band gap. For example, band gaps of anatase-type titania (TiO_2) and zinc oxide (ZnO) are ca. 3.2 eV [Gleria 1975]. They are almost similar, but chemical formulas are completely different. When a sample can be formed into an electrode shape, the flat band potential can be obtained by AC impedance analysis (Mott-Schottky Plot) [Kavan 1996]. When a given metal-oxide powder can be regarded as an n-type semiconductor, it is often considered that the flat band potential is almost equal to the CBB position. However, whether the shaped electrode maintains the form of a powder particle has been not known. For determination of structural information including composition of a given metal-oxide powders, XRD pattern analysis is a useful way to do. The diffraction caused by X-rays was discovered in 1912 [Krastev 2013], and this was an important step in the development of XRD pattern analysis.

After that, patterns of reflected X-ray produced by crystalline solids was discovered and Bragg's law was established [Bragg 1913]. Beams having the same wavelength and phase approach the crystalline solid and they are scattered from two different atoms therein. The lower beam traverses an extra length of $2d \sin\theta$. If this length is equal to an integer multiple of the wavelength of the radiation, interference will occur. Crystal structure determination by XRD was applied to of powder samples such as graphite [Hull 1917]. For identification and quantification of constituent components and to know crystal size and crystallinity, XRD pattern analysis has been often used for metal-oxide powders. It is well known that titania has mainly two crystalline phases, including anatase and rutile, and the crystalline phase of titania is mentioned in all paper. Determination of anatase and rutile ratio in titania powders has been achieved by measuring the intensity ratios of XRD peaks [Spurr 1957], however, a standard sample with single crystals of macro size and existence of amorphous phase causes the problem of the estimation. In regarded to this point, quantitative analysis of amorphous contents in titania powders have achieved by Rietveld analysis [Kawase 2010]. Thus, XRD can

be widely used for evaluating composition, which is expressed by chemical formula, of metal-oxide powders. Thus, compositions of metal-oxide powders have been evaluated by crystalline structure based on content ratio of crystal phase and amorphous phase and electron energy structure such as band gap width and CBB position.

As mentioned above paragraph, primary particle size as crystalline diameter can be estimated by the Scherrer equation using the corrected full width at half maximum of the most intense XRD peaks [Ohtani 2010]. A particle in which the primary particles are agglomerated is called a secondary particle and the secondary particle size as a volume-average particle size can be obtained from the particle size distribution. Specific surface area which is the surface area per unit mass of powders is obtained by analyzing the pressure dependency of the nitrogen adsorption amount at the liquid nitrogen temperature by using the Brunauer-Emmett-Teller (BET) equation to determine the monolayer adsorption amount and multiplying this by the nitrogen adsorption cross section. With titania powders, multiplying SSA (unit: m^2 g^{-1}) by primary particle size (unit: nm) yields ca. 1500. Since SSA gives the average information on all the particles in the sample, it is different from some of the particle size measurement methods, and an average primary particle diameter can be obtained. Therefore, although SSA contains information on surface area, SSA can express the size of metal-oxide powders. Thus, sizes of metal-oxide powders have been evaluated by measuring primary particle size, secondary particle size, and SSA.

However, whether a given metal-oxide powders is an industrial product or a laboratory prepared product, structural properties except for above mentioned composition or crystal structure represented by the chemical formula and particle size or size distribution and SSA have been only indicated. In fact, even when the composition and particle diameter of metal-oxide powders are almost the same, their performances often vary. This means that only information about composition and particle size cannot specify structures of metal-oxide powders, that is, metal-oxide powders have been not identified as chemical substances. Thus, in both cases of fundamental studies and applications, performances of metal-oxide powders have been discussed without identification, since an evaluation method of structural characteristics that dominate performances of metal-oxide powders has not been developed.

1.1.3 Difficulty in Identification of Powders Compared to Molecules

Specifying what a substance is, identification, and scientific and technological discussion on the substance should not be done without identifying the target substance. Identification can be thought of as describing the structure of the substance as words, that

is, the name is uniquely determined. Although it seems easy at the first sight, whether identification is possible or not depends not on a problem of whether the structure can be clearly elucidated by analyzing the target substance, but on whether the structure to be described can be defined.

Currently, three rules and guidelines established by the International Union of Pure and Applied Chemistry (IUPAC) are used to determine the name of a substance. Regarding molecules or metal complexes of organic or inorganic compounds, regardless of solids, liquids or gases, they are named on the basis of the skeleton structure of the molecule or metal complex and are named unambiguously from the structural formula. In other words, if a structural formula is drawn, molecules or metal complexes can be described according to the naming rules. This seems to be because a substance behaves as a single molecule or metal complex, which is actually used as a gas or a solution even if the substance is in a solid state. Therefore, even if a molecule or a metal complex is in the form of powder, there is no problem in naming it, and it can be said that there is no question as to what kind of aggregate state including the crystal structure.

One of the essential qualifications for identification in the fields of synthetic organic chemistry is that an elemental composition of an isolated chemical matches the estimated structure and that spectroscopic data considered to be specific for a structure can consistently be explained. It is often demonstrated that the substance is definitely isolated, in other words, does not contain impurities, by ^{1}H or ^{13}C nuclear magnetic resonance (NMR) spectrum which can be explained by a single component chemical substance. A new method of measuring nuclear magnetic moment was reported in 1938 [Rabi 1938]. The NMR signal was detected by using a beam of molecules for lithium chloride traversing a magnetic field, has been observed. In 1945, the absorption of radiofrequency energy, due to transitions in a solid material, paraffin, containing protons was observed [Purcell 1945]. At the same time, greatly increased sensitivity of nuclear induction offered the possibility to observe the effect not only in liquids and solids but also gases under no excessive pressure [Bloch 1946]. In this way, the technique was expanded for use on liquids and solids. After that, separated two different resonances of ^{14}N arise from ammonium ion and nitrate ion were observed [Proctor 1950]. Henceforth NMR spectroscopy has been kicked off by discovering chemical shift. When ^{1}H nucleus and ^{13}C nucleus are placed in the magnetic field, the spins are aligned parallel or antiparallel to the external magnetic field. When irradiated with a radio wave, energy is absorbed and the nuclear spin is inverted from a low energy state to a high energy state. Absorption of this energy is detected, amplified and displayed as NMR spectrum. By NMR spectroscopy, what carbon-hydrogen configuration exists is

elucidated. Not only NMR but also X-ray crystallography, mass spectroscopy (MS), ultraviolet spectroscopy (UV), and infrared spectroscopy (IR) have also been used for structural determination of organic molecules. Although three-dimensional molecular structure can be obtained by X-ray crystallography, it is limited for only when a molecule becomes crystal. Molecular weight and molecular formula of ionized organic molecule, presence of conjugated π electrons, and what molecular functional groups possessing specific infrared absorption are present can be acquired by MS, UV, and IR, respectively. In this sense, identification and characterization method has been already established in the field of organic chemistry. If a structure of a given organic compound is unknown, the molecule should be deemed to be identified by elemental analysis and NMR pattern matching with standard or calculated values. For example, both proton and carbon NMR data and either accurate mass or elemental analysis data, elemental analytical values for carbon and hydrogen agreeing with calculated values within 0.4%, should be included as evidence to identify new compounds for submitting a paper to Journal of Organic Chemistry.

However, when an inorganic compound such as salt which is not a molecule or a metal complex is in a solid state such as powder, there is no clear systematic rule on what kind of structural information can be named. For example, according to "Inorganic Chemistry Nomenclature - IUPAC 2005 Annual Meeting", it is written in practice that it is difficult to construct a completely systematic name when detailed structural information should be transmitted for inorganic solids, and only the notation of composition and crystal structure and mineral name are shown. That is, at present, it is not possible to identify the powder of the inorganic compound since the structural information corresponding to the "structural formula" of the molecular compound cannot be identified and there is no systematic nomenclature. Conversely speaking, identification can become possible if the structure information expressing the accurate structure of the powder is decided.

1.1.4 Surface Structure of Metal-oxide Powders

As mentioned above, there has been no concept of identification and no method of evaluating structural characteristics that dominate performances toward powdered materials including metal-oxide powders heretofore. There may be three main reasons why it has been said that decision of required structural information is difficult. First, both surface and bulk structures are required. This may be caused by that the number of atoms exposed on the surface is not negligible compared to the number of atoms in the bulk which is a part not in contact with the interface. Even if the surface atomic ratio is

very low, the physical properties such as fluidity and dispersibility of the powders and the chemical properties that govern the functions of the catalyst and the electrode material may be almost dominated by the surface structure. Also, in addition to the respective structures, the size of both the bulk and the surface must be measured. Secondary, macroscopic measurement is required. Scanning electron microscope (SEM) and transmission electron microscope (TEM) are often used to observe surface structure of metal-oxide powders by enlarging an object with an electron beam [Kingsley 1988/Poizot 2001]. Scanning probe microscope such as a scanning tunneling microscope (STM) [Binnig 1982] using a minute current, an atomic force microscope (AFM) [Binnig 1986] are also used to observe magnified surface states of metal-oxide powders [Friedbacher 1991]. However, between surface and bulk structures, in particular, such a measurement using electron and probe microscopes for the surface structures and properties is mostly microscopic, and there is no guarantee that the obtained result can be expanded beyond the observation part. The method of macroscopically measuring the surface structure of the powder has been limited to measurement of the zeta potential or isoelectric point based on the determination of the acid point or the base point of the surface or the acid dissociation of the surface hydroxyl group. Although SSA determined by macroscopic measurement seems to be like the surface characteristics at first glance, it does not change if the particle size is the same even if the surface structure is different, so the size of the bulk is expressed only. Finally, bulk does not consist of only crystalline. It seems to be easy to determine bulk structures compared to surface structures, but it is the case powders consist of only crystals and able to be measured by powder XRD technique. Actually, non-crystalline ingredients, including amorphous of which composition is same with crystalline component and have no long-distance periodic structure and precursor of powder preparation, and impurities such as intermediate and moisture, should be considered.

Considering these facts, three parameters of bulk composition, bulk size, and surface structure as structure information for identification or characterization of powder samples are required at least. Therefore, what is needed for identification of metal-oxide powders is a structural index reflecting surface structural property. In this study, electron-trap density is focused on as a candidate of the structural index. Explanation of electron traps, why electron -trap density is chosen, and how electron-trap density has been evaluated is described in next chapter *1.2.1*.

1.2 Electron-trap Density

1.2.1 Electron Traps as Vacant Energy Level

Since oxygen anions of metal oxides are easily apt to be detached to leave electrons in an oxygen defect, almost all metal oxides are classified as n-type semiconductors which have electron-filled donor levels below CBB [Ohtani 2013]. If those donor electrons flow out to adsorbed water or surface hydroxyl groups, those donor levels become vacant and can be sites accepting electrons. On the other hand, it has been well known that color change is induced by calcination of metal-oxide powders under hydrogen atmosphere or in vacuum, photoirradiation of suspended metal-oxide powders in the presence of electron donors under deaerated conditions or cathodic reduction of particulate metal-oxide electrodes. For titania and tungsten(VI) oxide (WO_3), they turn gray and blue by such a treatment, respectively, and those colorations are attributable to trivalent titanium ions (Ti^{3+}) [Kawaguchi 1968/Ghosh 1969/Inoue 1970/Hasegawa 1971/Kölle 1985/Howe 1985] and pentavalent tungsten ions [Ohtani 1988] accompanied by proton insertion. The generation of these reduced species is attributable to accumulation of electrons in electron acceptable sites (**Fig. 1-1** right). In this study, those sites are called "electron traps". The idea, assuming Ti^{3+} species on the surface occurring in titania as accumulated electrons captured in "electron traps", has been reported since 1968 [Kawaguchi 1968]. It has been also suggested that electron traps were predominantly located on the surface of metal oxides [Inoue 1970/ Hasegawa 1971/Kölle 1985], though this suggestion is described in later by using acquired data. Thus, "electron traps" can contain a parameter reflecting surface structure and this is the reason that "electron traps" have been focused on. For titania powders, molar amount of accumulated Ti^{3+} in titania particles in photoirradiated suspensions containing electron

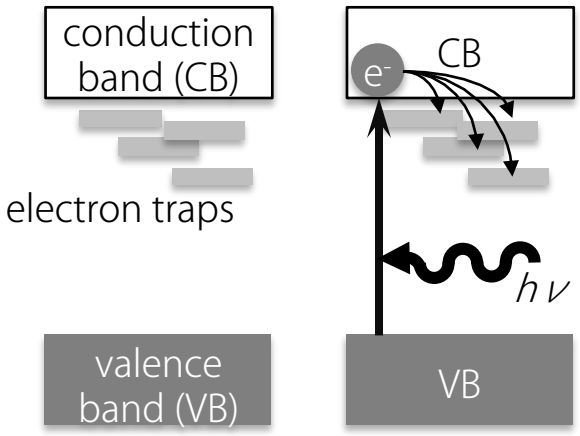

Fig. 1-1 Band structure and electron traps of metal-oxide powders.

donors, measured by chemical titration with methyl viologen (MV^{2+}), was saturated and the saturation amounts were different depending on the kind of titania samples [Ikeda 2003]. Therefore, metal-oxide powders such as titania have respective electron-trap density. Electron-trap densities in metal oxides have been analyzed by various methods.

1.2.2 Diffuse-reflectance Infrared Fourier Transform Analysis

Surface density of electron traps was estimated by diffuse-reflectance infrared Fourier transform (DRIFT) analysis of nitrobenzene adsorbed onto anatase and rutile titania powders due to photocatalytic reduction of nitroaromatics to amines on titania can be promoted on Ti^{3+} atoms located at the surface [Shiraishi 2013/Shiraishi 2014] (**Fig. 1-2**). Surface density of electron traps is equal to twice the amount of adsorbed nitrobenzene that is determined by the intensity ratio of 1522 cm^{-1} and 1346 cm^{-1} bands assigned to the asymmetric and symmetric stretching vibration of the nitro group adsorbed onto the surface Ti-OH group and the surface Ti^{3+} atoms, respectively. Electron traps can exist not only on surface but also in bulk, and surface density of electron traps measured by this method is surely smaller than total density of electron traps measured by later described photochemical method. In DRIFT study, ration of surface density of electron-trap density is suggested to be a decisive factor for chemoselective hydrogenation of nitroaromatics [Shiraishi 2013]. However, *y*-intercepts of relation between SSA and surface density of electron traps measured by DRIFT are not zero for both anatase and rutile titania powders (**Fig. 1-3**). Therefore,

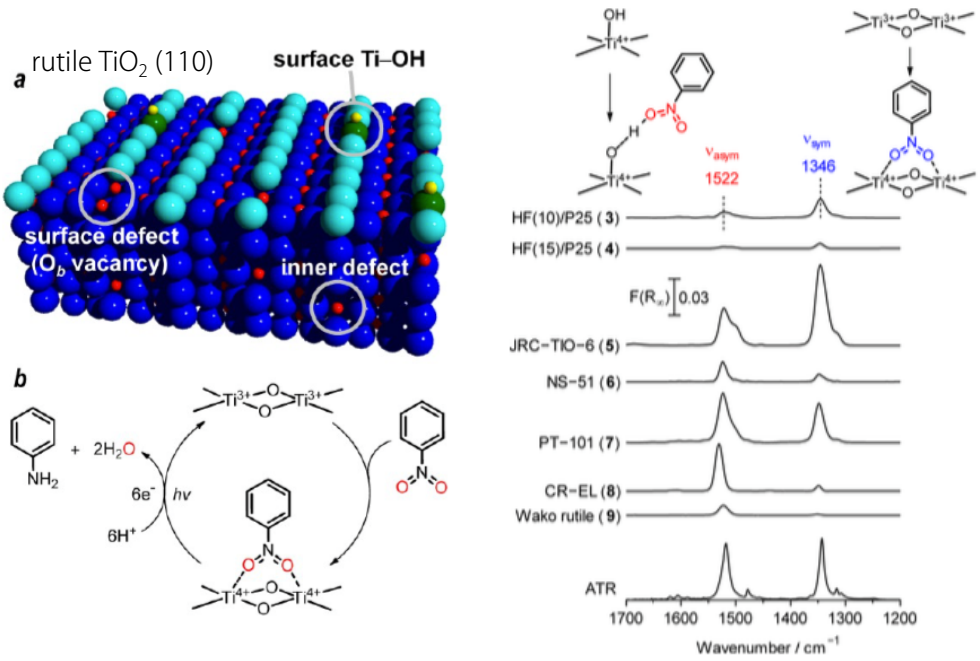

Fig. 1-2 Diffuse-reflectance Fourier transform analysis of surface density of electron traps [Shiraishi 2013].

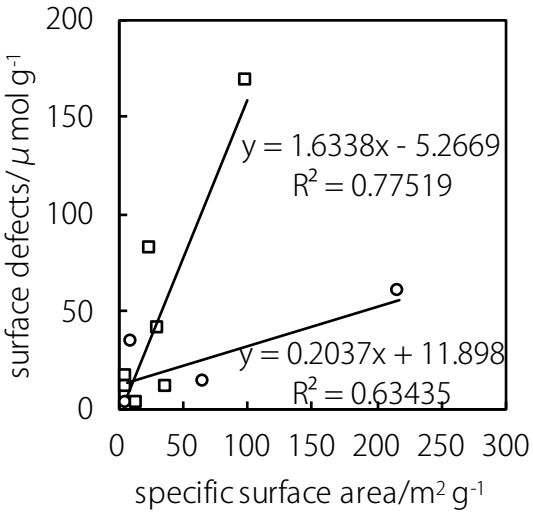

Fig. 1-3 Relation between specific surface area and surface density of electron traps measured by DRIFT.

values of electron-trap density of DRIFT may not reflect only surface density. In any case, only surface-vicinal electron-trap density is measurable by DRIFT.

1.2.3 Analysis of Total Density of Electron Traps by Photochemical Method

Total density of electron traps in titania samples have been measured, by the above-mentioned photochemical method using MV^{2+} [Ikeda 2003] as shown in **Fig. 1-4**. In photochemical method analysis, titania suspensions were UV photoirradiated in the presence of electron donors such as triethanolamine and methanol or for several days to fill up all electron traps with electrons, MV^{2+} was injected to make trapped electrons reduce MV^{2+} into methyl viologen cation radical ($MV^{\bullet+}$) and the molar amount of $MV^{\bullet+}$

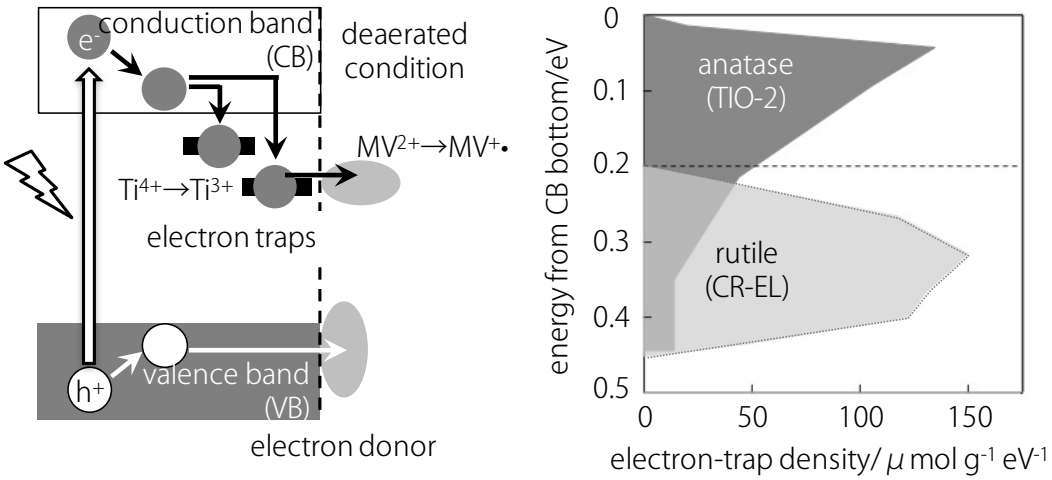

Fig. 1-4 Analysis of electron-trap density by photochemical method [Ikeda 2003].

was measured by photoabsorption spectroscopy. Thus, total density of electron traps can be quantitatively measured using chemical titration methods. Problems of this measurement is described in *1.2.5*.

1.2.4 Analysis of Total Density of Electron Traps by Double-beam Photoacoustic Spectroscopy

By accumulation of electrons via conduction band by interband transition like photochemical method, total density of electron traps was tired to be measured by double-beam photoacoustic spectroscopy (DB-PAS) [Murakami 2007]. Although precise explanation is described in Chapter 2, photoabsorption of accumulated electrons assigned to be Ti^{3+} was measured by intermittent light during both intermittent light for detection and continuous light for excitation in DB-PAS. Saturated intensity of photoaocutsic signal was similar to total density of electron traps shown in **Fig. 1-5**, thus DB-PAS can be also used for estimation of total density of electron traps. However, it is impossible to accomplish energy-resolved measurement of electron-trap density by DB-PAS since electrons are accumulated in electron traps from conduction band at random and intermittent light absorbs all accumulated electron traps.

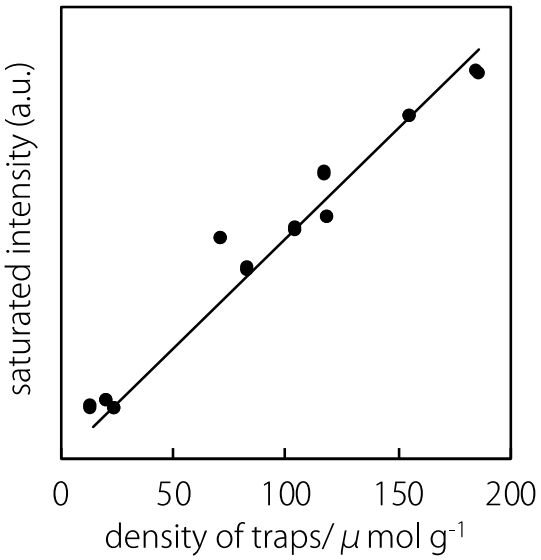

Fig. 1-5 Relation between density of electron traps evaluated by photochemical method and double-beam photoacoustic spectroscopy [Murakami 2007].

1.2.5 Energy Level of Electron Traps in Other Than Powders

Although total density of electron traps can be measured by counting numbers of accumulated electrons, there have been only several papers reporting the analytical results of energy-resolved distribution of electron traps (ERDT) for metal-oxide powders.

In the field of semiconductor physics, as energy-resolved measurement of density of crystalline defects, a kind of electron traps, in semiconductor materials, a thermally stimulated capacitance [Gonzalez 1997] and current methods [Nishimoto 1983] were used in the past and deep-level transient spectroscopy (DLTS) with higher sensitivity is now frequently used [Lang 1974/Miyagi 2001/Miyagi 2004]. A fundamental basis of DLTS lies in the concept of p-n junction capacitance transient for filling and emptying traps at a fixed temperature [Lang 1974]. An example of metal-oxide ERDT measurements by DLTS was those for anatase films epitaxially grown by metal organic chemical vapor deposition. For example, the reported electron-trap densities were 0.0025 and 0.027 μmol g^{-1} at 0.12 eV and 0.96 eV from CBB, respectively [Miyagi 2001]. The data converted assuming density of anatase crystal to be 4 g cm^{-3} and these densities seemed much lower than the total density of electron traps for titania powders by photochemical method, ten to several tens μmol g^{-1}. Thus, it has been found that deep traps exist in titania thin films, although electron-trap density differs between powders and thin films. However, in DLTS measurement, since the width of space charge layer is narrow with respect to the film thickness and a carrier concentration which shows electric conductivity are required, there seems to be no report on DLTS measurement for powder samples having a space charge layer width larger than the particle size. Furthermore, DLTS detects only deep traps presumably in the bulk of samples. Those problems can be obstacles for identification and characterization of metal-oxide powders.

1.2.6 Energy-resolved Measurement by Photochemical Method

One of the successful methods for ERDT analysis is the above-mentioned photochemical method. For the ERDT measurements, MV^{2+} was added by changing the pH of photoirradiated titania suspensions from lower side to higher side. Since, as is well known, band positions, as well as electron-trap levels, of metal oxides are shifted depending on the pH of electrolyte solution, electron-trap energy can be increased with the increase in pH by ca. 59 mV per decade, while electrode potential of $MV^{2+}/MV^{\bullet+}$ redox couple is constant, not depending on pH. It has been reported that mainly electron traps are located 0.1–0.2 eV below CBB (**Fig. 1-4**). Observed ERDT for titania samples by photochemical method may be sole example of ERDT analysis of metal-oxide samples in the form of powder. However, photochemical method requires very careful operation to avoid leakage of oxygen from the atmosphere and measurable energy range and energy resolution, governed by the accuracy in pH control, were limited and low, respectively. For establishing identification and characterization of metal-oxide powders, those problems must be solved.

1.2.7 Energy-resolved Measurement by Spectroelectrochemical Method

Spectroelectrochemical method using electrodes prepared from powder samples set in a diffuse-reflectance spectrometer reported ERDT of titania samples [Buchalska 2015] and seems better than photocehmical method in that electrons traps are filled from deeper side to shallower side as shown in **Fig. 1-6**. In this method, electrochemical reduction of titania generates Ti^{3+} which can absorb visible light of 780 nm assign to localized electron traps below CBB. Reflectance changes measured at 780 nm as a function of the electrode potential and transformed to the KM function shows curves correspond to the onset reduction potentials at which trapping of electrons occurs. In spectroelectrochemical method, it seems to be ideal for ERDT measurement since electrons are accumulated from deeper side in sequence unlike with photochemical method and DLTS. However, the electrode preparation process might change the surface structure of samples to result in the change in ERDT and there seems no guarantee that all the particles in the electrodes participate in the electrochemical process. Thus, innovation for ERDT-analysis methodology using powder samples without changing their form is highly desirable.

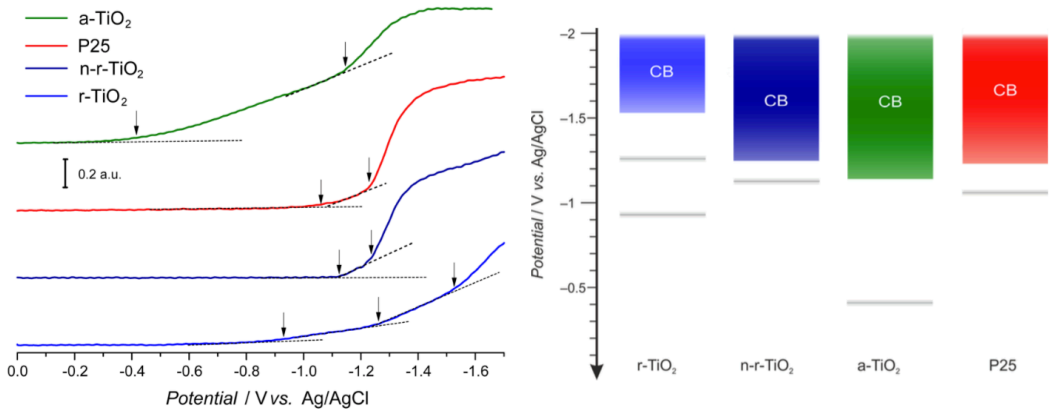

Fig. 1-6 Analysis of energy-resolved measurement of electron traps by spectroelectrochemical method [Buchalska 2015].

1.3 Purpose of This Study

Although mensuration techniques of bulk composition and bulk size and microscopic measurement techniques for surface structural properties have existed so far, identification and structural evaluation of metal-oxide powders have been prevented by lack of methodology which measures surface structure macroscopically. In this study, ERDT was focused on as a novel structural index to identify and characterize metal-oxide powders based on a prediction that electron traps were located mainly on the surface of

metal-oxide powders. There have been several methods for evaluating electron-trap density, however energy-resolved measurement of electron-trap density in particulate metal oxides has been achieved by only one method which has problems in energy resolution and measurable energy range. Thus, development of a new method of energy-resolved measurement of electron-trap density is required for identification and characterization. Ideal method of evaluating ERDT is to measure electron-trap density in powder formed metal oxides, while sequentially filling electrons in electron traps from deeper side. Therefore, use of direct excitation of electrons from valance band to electron traps was tried in Chapter 2.

As establishment of identification and characterization of metal-oxide powders by using the new method, titania powders were mainly focused on because of ease to procurement and high redox ability directly linked to their performances. For performances of metal-oxide powders, photocatalysis was focused on since decisive factors of photocatalytic activities have been not elucidated based on bulk structures such as crystalline composition and SSA and electron traps can affect both recombination of electrons and holes and electron transfer without recombination which may occur between conduction band and relatively shallow traps. Suggestion of identification and characterization and performance of metal-oxide powders was tried to evaluate identicalness/similarity/differentness of two metal-oxide powders. This is shown in Chapter 3.

Direct excitation of electrons from valence band to electron traps is a newly method but position of valence-band top (VBT) cannot be measured. If VBT positions are different, comparison of ERDT is difficult. Then, for precise characterization of metal-oxide powders, estimation of relative VBT positions was also tried. This is described in Chapter 4.

1.4. References

Binnig 1982 Binnig, G.; Rohrer, H.; Gerber, C.; Weibel, E., Tunneling through a controllable vacuum gap, *Appl. Phys. Lett.*, **40**, 178–180 (1982).

Binnig 1986 Binnig, G.; Quate, C. F., Atomic Force Microscope, Phys. Rev. Lett., 56, 930–934 (1986).

Bloch 1946 Bloch, F., Nuclear Introduction, *Phys. Rev.*, **70**, 460–474 (1946).

Bragg 1913 Bragg, W. H.; Bragg, W. L., The Reflection of X-rays by Crystals, *Proc. R. Soc. Lond. A*, **88**, 428–438 (1913).

Buchalska 2015 Buchalska, M.; Kobielusz, M.; Matuszek, A.; Pacia., M.; Wojtyła, S.; Macyk, W., On Oxygen Activation at Rutile- and Anatase-TiO_2, *ACS Catal.*, **5**, 7424–7431 (2015).

Friedbacher 1991 Friedbacher, G.; Hansma, P. K.; Ramli, E.; Stucky, G. D., Imaging Powders with the Atomic Force Microscope: From Biominerals to Commercial Materials, Science, 253, 1261–1263 (1991).

Ghosh 1969 Ghosh, A. K.; Wakim, F. G.; Addiss, Jr., R. R., Photoelectronic Processes in Rutile, *Physical Review*, **184** 979–988 (1969).

Gleria 1975 Gleria, M; Memming, R., CHARGE TRANSFER PROCESSES AT LARGE BAND GAP SEMICONDUCTOR ELECTRODES: REACTIONS AT SiC-ELECTRODES, *J. Electroanal. Chem.*, **65**, 163–175 (1975).

Goodeve 1937 Goodeve, C. F., The absorption spectra and photo-sensitising activity of white pigments, Trans. Faraday Soc., **33**, 340–347 (1937).

Harriman 1988 Harriman, A.; Pickering, I. J.; Thomas, J. M., Metal Oxides as Heterogeneous Catalysts for Oxygen Evolution under Photochemical Conditions, *J. Chem. Soc., Faraday Trans. 1*, **84**, 2795–2806 (1988).

Hasegawa 1971 Hasegawa, S.; Kawaguchi, T., Surface properties and photoconductivity of hydrogen-reduced titanium(IV) oxide, **92**, 389–392 (1971).

Hitoki 2002 Hitoki, G.; Ishikawa, A.; Takata, T.; Kondo, J. N.; Hara, M.; Domen, K., Ta_3N_5 as a Novel Visible Light-Driven Photocatalyst (< 600 nm), Chem. Lett., 736–737 (2002).

Howe 1985 Howe, R. F.; Grätzel, M.; EPR Observation of Trapped Electrons in Colloidal TiO_2, J. Phys. Chem., **89**, 4495–4499 (1985).

Hull 1917 Hull, A. W., A NEW METHOD OF X—RAY CRYSTAL ANALYSIS, *Phys. Rev.*, **10**, 661–696 (1917).

Ikeda 2003 Ikeda, S.; Sugiyama, N.; Murakami, S.; Kominami, H.; Kera, Y.; Noguchi, H.; Uosaki, K.; Torimoto, T.; Ohtani, B., Quantitative analysis of defective sites in titanium(IV) oxide photocatalyst powders, *Phys. Chem. Chem. Phys.*, **5**, 778–783 (2003).

Inoue 1970 Inoue, Y.; Hasegawa, S.; Kawaguchi, T.; Surface properties and catalytic function of a few metal oxides, *Nippon Kagaku Zasshi*, 91, 1034–1038 (1970).

Ito 2007 Ito, S.; Chen, P.; Comte, P.; Nazeeruddin, M. K.; Liska, P.; Péchy, P.; Grätzel, M., Fabrication of Screen-Printing Pastes From TiO_2 Powders for Dye-Sensitised Solar Cells, *Prog. Photovolt: Res. Appl.*, **15**, 603–612 (2007).

Kavan 1996 Kavan, L.; Grätzel, M.; Gilbert, S. E.; Klemenz, C.; Scheel, J., Electrochemical and Photoelectrochemical Investigation of Single-Crystal Anatase, *J. Am. Chem. Soc.*, **118**, 6716–6723 (1996).

Kawaguchi 1968 Kawaguchi, S.; Hasegawa, S.; Kaseda, K.; Kurita, S.; Studies on the Surface Electron Traps in Photoconductors (I) DPPH Method and Hammett Method, *Denshi Shashin*, **8**, 92–100 (1968).

Kawase 2010 Kawase, S.; Sugimoto, K.-i; Fujiwara, R.; Ono, S., Quantitative Analysis of Amorphous Contents in Photocatalytic Titania Powders, *Bunseki Kagaku*, **59**, 921–926 (2010).

Katelnikovas 2012 Katelnikovas, A.; Plewa, J.; Sakirzanovas, S.; Dutczak, D., Enseling, D.; Baur, F.; Winkler, H.; Kareiva, A.; Jüstel, T, Synthesis and optical properties of $Li_3Ba_2La_3(MoO_4)_8:Eu^{3+}$ powders and ceramics for pcLEDs, *J. Mater. Chem.*, **22**, 22126–22134 (2012).

Kingsley 1988 A NOVEL COMBUSTION PROCESS FOR THE SYNTHESIS OF FINE PARTICLE a-ALUMINA AND RELATED OXIDE MATERIALS, **6**, 427–432 (1988).

Kölle 1985 Kölle, U.; Grätzel, M., Dynamics of Interfacial Charge-Transfer Reactions in Semiconductor Dispersions. Reduction of Cobaltoceniumdicarboxylate in Colloidal TiO_2, *Inorg. Chem.*, **24**, 2253–2258 (1985).

Krastev 2013 Krastev, V.; Exner, G. K., 100 years of X-ray diffraction: from Röntgen's discovery to top-of-the-art synchrotron source applications, Bulgarian Chemical Communications, **45**, 411–417 (2013).

Lang 1974 Lang, D. V., Deep-level transient spectroscopy: A new method to characterize traps in semiconductors, *J. Appl. Phys.*, **45**, 3023–3032 (1974).

Lazar 2012 Lazar, M. A.; Varghese, S.; Nair, S. S., Photocatalytic Water Treatment by Titanium Dioxide: Recent Updates, *Catalysts*, **2**, 572–601 (2012).

McCune 2012 McCune, M.; Zhang, W.; Deng, Y., High Efficiency Dye-Sensitized Solar Cells Based on Three- Dimensional Multilayered ZnO Nanowire Arrays with "Caterpillar- like" Structure, *Nano Lett.*, **12**, 3656−3662 (2012).

Matsumura 1983 Matsumura, M.; Saho, Y.; Tsubomura, H., Photocatalytic Hydrogen Production from Solutions of Sulfite Using Platinized Cadmium Sulfide Powder, *J. Phys. Chem.*, **87**, 3807–3808 (1903).

Miyagi 2001 Miyagi, T.; Ogawa, T.; Kamei, M.; Wada, Y.; Mitsuhashi, T.; Yamazaki, A.; Ohta, E.; Sato, T., Deep Level Transient Spectroscopy Analysis of an Anatase Epitaxial Film Grown by Metal Organic Chemical Vapor Deposition, *Jpn. J. Appl. Phys.*, **40**, L404–L406 (2001).

Miyagi 2004 Miyagi, T.; Kamei, M.; Sakaguchi T.; Mitsuhashi, T.; Yamazaki, A, Photocatalytic Property and Deep Levels of Nb-doped Anatase TiO_2 Film Grown by Metalorganic Chemical Vapor Depostion, *Jpn. J. Appl. Phys.*, **43**, 775–776 (2004).

Murakami 2007 Murakami, N.; Prieto-Mahaney, O.-O.; Abe, R.; Torimoto, T.; Ohtani, B.; Double-Beam Photoacoustic Spectroscopic Studies on Transient Absorption of Titanium(IV) Oxide Photocatalyst Powders, *J. Phys. Chem. C*, **111**, 11927–11935 (2007).

Niu 2004 Niu X.; Du, W.; Du, W., Preparation and gas sensing properties of ZnM_2O_4 (M = Fe, Co, Cr), *Sensors and Actuators B*, **99**, 405–409 (2004).

Ohtani 1998 Ohtani, B.; Atsumi, T.; Nishimoto, S.-i.; Kagiya, T., Multiple-mode Responsive Device. Photo- and Electro-Chromic Composite Thin Film of Tungsten Oxide with Titanium Oxide, *Chem. Lett.*, **17**, 295–298 (1988).

Ohtani 2010 Ohtani, B.; Prieto-Mahaney, O.-O.; Amano, F.; Murakami, N.; Abe, R., What Are Titania Photocatalysts?—An Exploratory Correlation of Photocatalytic Activity with Structural and Physical Properties, *J. Adv. Oxid. Technol.*, **13**, 247–261 (2010).

Ohtani 2013 Ohtani, B., Titania Photocatalysis beyond Recombination: A Critical Review, *Catalysts*, **3**, 942–953 (2013).

Ohtani 2014 Ohtani, B., Revisiting the Fundamental Physical Chemistry in Heterogeneous Photocatalysis: Its Thermodynamics and Kinetics, *Phys. Chem. Chem. Phys.*, **16**, 1788–1797 (2014).

Poizot 2001 Poizot, P.; Laruelle, S.; Grugeon, S.; Dupont, L.; Tarascon, J.-M., Searching for new anode materials for the Li-ion technology: time to deviate from the usual path, Journal of Power Sources, **97–98**, 235–39 (2001).

Proctor 1950 Proctor, W. G.; Yu, F. C., The Dependence of a Nuclear Magnetic Resonance Frequency upon Chemical Compound, *Phys. Rev.*, 717–717 (1950).

Purcell 1945 Purcell, E. M.; Torrey, H. C.; Pound, R. V., Resonance Absorption by Nuclear Magnetic Moments in a Solid, Phys. Rev., **69**, 37–38 (1945).

Rabi 1937 Rabi, I. I.; Zacharias, J. R.; Millman, S.; Kusch, P., A New Method of Measuring Nuclear Magnetic Moment, *Phys. Rev.*, **53**, 318–327 (1938).

Sato 1980 Sato, S.; White, J. M., PHOTODECOMPOSlTlON OF WATER OVER Pt/TiO_2 CATALYSTS, *Chem. Phys. Lett.*, **72**, 83–86 (1980).

Shiraishi 2013 Shiraishi, Y.; Hirakawa, H.; Togawa, Y.; Sugano, Y.; Ichikawa, S.; Hirai, T., Rutile Crystallites Isolated from Degussa (Evonik) P25 TiO_2: Highly Efficient Photocatalyst for Chemoselective Hydrogenation of Nitroaromatics, *ACS Catal.*, **3**, 2318–2326 (2013).

Shiraishi 2014 Shiraishi, Y.; Hirakawa, H.; Togawa, Y.; Hirai, T., Noble-Metal-Free Deoxygenation of Epoxides: Titanium Dioxide as a Photocatalytically Regenerable Electron-Transfer Catalyst, *ACS Catal.*, **4**, 1642–1649 (2014).

Spurr 1957 Spurr, R. A.; Myers, H., Quantitative Analysis of Anatase-Rutile Mixtures with an X-Ray Diffractometer, *Anal. Chem.*, **29**, 760–762 (1957).

Zhong 2010 Zhong, K.; Xia, X; Zhang, B; Li, H.; Wang, Z.; Chen, L., MnO powder as anode active materials for lithium ion batteries, *Journal of Power Sources*, **195**, 3300–3308 (2010).

Chapter 2

Development of Reversed Double-beam Photoacoustic Spectroscopy

2.1 Introduction

2.1.1 Photoacoustic Spectroscopy

Photoacoustic spectroscopy (PAS), in which a sound wave is generated from a sample when intermittent light is irradiated on the sample, can be a candidate for evaluating electron-trap density. The phenomenon of photoacoustic (PA) effect that is the principle of PAS has been discovered by Bell, inventor of the telephone, in 1880 ([Bell 1880]). Initially, research as a gas spectroscopy had been mostly carried out, but in 1976, a theory of solid PA effects was established, and it has been widely used since then [Rosencwaig 1976]. As one of the photothermal spectroscopies, PAS is a method to detect heat released when excited species generated by light absorption are deexcited as sound wave caused by thermal expansion of atmospheric substance. If excited species are not consumed by other reactions, heat corresponding to light absorption is released, so that it is possible to estimate light absorption by detecting the generated sound waves with a microphone (**Fig. 2-1**).

It has been suggested that a main source of PA signal arises from a periodic heat flow, from a solid to the surrounding gas, that causes an oscillatory motion of a narrow layer of gas at the solid-gas boundary [Rosencwaig 1976]. A one-dimensional model of the heat flow in the cell resulting from absorbed light energy as a theory regarding PA

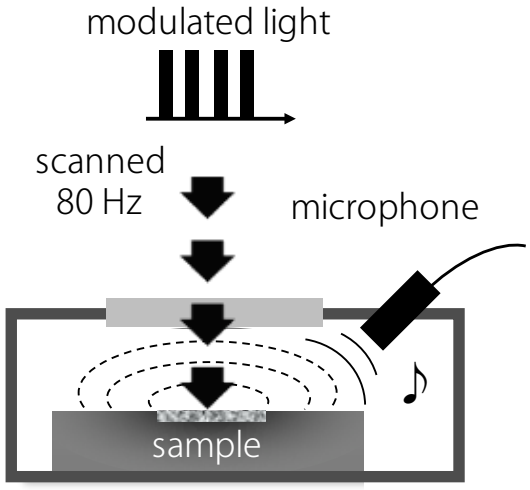

Fig. 2-1 Principle of photoacoustic spectroscopy.

effect of solids has been also reported and it has been suggested that PA signal is ultimately governed by the magnitude of the thermal diffusion length of the solids.

As mentioned before, PAS is a method of evaluating light absorption by sound waves, and since there is no need to detect light after irradiation at a sample like transmission/reflection spectroscopy, influence of light scattering which becomes a problem in spectroscopic measurement of fine particles can be avoided. Also, since the PA signal increases in proportion to the intensity of the excitation light, highly sensitive measurement can be performed by optimizing the light source and the sensor. Given above advantages, PAS has features that are not in conventional spectroscopy, such as depth analysis and reflection of thermal characteristics of the signal, and it is applied to various fields including biological imaging, gas analysis, non-destructive inspection of substances. For example, in the field of PA imaging, imaging of deep body with high contrast without being affected by light scattering and decreasing resolution and sensitivity, can be achieved because of acoustic detection that the scatter coefficient is small compared to light, and excitation of a particular absorber selectively can be also achieved by arranging wavelength of light appropriately toward a target. If it becomes possible to image minute cancer cells located in deep body, breakthrough of cancer therapy will be expected. To solve a problem of being low sensitivity since many disorders do not show PA contrast, studies on PA probe such as gold nanoparticles have been done [Thakor 2011]. There have also been reported that PAS technique was available to metal-oxide powders such as ceramic zinc oxide (ZnO) doped with 1 mol% bismuth oxide (Bi_2O_3) [Toyoda 1998], mixed titania nanocrystals with anatase and rutile structures [Toyoda 2003], and titania powders [Toyoda 2000]. From the report regarding PAS analysis of titania powders, it has been suggested that the onset of quantum size effect is caused by decreasing particle size from comparing band gap of size different anatase powders, and that anatase type has increasing energy due to the displacement of atoms, specifically due to oxygen vacancies and/or chlorine impurities in the production process of the powders, by comparing PA intensities of rutile and anatase plotted semi logarithmically [Toyoda 2000].

A comparison of diffuse reflectance spectrum and PA spectrum of a given titania powders is shown in **Fig. 2-2**. Modulated light (80 Hz for the case of **Fig. 2-2**) is scanned from longer wavelength side to shorter wavelength side to get PA spectrum. For titania, PA signal does not increase under visible light irradiation with nitrogen atmosphere. This means that there is nothing to absorb visible light. On the other hand, PA signal starts increasing under ultraviolet (UV) region.

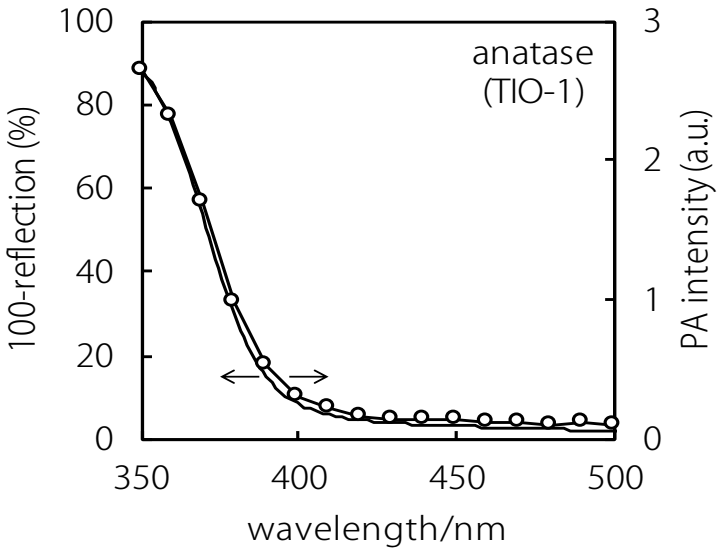

Fig. 2-2 Diffuse reflectance spectrum and PA spectrum for a titania powder.

This is attributable to photoabsorption of the titania powder. It seems that PA spectrum corresponds to diffuse reflectance spectrum. Integrating sphere is used to measure intensity of scattering light for powders scattering incident light, in diffuse reflectance spectroscopy (DRS). Thus, PA spectrum is similar to DR spectrum, however, PAS enables measurement of signal intensity that is proportional to light absorbed amount, which differs DRS using subtraction procedure. For example, if DR spectra of titania powders with specific surface area (SSA) higher than 250 m^2 g^{-1} are measured, 100-reflection is almost 0% at visible light region, however, PA signal for those titania powders measured in air increases from ca. 500 nm to ca. 400 nm. Those results indicate that titania can absorb only UV light and something absorbs visible light corresponds to ca. 400 nm ~ ca. 500 nm. This photoabsorption is attributable to surface peroxide species produced by hydrogen peroxide (H_2O_2) resulted from reductive reaction with large amount of adsorbed molecular oxygen (O_2) and protons by photoexcited electrons or from superoxide anion (O_2^-) since titania samples of high SSA has large amounts of physisorbed water and hydroxyl groups [Murakami 2006/Murakami 2007]. The increase of PA signal for titania powders with high SSA measured in air cannot be observed when the atmosphere is nitrogen (N_2) gas or argon (Ar) gas. Thus, PAS is very sensitive for photoabsorption including not only target materials but also surface adsorbed species produced by light irradiation, and appropriate measurement atmosphere and attribution of photoabsorption are important. As shown in **Fig. 2-3**, experimental fact that absorption-edge wavelength of anatase is shorter than that of rutile is corresponding reported band gap of anatase (ca. 3.2 eV) [Tang 1993] and rutile (ca. 3.0 eV) [Minoura

1985]. It is well known that calcination of titania powders under hydrogen (H_2) gas atmosphere induces titanium trivalent ion (Ti^{3+}) formation, and PAS can detect photoabsorption of the electrons at donor levels of H_2 reduced titania sample prepared based on reported method [Amano 2016] as shown in **Fig. 2-4**. However, information on electron traps is not acquired by using only intermittent light for untreated metal-oxide powders.

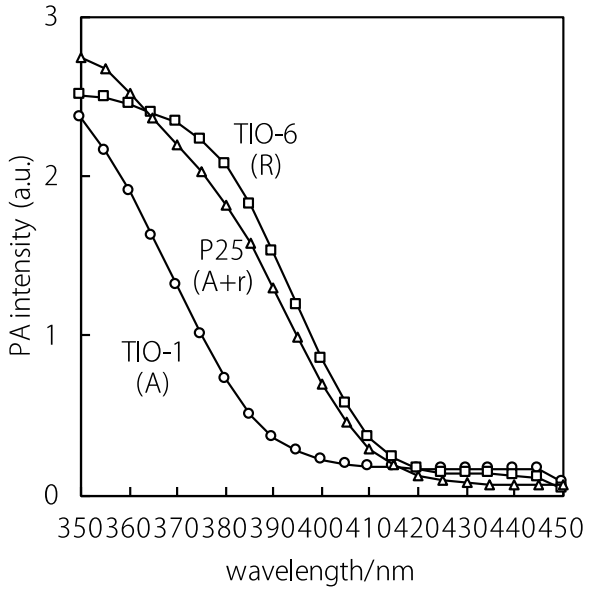

Fig. 2-3 Representative PA spectra for titania powders with different crystalline composition.

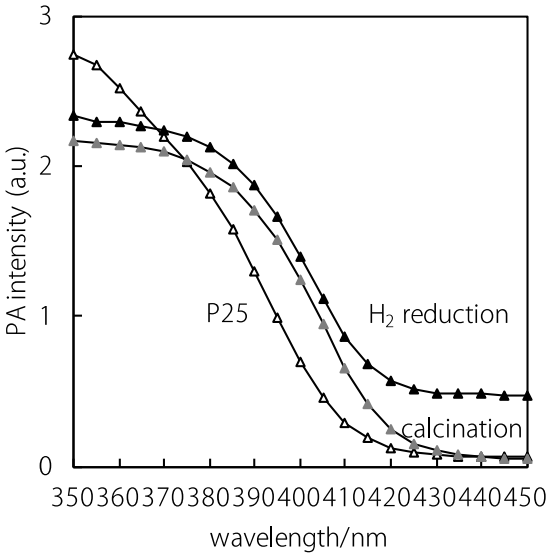

Fig. 2-4 Representative PA spectra for titania powders with and without treatment.

2.1.2 Double-beam Photoacoustic Spectroscopy

As described in **1-2**, photoirradiation of metal-oxide powders under deaerated condition in the presence of electron donors induces color change due to accumulated electrons in electron traps. By riding the strength on lock-in detection, detecting method of minute signal deriving only synchronous component with specific frequency from alternating-current signal, double-beam photoacoustic spectroscopy (DB-PAS) has been developed [Murakami 2006/Murakami 2007/Murakami 2007b/Murakami 2008]. Double beam means use of two lights; one is intermitted light and the other is continuous light. The role of continuous light is excitation of electrons in valence band to electron traps via conduction band and intermittent light is detection of photoabsorption for accumulated electrons. Under UV-continuous light irradiation during PAS measurement with methanol saturated argon gas atmosphere, PA signal increased even in visible region compared with intensity of PA signal under only intermittent light (single beam) irradiation as shown in **Fig. 2-5**.

In DB-PAS measurement, electrons in valence band are excited to conduction band to be accumulated in electron traps since holes are scavenged by methanol vapor as electron donor, and these accumulated electrons can absorb visible light. Since PA signal increases slightly accompanied with time and is saturated. Since saturated intensities of PA signal for titania powders differ from each other, saturated intensity corresponds to total amounts of accumulated electrons in electron traps. To estimate saturated intensities of PA signal for titania powders, time-resolved measurement of PA signal has been done [Murakami 2007]. In time-resolved measurement, wavelength of modulated light is not scanned but fixed to chase accumulation of electrons and 625 nm

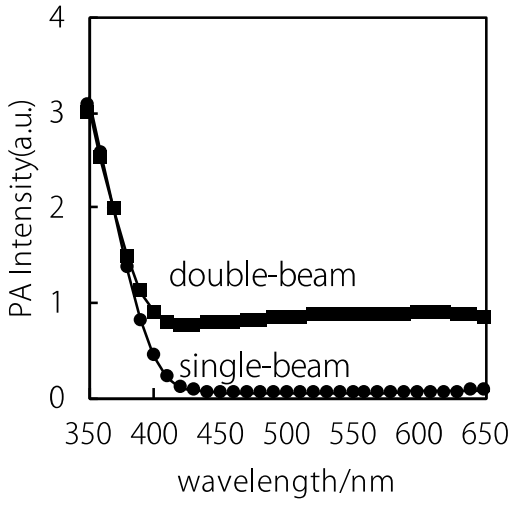

Fig. 2-5 Representative PA and DB-PA spectra for titania powders.

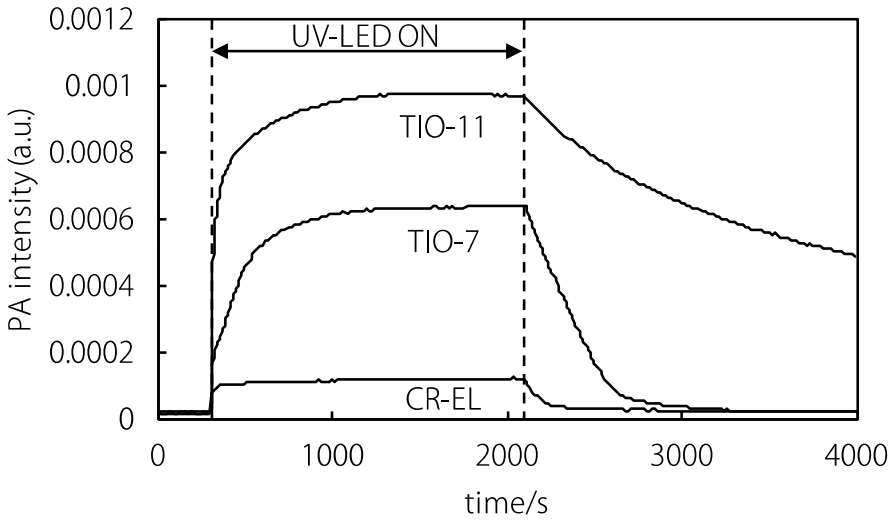

Fig. 2-6 Time course curves of PA spectra for titania powders.

has been chosen to avoid containing photoabsorption of surface peroxide species. Representative time course curves of PA signal for titania powders are shown in **Fig. 2-6**. At first, intensity of PA signal is low and almost flat during only intermittent light irradiation because untreated titania powders cannot absorb light at 625 nm. After UV-continuous light is irradiated at the same time, PA signal increases drastically and becomes gradually saturation. Saturated intensities are estimated by fitting time-course curves to a set of three exponential functions I (**eq. 2-1**).

$$I(t) = \sum_{i=1}^{3} a_i \left[1 - exp\left(-\frac{t}{\tau_i}\right)\right] \qquad \textbf{(eq.2-1)}$$

where t, a, τ show irradiation time of intermittent light, coefficient, and time constant, respectively. Saturated intensity of PA signal I_{sat} at 625 nm is obtained from summation (**eq. 2-2**).

$$I_{sat} = \sum_{i=1}^{3} a_i \qquad \textbf{(eq. 2-2)}$$

Total density of electron traps estimated by photochemical method [Ikeda 2003] and saturated intensity of PA signal I_{sat} are compared, and almost proportional relation has been obtained [Murakami 2007]. In this sense, signal increase observed in **Fig. 2-5** under UV-continuous light irradiation is attributable to accumulated electrons in electron traps. Thus, DB-PAS is an effective measure of evaluating total density of electron traps.

Not only quantitative estimation of electron-trap density but also evaluation of electron mobility has been studied by DB-PAS [Murakami 2007b]. In **Fig. 2-6**, PA signal decreases after stopping UV-continuous irradiation. This is caused by consumption of accumulated electrons and decay rates depend on kinds of titania powders.

When time-resolved measurement is done under methanol saturated O_2 atmosphere, decay is clearly fast, suggesting electron transfer from electron traps to O_2. On the other hand, no correlation has been observed between SSA and decay rate, thereby it has been suggested that main factor of decay rate is attributable to reactivity of accumulated electrons in electron traps. Decay curve has been fitted for a set of two exponential functions I (**eq. 2-3**) and the weighted mean decay rate constant (k_{wm}) has been calculated from the components (**eq. 2-4**).

$$I(t) = \sum_{i=1}^{2} a_i exp(-k_i t) \qquad \textbf{(eq. 2-3)}$$

$$k_{wm} = \frac{\sum_{i=1}^{2} a_i k_i}{\sum_{i=1}^{2} a_i} \qquad \textbf{(eq. 2-4)}$$

Although photocatalytic activities are almost constant in a region with fast decay rate, relation of monotonic increase between decay rate of PA signal for titania powders k_{wm} and photocatalytic activity of methanol dehydrogenation using platinum-loaded titania powders has been confirmed. Possible reason of the relation is electron transfer depending on energy-resolved density of electron traps (ERDT). One hypothesis is that deep traps facilitate recombination of electrons and holes, since electrons in deep traps may stay or be trapped deeper level slowly, and shallow traps that are located within ca. 0.026 eV, corresponding to thermal energy of electrons from CBB at room temperature, inhibit being trapped in deep traps by hopping [Böttger 1976] between conduction band and shallow traps, because electrons in shallow traps can be thermally excited to conduction band again. In this sense, ERDT may be important for electron transfer reaction of using metal-oxide powders such as photocatalysts, dye-sensitized solar cells, catalysts, and fuel cells. Thus, DB-PAS can be the method to evaluate electron transfer by analyzing decay rate of PA signal.

Not only evaluation of total density of electron traps and of electron transfer but also of reduction co-catalyst performance [Abe 2008], electron injection [Murakami 2010], and component separation of reaction heat [Murakami 2008] have been proposed for application of DB-PAS. Time-course curves of PA signal for a platinum (Pt) loaded titania powder prepared by photodeposition method [Kraeutler 1978] under methanol saturated Ar gas atmosphere is shown in **Fig. 2-7**. In the photodeposition method, Pt metal is loaded on metal-oxide powders by photocatalytic reaction; holes oxidize methanol and photoexcitated electrons reduce divalent platinum ion at first and protons to evolve H_2 after photodeposition. Maximum intensities of PA signal decrease with increase in Pt-loaded amount and decay rate of PA signal becomes steeply fast by Pt loading. This indicates that accumulation of electrons in electron traps is inhibited by

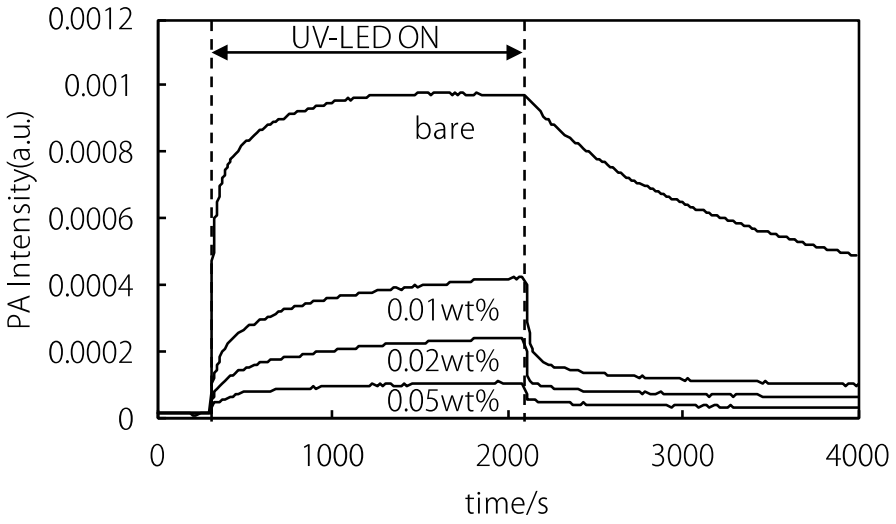

Fig. 2-7 Time course curves of PA spectra for platinum (Pt) loaded titania powders.

electron transfer from conduction band or electron traps to Pt. Decay rate constant k_{wm} becomes large by increase in Pt-loading amount from 0.01% to 0.05% and H_2 evolution activities increases with increase in k_{wm}, thereby electron transfer can be facilitated by Pt-loading. Although there are a lot of candidates as co-catalysts, inquest of co-catalysts for tungsten(VI) oxide (WO_3) powders toward decomposition of organic compounds has been done by analyzing decay rate [Abe 2008]. If visible-light sensitizer such as iron(III) ion is modified on titania powders, electron injection from the compounds to conduction band of titania powders can be also evaluated by DB-PAS [Murakami 2010]. If PAS is applied to fields where photochemical reactions can occur, not only heat release accompanied by deexicitation of photoexcited species but also reaction heat generated by photochemical reaction, and also pressure change accompanied by gas production and consumption can affect PA signal. However, since these components are observed at the same time, respective information is not elucidated. The components generated by such photoexcitation have their own time response characteristics. For example, it is well known that recombination process in titania powders occurs in picosecond region [Ikeda 2001], whereas oxygen active species involved in photocatalytic reactions in air has a lifetime slower than recombination. It has been estimated that lifetime of active species involving oxidative reaction of methanol is the order of 10 ms by reaction heat analysis [Murakami 2008].

As mentioned above, various evaluation of metal-oxide powders has been achieved by DB-PAS. However, it is impossible to measure ERDT since electrons excited in conduction band are captured in electron traps at random in DB-PAS measurement due to UV-continuous light irradiation.

2.1.3 Direct Excitation from Valence Band to Electron Traps

In ordinal PAS measurement shown in **Fig. 2-8**, PA signal started increasing at slightly longer wavelength side under methanol saturated Ar gas atmosphere than that under Ar gas atmosphere.

Absence of methanol vapor in DB-PAS measurement causes low PA signal because holes can react with accumulated electrons to recombine each other. In this sense, early increased PA signal in **Fig. 2-8** indicates that direct excitation from valence band to shallow traps close to CBB occurs. Thus, if electron traps are accumulated from deeper sides to shallower sides in sequence, ERDT can be achieved by using PAS. However, extinction coefficient of direct excitation from valence band to electron traps seems to be almost zero or negligibly small since direct excitation may occur only near band gap even in the presence of methanol vapor considering ERDT distributed within at least 0.25 eV below CBB estimated by photochemical method. Thus, another light for direct excitation from valence band to electron traps is needed separately from intermittent light for detection of accumulated electrons. In this study, reversed double-beam photoacoustic spectroscopy (RDB-PAS), in which wavelength scanned monochromatic light was used as excitation continuous light to accumulate electrons from deeper sides to shallower sides by direct excitation and monochlomatic LED light was used as intermittent light, was developed. Reversed means monochromatic light that has been used as the intermittent light so far is converted the continuous light in RDB-PAS measurement. Various kinds of metal-oxide powders were used and ERDT was evaluated as energy function from VBT.

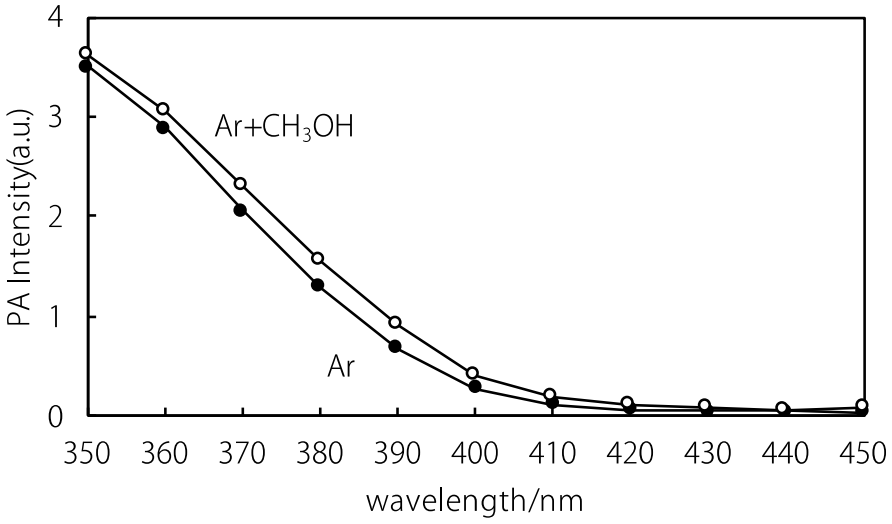

Fig. 2-8 Difference of PA spectra with or without existence of methanol vapor.

2.2 Experimental

2.2.1 Materials

Forty-nine titania powders from commercial source and reference catalysts supplied by the Catalysis Society of Japan (CSJ) were used. Platinum-loaded titania powders were prepared by photodeposition method. A suspension containing 600 mg of titania powders, 14.3 ml of methanol solution (Wako Pure Chemical Industries, Ltd.), 14.3 ml of pure water, and appropriate amount of hexachloroplatinic(IV) acid ($H_2PtCl_6 \bullet 6H_2O$) as the source of Pt was photoirradiated (400-W high-pressure mercury arc (Eiko-sha) at 298 K) under Ar gas atmosphere with magnetic stirring (1000 rpm). Platinum-loading was confirmed by gray coloration and by analyzing liberation of H_2 by gas chromatography (Shimazu GC-8A gas chromatograph equipped with a TCD and column of molecular sieve 5A). The prepared sample was dried at 70 °C for 12 hours.

Commercially available WO_3 supplied by Kojundo Chemical Laboratory, cerium(IV) oxide (CeO_2) supplied by Kojundo Chemical Laboratory, strontium titanate ($SrTiO_3$) supplied by Sigma-Aldrich, tin(IV) oxide (SnO_2) supplied by Wako Pure Chemical Industries, zinc oxide (ZnO) supplied by Wako Pure Chemical Industries, and potassium tantalite ($KaTaO_3$) supplied by Kojundo Chemical Laboratory were also used as metal-oxide powders other than titania powders.

2.2.2 Experimental Set Up

A 15–150 mg (depending on the apparent bulk density of a sample)-portion of a powder sample loaded on a stainless steel sample holder (standard sample thickness: 1.0 mm) was placed in a laboratory-made PAS cell (upper and bottom parts were made of aluminum and stainless steel, respectively) equipped with a microphone (Knowles Electronics SP0103NC3-3 electret condenser microphone) and a quartz window on the upper part.

For the PAS measurement to estimate bandgap of samples, the PAS cell was tightly sealed and placed in a glove box (Unico UN650F) under nitrogen atmosphere, and a monochromatic light beam from a xenon lamp (Spectral Products ASB-XE-175 xenon light source) with a grating monochromator (Spectral Products CM110) modulated at 80 Hz by a light chopper (NF Corporation 5584A) was irradiated from the top of the cell with wavelength scanning from 650 nm to 350 nm. The PA signal was detected using a digital lock-in amplifier (NF Corporation LI5630) and calibrated with spectral response

with a graphite sample, absorbing whole range of irradiated light, to compensate wavelength-dependent monochromatic light intensity. Position of CBB (E_{CBB}) was estimated as a function of energy from VBT from the onset wavelength of a PA spectrum using an equation. Since absorption-edge wavelength means that electrons cannot be excited at energy below the band gap, E_{CBB} shows energy between CBB and VBT.

In the RDB-PAS measurements, ambient-temperature methanol-saturated argon gas was passed (ca. 30 mL min^{-1}) through a sample-loaded PAS cell in a nitrogen-filled glove box for at least 30 min. and the cell was tightly closed. Methanol was used for scavenging positive holes left by photoexcitation of VB electrons to electron traps. Two light beams were combined and introduced to the PAS cell using a UV quartz combiner light guide (Moritex MWS5-1000S-UV3); one is a probe light beam from a 625-nm (1.98 eV) light-emitting diode (LED; Luxeon LXHL-ND98) intensity modulated (80 Hz) by a digital function generator (NF Corporation DF-1906) and the other is continuous monochromatic light from the xenon lamp-monochromator used in PAS measurement, as depicted in **Fig. 2-9**. PA signal was recorded similarly to the above-mentioned PAS measurement by scanning continuous-light wavelength from 650 nm (1.91 eV) to 350 nm (3.54 eV) with a 5-nm step. Continuous-light intensities at 650 nm, 600 nm, 500 nm, 450 nm, 400 nm, and 350 nm are 1.04 mW, 1.14 mW, 1.20 mW, 1.00 mW, 0.873 mW, 0.420 mW, and 0.199 mW, respectively. Standard waiting and acquisition times at each wavelength were 255 s and 20 s, respectively. The observed signal intensity was plotted against energy of continuous light and the RDB-PA spectrum was differentiated from the lower energy side to higher energy side, and the obtained

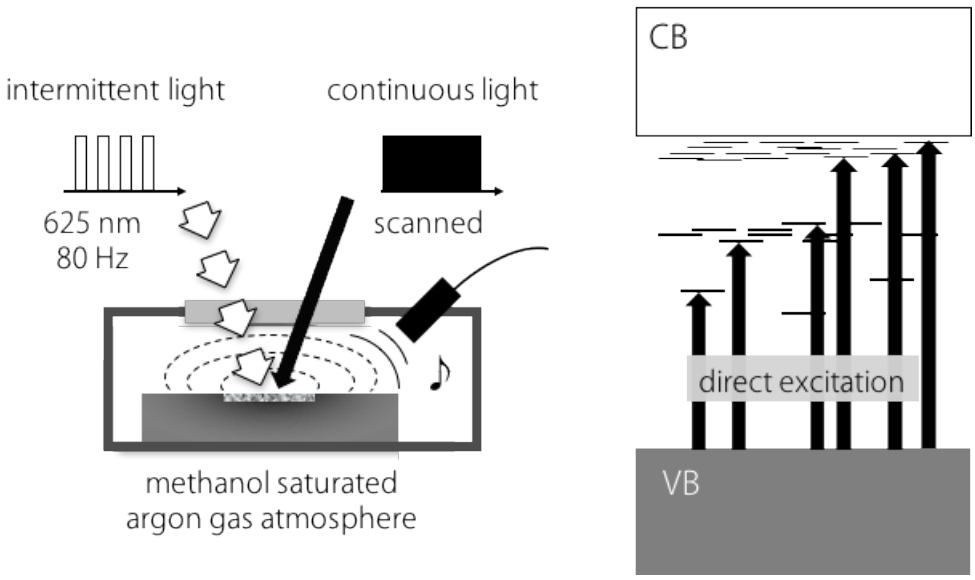

Fig. 2-9 Principle of reversed double-beam photoacoustic spectroscopy.

value was converted into electron-trap density in the unit of μmol g^{-1} eV^{-1} with conversion coefficient determined for each cell. The thus-obtained ERDT was a function of energy from VBT and replotted as a bar-graph with a 0.05 eV pitch. In RDB-PAS, direct excitation of electrons has to be assumed from VBT whether it occurs from VBT or not. In this respect, the meaning of energy from VBT for ERDT in **Fig. 10** is different from that for CBB estimated from the absorption-edge wavelength.

Titanium oxide powders were immersed in anhydrous acetonitrile solution and pulverized to be thin with an agate mortar and breast. This titanium oxide solution was coated on the platinum foil to form an opaque thin working electrode. A platinum wire and silver/silver chloride (Ag/AgCl) as the counter and reference electrodes, respectively, were placed in a cuvette with a quartz window filled with acetonitrile containing 0.1 mol dm^{-3} of $LiClO_4$ solution. Before and during the experiment, bubbling with argon gas was performed to remove oxygen. The cuvette was placed in front of the integrating sphere so that the working electrode faces the light source. The electrode potential was controlled by an electrochemical analyzer and the potential was lowered by 0.025 V every 10 minutes from 0 V Vs Ag/AgCl. The change in reflectance at 780 nm with respect to the potential was converted to Kubelka-Munk, and the state density (DOS) of the electron trap was obtained.

2.3 Results and Discussion

2.3.1 Role of Methanol Saturated Argon Gas

Acquired RDB-PA spectrum for a given titania powder is shown in **Fig. 2-10**. Like **Fig. 2-2**, PA signal started increasing from ca. 400 nm, ca. 3.1 eV. This energy corresponds band gap, that is E_{CBB} based on VBT. On the other hand, RDB-PA spectrum started increasing from wavelength longer than absorption-edge wavelength under methanol saturated Ar gas atmosphere. This means that something except for surface peroxide species which absorbs light from 400 nm (3.10 eV) to 500 nm (2.48 eV) absorbs 625 nm of light. If RDB-PAS measurement was done under Ar gas atmosphere without methanol vapor, however, increase of RDB-PA signal shown in **Fig. 2-10** was scarcely observed. Existence or absence of methanol vapor contributes whether holes are scavenged or not. In this sense, it is suggested that electrons in valence band were directly excited to electron traps by wavelength-scanned continuous light having energy smaller than the band gap and photoabsorption of accumulated electrons was detected by 625 nm of intermittent light because holes were effectively scavenged by methanol

irreversibly. In other words, absence of methanol vapor prevents accumulation of electrons in electron traps by continuous light. Explanation of the middle graph of **Fig. 2-10** is described in 2.3.3.

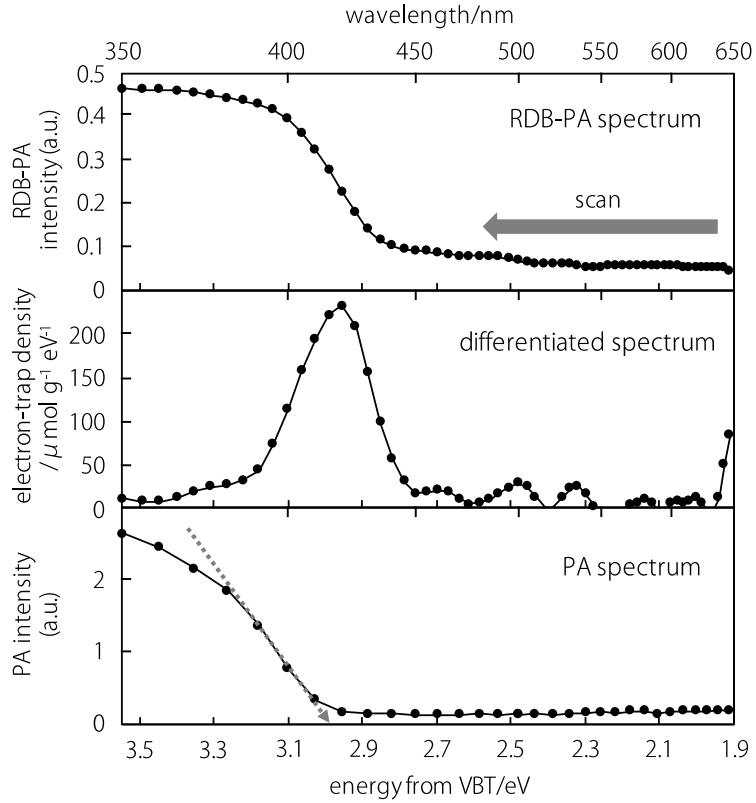

Fig. 2-10 Acquired RDB-PA spectrum and the differentiated spectrum.

2.3.2 Effect of Platinum-loading on Metal-oxide Powders

Although PA signal from accumulated electrons is hardly obtained if large amounts of Pt (>0.1wt%) are loaded on metal-oxide powders because of large photoabsorption of Pt itself, small amount of Pt loading such as 0.01wt% avoids large photoabsorption derived from Pt. Obtained RDB-PA spectrum for 0.01wt% of Pt-loaded titania powder is shown in **Fig. 2-11**. Although RDB-PA intensity was high because of photoabsorption of Pt itself, increase of RDB-PA signal at wavelength around 425 nm disappeared by Pt loading. It is well known that dehydrogenation of methanol to evolve H_2 using metal-oxide powders is drastically promoted by Pt loading to capture excited electrons efficiently. As shown in **Fig. 2-8**, it is assumed that a lot of excited electrons in conduction band are trapped by not electron traps but Pt. Although it is speculated that only a part of accumulated electrons is excited to conduction band by intermittent light by using ND filter in order to avoid change of position of accumulated electrons in RDB-PAS measurement, electrons once excited to conduction band may be mainly captured by not electron traps but Pt. This can be predicted by low saturated

intensity and large decay rate of PA signal in **Fig. 2-7**. Thus, RDB-PA signal is attributable to accumulated electrons in electron traps.

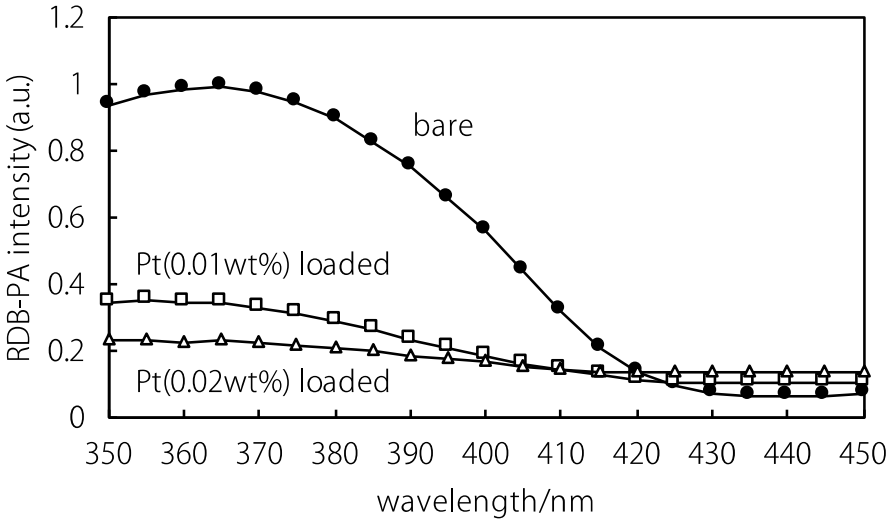

Fig. 2-11 Effect of Pt-loading on titania powders toward PA signal.

2.3.3 Acquisition of Energy-resolved Density of Electron Traps

As shown in **Fig. 2-10**, RDB-PA signal increased without decay and was eventually saturated. Given the relationship between total density of electron traps estimated by photochemical method and saturated intensity of DB-PA signal at 625 nm from time-resolved measurement, saturated intensity of RDB-PA signal can also correspond to total amounts of electron traps. In PAS measurement, intensity is given in relative value due to division of PA signal for a given sample by PA signal of graphite absorbing all range of UV and visible light to adjust light intensity of light source. A relationship between total density of electron traps measured by photochemical method and saturated intensity of RDB-PA signal is shown in **Fig. 2-12**. Although TIO-6 and some samples with high SSA were exception, linear relation was obtained between both parameters to give conversion factor. Thus, RDB-PA signal can be expressed as electron-trap density by using conversion factor. As is the report of relation between total density of electron traps and saturated intensity of PA signal, TIO-6 was only exception from linear relation. The reason has been proposed that steady-state generation of electrons might be insufficient due to a high recombination rate or a large amount of amorphous phase [Murakami 2007]. A possible reason of low value of saturated intensity for titania powders with high SSA compared to total density of electron traps might be large amounts of surface adsorbed water or surface hydroxyl groups on the powders. Considering the possibility of holes reacting with surface adsorbed water or

surface hydroxyl groups to produce peroxide species even in the presence of methanol vapor as hole scavenger, those peroxide species might react with accumulated electrons to reduce whole RDB-PA signal. Another possibility is low light power of xenon lamp for electrons to be excited to electron traps since 350 nm is enough large energy for band transition. In other words, high light intensity and long measurement time may solve this problem. Since electron traps are filled from deeper sides to shallower sides and photoabsorption of those accumulated electrons are detected by PAS, intensity of RDB-PA signal at a given wavelength can correspond to total quantity of electrons including so far electrons accumulated by continuous light having longer wavelength than the irradiation wavelength. So, after intensity of RDB-PA signal and wavelength was converted to electron-trap density in the unit of μmol g^{-1} and energy from VBT in the unit of eV, respectively, the spectrum was differentiated from lower energy side (**Fig. 2-10**).

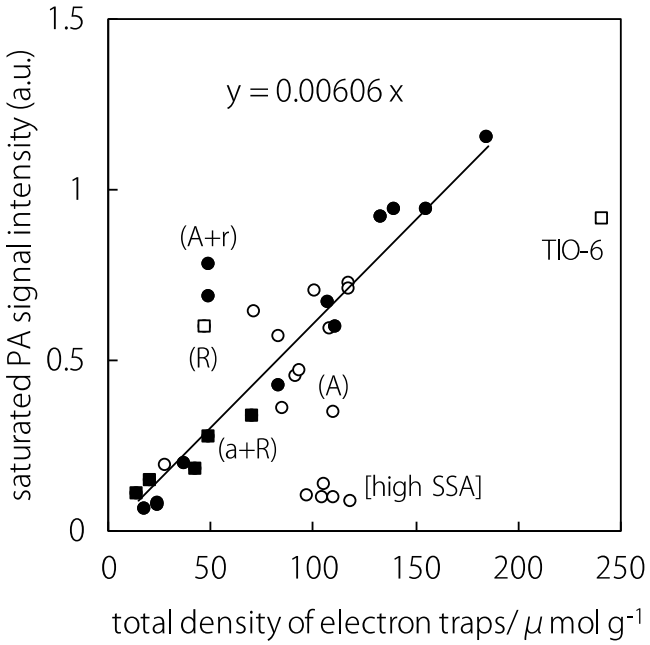

Fig. 2-12 Relation between total density of electron traps and saturated intensity.

Although there was increase of derivative spectrum at lower energy side cause by fluctuation of RDB-PA signal, ERDT of 5-nm step was obtained.

2.3.4 Comparison with Previous Results

Although various method for measuring electron-trap density has been reported, ERDT of powder form metal oxides has been reported by only photochemical method. Two kinds of ERDT for anatase and rutile type titania powders, TIO-2 and CR-EL, have been already measured [Ikeda 2003]. It has been reported that most electron traps are located 0.1 eV–0.2 eV below CBB. A comparison data of ERDT by photochemical

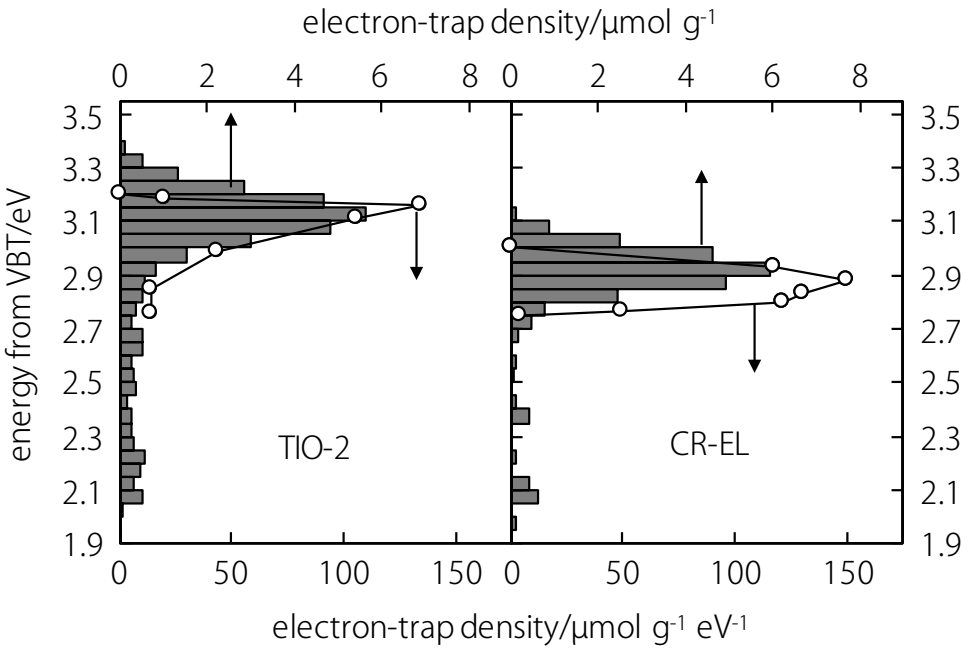

Fig. 2-13 Comparison of ERDT patterns of TIO-2 (anatase) and C-EL (rutile rich) measured by RDB-PAS (bar graphs) and photochemical method (lines with markers).

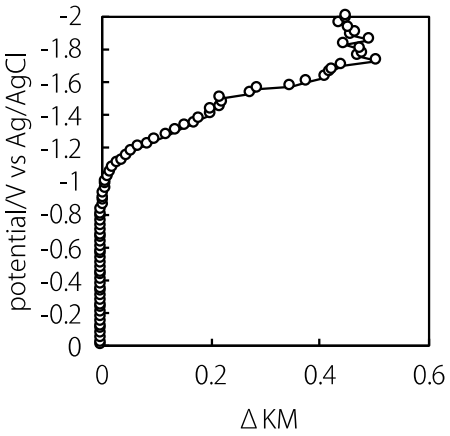

Fig. 2-14 Result of spectroelectrochemical measurement (for TIO-1).

method is shown in **Fig. 2-13**. Although energy difference of CBB positions between anatase and rutile has been assumed to be 0.24 eV by values of flat band potentials estimated by Mott-Schottky plots, to compare ERDT between RDB-PAS and photochemical method, ERDT estimated by photochemical method was shown as an energy function from VBT using reported bandgap values of 3.2 eV and 3.0 eV for anatase and rutile, respectively, analyzed by photocurrent action spectrum [Kavan 1996]. Distribution profiles of ERDT measured by RDB-PAS were similar to those of ERDT measured by photochemical method and it was unveiled that RDB-PAS measured the same parameter measured by photochemical method. Therefore, it is suggested that photoabsorption coefficient of electrons in electron traps at 625 nm is constant not

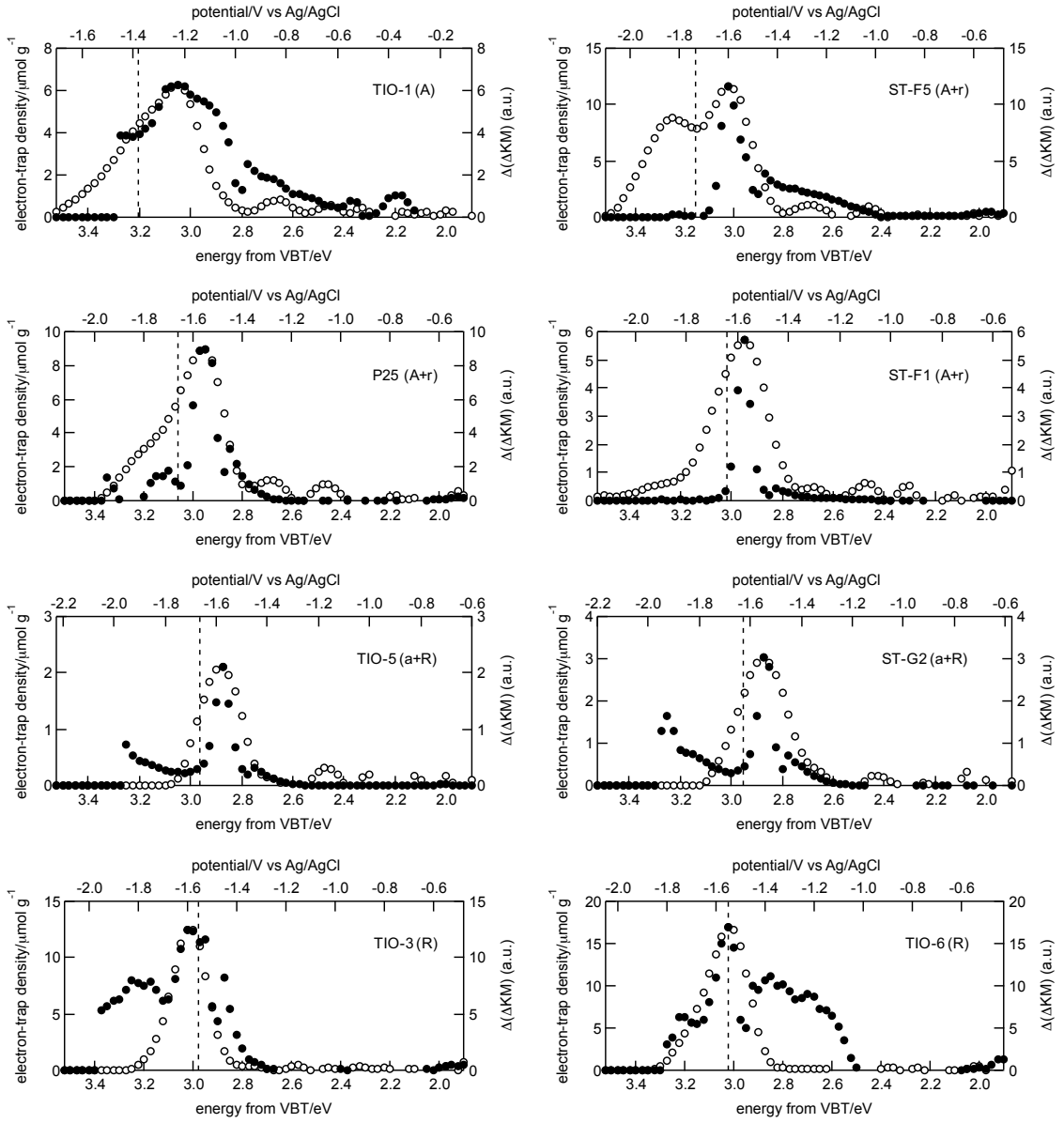

Fig. 2-15 Comparison of ERDT patterns measured by SEC. Closed and opend circles are ERDT measured by SEC and RDB-PAS, respectively. Values below sample name show differences of maximum energy and minimum potential.

depending on energy level and ERDT measurement by RDB-PAS is achieved. Energy resolution is higher and energy range is wider in ERDT measurement by RDB-PAS compared with photochemical method. The difference of energy scale in ERDT patterns is described in *2.3.5*.

ERDT patterns of titania powders were tried to be measured by spectroelectrochemical method (SEC) [Buchalska 2015]. In the method, changes of KM values were measured accompanied with changing electrode potential (**Fig. 2-14**). Density of states of electron traps was obtained by differential of a spectrum of **Fig. 2-14**. Obtained ERDT pattern were also similar to ERDT measured by spectroelectrochemical method till energy lower than CBB shown in **Fig. 2-15**. Potential was adjusted based

on the peak top of ERDT patterns measured by both methods. In the SEC method, electron traps were filled by electrons from deeper side to shallower side without generation of holes. Those electrons can be accumulated in conduction band. This may be one of the reasons for different shape of ERDT at energy higher than CBB. Another possibility is difference in shape of titania in RDB-PAS and SEC method. Although total density of electron traps cannot be ontained from SEC method, RDB-PAS could give the value. Except for TIO-1, values of differences between maximum energy and minimum potential were almost the same in titania powders. TIO-1 is synthesized by sulfide method and high pH value is attributable to make the value of difference large. Based on energy from VBT, ERDT patterns of anatase are apt to be located higher than energy of rutile and the ERDT/CBB patterns can be complex, however, there seems to be a little difference based on CBB.

2.3.5 Energy-resolved Density of Electron Traps for Metal-oxide Powders

Bar graph in 0.05 eV energy range of ERDT patterns for titania powders are shown in **Fig. 2-16**. Dotted line and numbers in angle bracket indicates CBB and total density of electron traps, respectively, and sample name, SSA, and crystalline type (Mainly crystalline phase, anatase or rutile, is shown in capital “A” or “R” and minor crystalline phase is shown in lower-case “a” or “r”.) are shown below total density of electron traps. Most electron traps were located around CBB regardless of crystalline composition and SSA. Those ERDT patterns were change by measurement time. In other words, if the measurement time is short, accumulation of electrons by continuous light irradiation is inadequate and ERDT is shifted toward lower energy side without maintaining the shape. Saturation of RDB-PA signal was commonly observed for titania powders and linear relation was obtained between total density of electron traps and saturated intensity of RDB-PA signal, thereby all of electron traps were filled with electrons and no accumulation of electrons in conduction band occurred. However, electron traps are present above CBB. Possible factors of the reason are described in *2.3.6*.

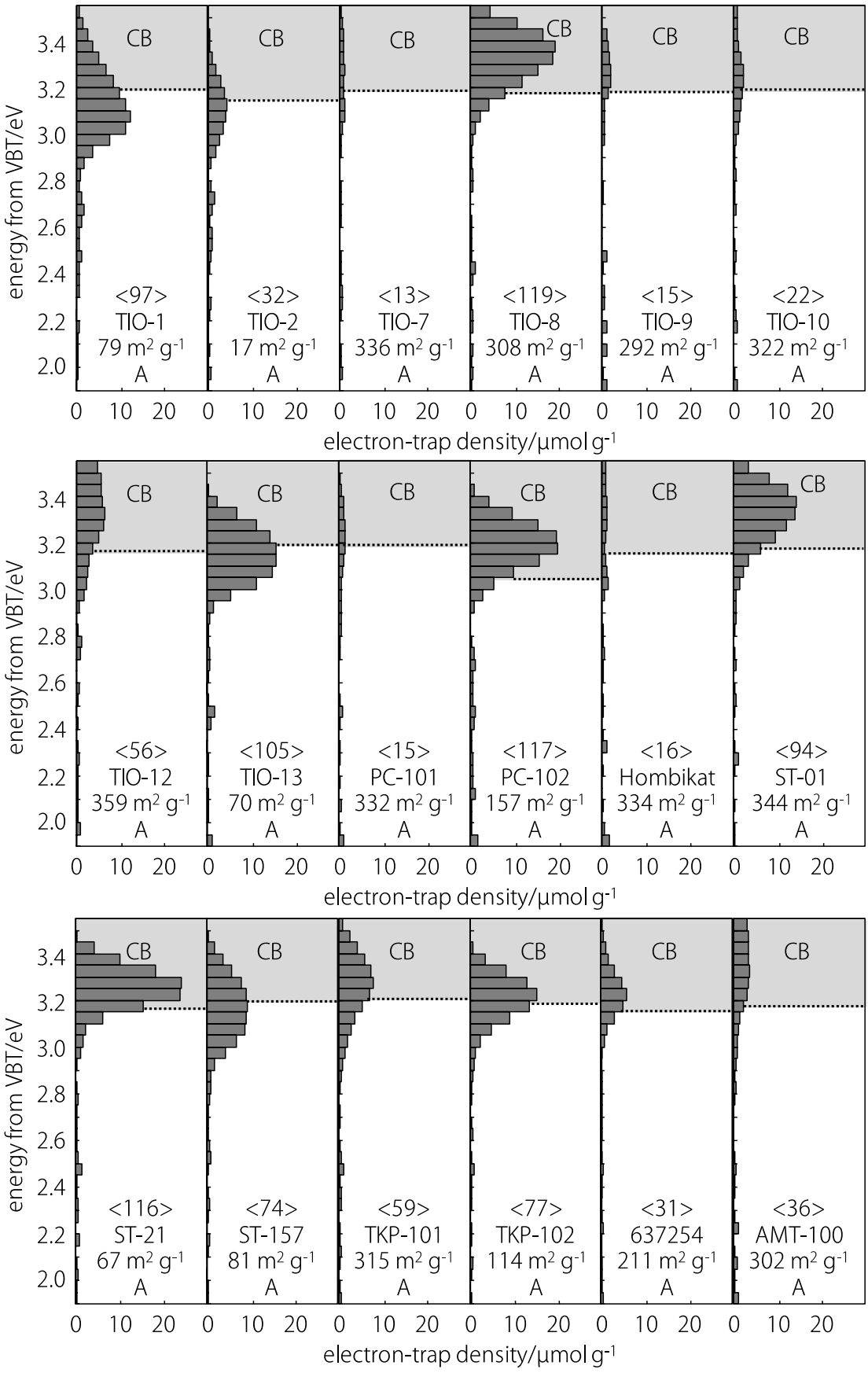

Fig. 2-16-1 Obtained ERDT patterns with conduction-band bottom (CBB) for titania powders.

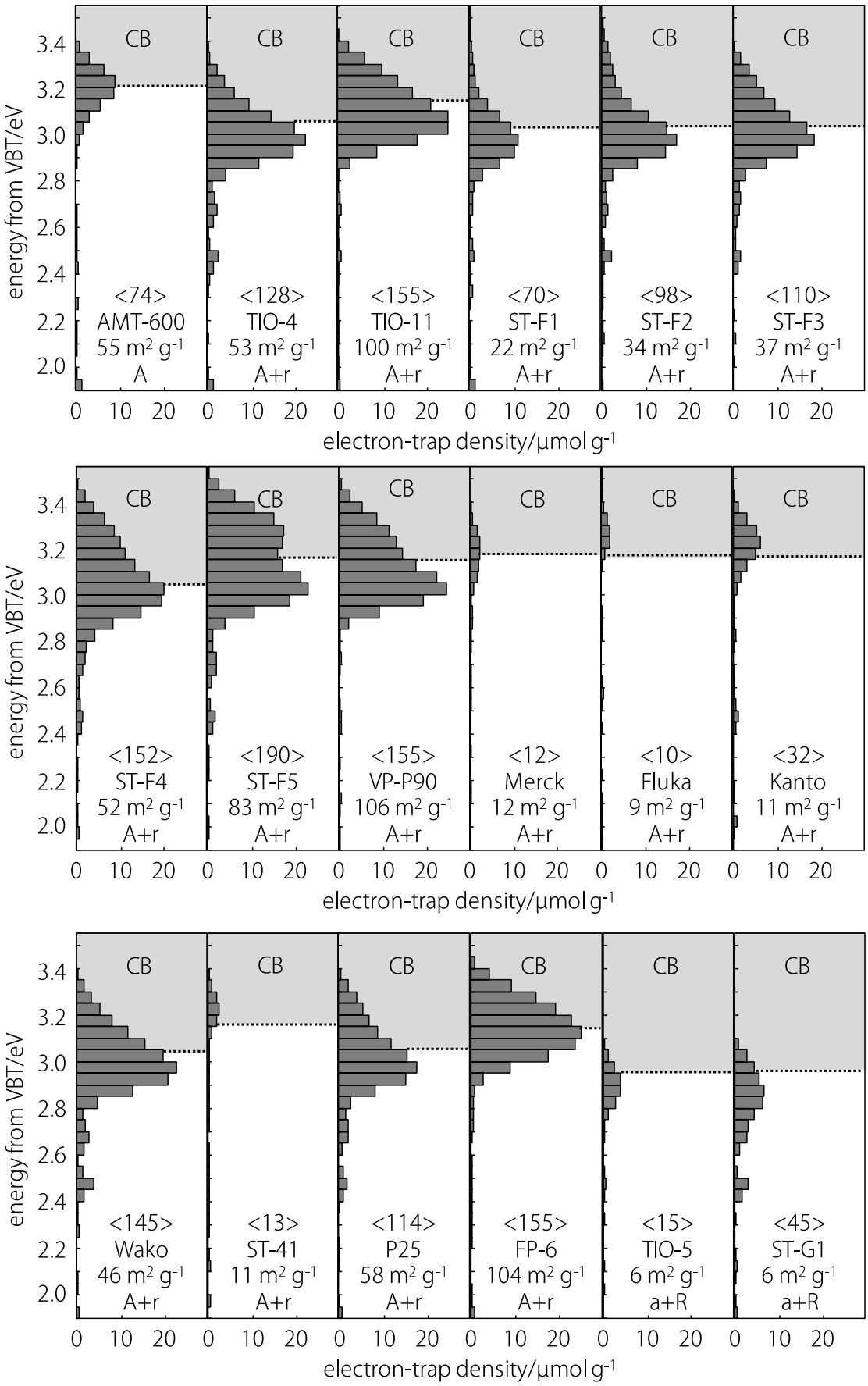

Fig. 2-16-2 Obtained ERDT/CBB patterns for titania powders.

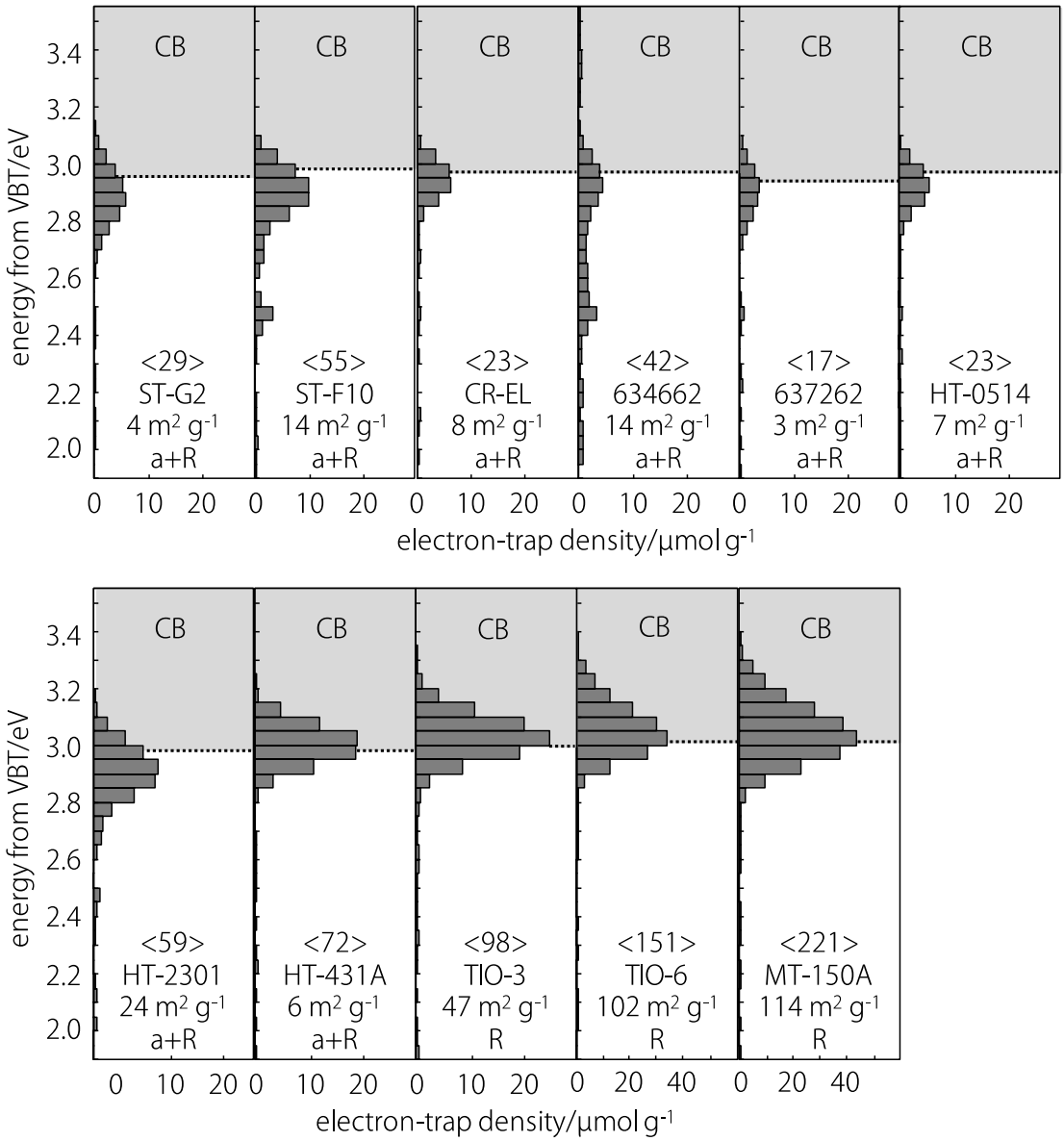

Fig. 2-16-3 Obtained ERDT/CBB patterns for titania powders.

Although ERDT measurement has been reported for only titania samples among metal-oxide powders, it is no wonder that metal-oxide powders other than titania may exhibit ERDT/CBB patterns similar to those shown in **Fig. 2-16** since most metal-oxides are classified as n-type semiconductors possessing band gap and donor levels below CBB. Representative ERDT patterns with CBB for commercially available WO_3, CeO_2, $SrTiO_3$, SnO_2, ZnO, and $KTaO_3$ are shown in **Fig. 2-17**. Since total density of electron traps for WO_3, CeO_2, $SrTiO_3$, SnO_2, ZnO, and $KTaO_3$ is unclear, conversion factor of titania powders was used simply. Positions of CBB estimated by absorption-edge wavelength of PA spectra corresponded to respective reported band gap of WO_3 [Bamwenda 1999], CeO_2 [Deus 2014], $SrTiO_3$ [Cardona 1965], SnO_2 [Miglio 2014], and

ZnO [Srikant 1998]. The ERDT patterns were also different depending on metal-oxide powders. Although total density of electron traps for ZnO was low, RDB-PAS measurement could be applied to various metal-oxide powders other than titania. Furthermore, ERDT/CBB patterns for hydrous niobic acid powders and niobium(V) oxide powders without crystalline phase that analysis was impossible for XRD measurement, zirconium(IV) oxide powders with wide band gap (ca. 5 eV), and titania thin film could be also obtained. Given that ERDT analysis of particulate metal-oxides has been achieved by only photochemical method for only titania powders, comparison of data with other method is difficult. However, RDB-PAS can be applied to various metal-oxide powders possessing electron traps. By improving sensitivity, light source, and wavelength-fixed intermittent-detection light, RDB-PAS can be used for much further kinds of metal-oxide powders and metal-oxide thin films.

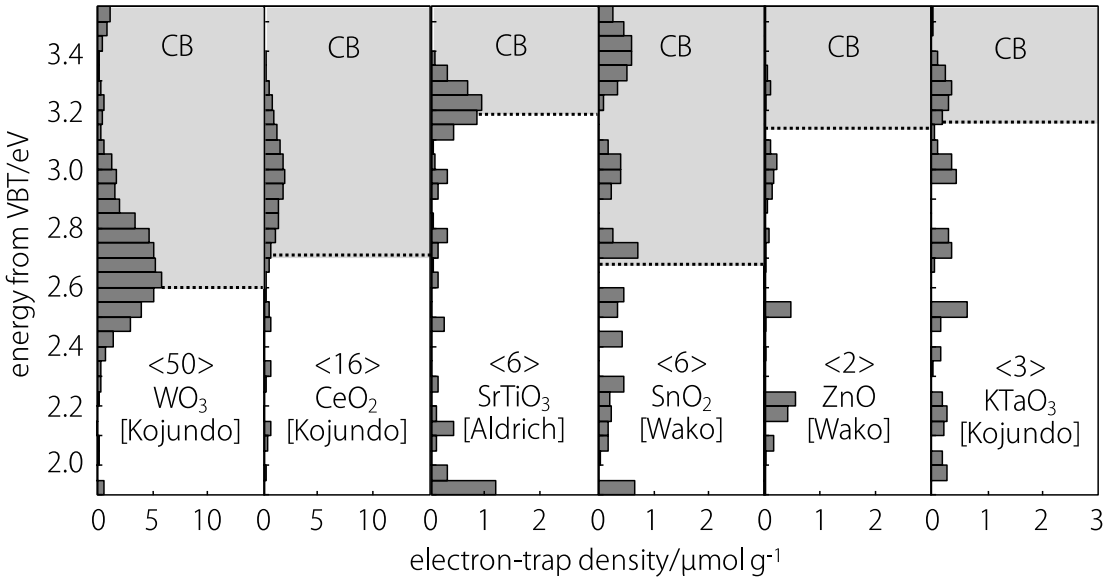

Fig. 2-17 Obtained ERDT/CBB patterns for metal-oxide powders.

2.3.6 Factors for Electron traps Exist in Conduction Band

Contrary to expectations, electron traps were located not only below CBB but also above CBB regardless of the crystalline composition and SSA. This phenomenon could be triggered by several considerable factors. Although direct excitation from valence band to electron traps occurs under continuous light irradiation, increase in PA signal at longer wavelength side corresponding to energy where electron traps exist was hardly observed under ordinary PAS measurement even under methanol saturated argon gas condition. In other words, difficulty in accumulation and detection of electrons in electron traps by only modulated light is attributable to quite small absorption cross-

section area of electron traps. Thus, direct excitation possibly occurs from high density of states (DOS) in valence band that is lower than VBT since electrons in VBT are negligible or lower. If electrons are directly excited from high energy of DOS, ERDT will be shifted to upward side caused by energy difference between VBT and high DOS states to be located at energy higher than CBB. In RDB-PAS measurement, it is impossible to determine absolute position of CBB and VBT because of the principle using direct excitation, energy axis of ERDT/CBB patterns is expressed as energy from VBT assuming direct excitation occurs from VBT. Possible another factor is difference between surface and bulk structures. Band structure model and well-known donner levels just below CBB are confined to matters of bulk structure. Since electron traps may be located on the surface [Kölle 1985], existence range of energy level for electron traps cannot be limited within band gap. There also seems to be a factor of electron traps located over CBB in estimation of CBB position. Absorption-edge wavelength of titania powders containing both anatase and rutile phases is affected by rutile to underestimate of CBB for mixed samples. Thus, ERDT of titania powders with anatase-rutile mixed phases may well be located over estimated CBB. Difference of ERDT at energy from VBT between photochemical method and RDB-PAS may be also affected by above several factors. Those factors are also discussed at **Chapter 4**.

2.4 Conclusions

In this chapter, RDB-PAS was developed as a new analysis method of ERDT for metal-oxide powders. In previously reported DB-PAS, UV light was irradiated simultaneously with intermittent light irradiation to accumulate electrons in electron traps via conduction band by interband transition. However, electrons were trapped at random to make it impossible to measure ERDT. On the other hand, in RDB-PAS, previously fixed continuous light was scanned from longer wavelength side to shorter wavelength side for electrons to be excited directly from valence band to electron traps, thereby it was possible to accumulate electrons from deep traps rather than accumulation of electrons at random electron like conventional photochemical method or DB-PAS. Increase of RDB-PA signal was observed when atmosphere was maintained as methanol saturated Ar gas, however no increase of RDB-PA signal was observed without methanol vapor or with Pt loading at visible light region. Therefore, RDB-PA signal is attributable to photoabsorption of accumulated electrons in electron traps. By using conversion factor from RDB-PA signal to electron-trap density based on the relation between total density of electron traps and saturated intensity of RDB-PA signal and differentiating RDB-PA spectrum from lower energy side, ERDT was easily acquired. Obtained ERDT

by RDB-PAS analysis was similar in shape to ERDT patterns of two kinds of titania powders different in crystalline form obtained by photochemical method, indicating that ERDT analysis can be achieved by RDB-PAS. This new ERDT measurement was applied to not only titania powders but also various metal-oxide powders such as WO_3 powders. Thus, RDB-PAS, which has high energy resolution and wide energy range, can be a standard evaluation method of ERDT for metal-oxide powders and for significant fundamental properties of functional inorganic materials such as photocatalysts, dye-sensitized solar cell, catalysts, and fuel cells.

2.5 References

Abe 2008 Abe, R.; Takami, H.; Murakami N.; Ohtani B., Pristine Simple Oxides as Visible Light Driven Photocatalysts: Highly Efficient Decomposition of Organic Compounds over Platinum-Loaded Tungsten Oxide, *J. Am. Chem. Soc.*, **130**, 7780–7781 (2008).

Amano 2016 Amano, F.; Nakata, M.; Yamamoto A.; Tanaka T., Effect of Ti^{3+} Ions and Conduction Band Electrons on Photocatalytic and Photoelectrochemical Activity of Rutile Titania for Water Oxidation, *J. Phys. Chem. C*, **120**, 6467–6474 (2016).

Bamwenda 1999 Bamwenda, R. G.; Sayama, K.; Arakawa, H., The effect of selected reaction parameters on the photoproduction of oxygen and hydrogen from a WO_3-Fe^{2+}-Fe^{3+} aqueous suspension, *J. Photochem. Photobiol. A*, **122**, 175–183 (1999).

Bell 1880 Bell, A. G., On the production and reproduction of sound by light, *Am. Jour. Sci.*, **20**, 305–324 (1880).

Böttger 1976 Böttger, H.; Bryksin V. V., Hopping conductivity in ordered and disordered solids (I), *Phys. Stat. Solid B*, **78**, 9–56 (1976).

Buchalska 2015 Buchalska, M.; Kobielusz, M.; Matuszek, A.; Pacia., M.; Wojtyła, S.; Macyk, W., On Oxygen Activation at Rutile- and Anatase-TiO_2, *ACS Catal.*, **5**, 7424–7431 (2015).

Cardona 1965 Cardona M., Optical Properties and Band Structure of $SrTiO_3$ and $BaTiO_3$, *Phys. Rev.*, **140**, A651–A655 (1965).

Deus 2014 Deus, R. C.; Foschini, C. R.; Spitova, B.; Moura, F.; Longo, E.; Simões, A. Z., Effect of soaking time on the photoluminescence properties of cerium oxide nanoparticles, *Ceramics International*, **40**, 1–9 (2014).

Ikeda 2001 Ikeda, S.; Sugiyama, N.; Pal, B.; Ohtani, B.; Noguchi, H.; Uosaki, K.; Marci, G.; Palmisano, L., Photocatalytic activity of transition-metal-loaded titanium(IV) oxide powders suspended in aqueous solutions: Correlation with electron-hole recombination kinetics, *Phys. Chem. Chem. Phys.*, **3**, 267–273 (2001).

Ikeda 2003 Ikeda, S.; Sugiyama, N.; Murakami, S.; Kominami, H.; Kera, Y.; Noguchi, H.; Uosaki, K.; Torimoto, T.; Ohtani, B., Quantitative analysis of defective sites in titanium(IV) oxide photocatalyst powders, *Phys. Chem. Chem. Phys.*, **5**, 778–783 (2003).

Kavan 1996 Kavan, L.; Grätzel, M.; Gilbert, S. E.; Klemenz, C.; Scheel, J., Electrochemical and Photoelectrochemical Investigation of Single-Crystal Anatase, *J. Am. Chem. Soc.*, **118**, 6716–6723 (1996).

Kölle 1985 Kölle, U.; Moser, J.; Grätzel, M., Dynamics of Interfacial Charge-Transfer Reactions in Semiconductor Dispersions. Reduction of Cobaltoceniumdicarboxylate in Colloidal TiO_2, *Inorg. Chem.*, **24**, 2253–2258 (1985).

Kraeutler 1978 Kraeutler, B.; Bard, A. J., Heterogeneous photocatalytic preparation of supported catalysts. Photodeposition of Platinum on Titanium Dioxide Powder and Other Substrates, *J. Am. Chem. Soc.*, **100**, 4317−4318 (1978).

Miglio 2014 Miglio, A.; Saniz, R.; Waroquiers, D.; Stankovski, M.; Giantomassi, M.; Hautier, G.; Rignanese, G.-M.; Gonze, X., Computed electronic and optical properties of SnO_2 under compressive stress, *Optical Materials*, **38**, 161−166 (2014).

Minoura 1985 Minoura, H.; Nasu, M.; Takahashi, Y., Comparative studies of photoelectrochemical behavior of rutile and anatase electrodes prepared by OMCVD technique, *Phys. Chem.*, **89**, 1064–1069 (1985).

Murakami 2006 Murakami, N.; Prieto-Mahaney, O.-O.; Torimoto, T.; Ohtani, B.; Photoacoustic spectroscopic analysis of photoinduced change in absorption of titanium(IV) oxide photocatalyst powders: A novel feasible technique for measurement of defect density, *Chem. Phys. Lett.*, **426**, 204–208 (2006).

Murakami 2007 Murakami, N.; Prieto-Mahaney, O.-O.; Abe, R.; Torimoto, T.; Ohtani, B.; Double-Beam Photoacoustic Spectroscopic Studies on Transient Absorption of Titanium(IV) Oxide Photocatalyst Powders, *J. Phys. Chem. C*, **111**, 11927–11935 (2007).

Murakami 2007b Murakami, N.; Abe, R.; Prieto-Mahaney, O.-O.; Torimoto, T.; Ohtani, B.; Photoacoustic Spectroscopic Estimation of Electron Mobility in Titanium(IV) Oxide Photocatalysts, *Stud. Surf. Sci. Catal.*, **172**, 429–432 (2007).

Murakami 2008 Murakami, N.; Abe, R.; Ohtani, B., In situ observation of photocatalytic reaction by photoacoustic spectroscopy: Detection of heat of exothermic photocatalytic reaction, *Chem. Phys. Lett.*, **451**, 316–320 (2008).

Murakami 2010 Murakami, N.; Ono, A.; Nakamura, M.; Tsubota, T.; Ohno, T., Development of a visible-light-responsive rutile rod by site-selective modification of iron(III) ion on {111} exposed crystal faces, *Appl. Catal. B: Environ.*, **97**, 115–119 (2010).

Nitta 2016 Nitta, A.; Takase, M.; Takashima, M.; Murakami, N.; Ohtani, B., A fingerprint of metal-oxide powders: energy-resolved distribution of electron traps, *Chem. Commun.*, **52**, 12096–12099 (2016).

Rosencwaig 1976 Rosencwaig, A.; Gersho, A., Theory of the Photoacoustic Effect with Solids, *J. Appl. Phys.*, **47**, 64–69 (1976).

Srikant 1998 Srikant, V.; Clarke, D. R., On the optical band gap of zinc oxide, *J. Appl. Phys.*, **83**, 5447–5451 (1998).

Tang 1993 Tang, H; Berger, H.; Schmid, P. E.; Levy, F.; Burri, G., Photoluminescence in TiO_2 anatase single crystals, *Solid State Commun.*, **87**, 847–850 (1993).

Thakor 2011 Thakor, A. S.; Jokerst, J.; Zaveleta, C.; Massoud, T. F.; Gambhir, S. S., Gold Nanoparticles: A Revival in Precious Metal Administration to Patients, *Nano Lett.*, **11**, 4029–4036 (2011).

Toyoda 1998 Toyoda, T.; Shimamoto, S., Effects of Bi_2O_3 Impurities in Ceramic ZnO on Photoacoustic Spectra and Current-Voltage Characteristics, *Jpn. J. Appl. Phys.*, **37**, 2827–2831 (1998).

Toyoda 2000 Toyoda, T.; Kawano, H.; Shen, Q; Kotera, A.; Ohmori; M., Characterization of Electronic States of TiO_2 Powders by Photoacoustic Spectroscopy, *Jpn. J. Appl. Phys.*, **39**, 3160–3163 (2000).

Toyoda 2003 Toyoda, T.; Tsuboya I., Apparent band-gap energies of mixed TiO_2 nanocrystals with anatase and rutile structures characterized with photoacoustic spectroscopy, *Rev. Sci. Instrum.*, **74**, 782–784 (2003).

Chapter 3

Identification and Characterization of Metal-oxide Powders by Electron Traps

3.1 Introduction

3.1.1 Identification of Organic Molecules

For organic compounds, anything manufactured at a high purity can be the same. If a structure of a given organic compound is unknown, the molecule is deemed to be identified by elemental analysis and nuclear magnetic resonance (NMR) pattern matching with standard or calculated values. For example, both proton and carbon NMR data and either accurate mass or elemental analysis data should be included as evidence to identify new compounds for submitting a paper to Journal of Organic Chemistry. In other words, identification method has been already established. Structure identification and structure verification by NMR spectral analysis seem to be powerful considering they can be largely automated in a software package and be performed in minutes [Dunkel 2007].

3.1.2 Identification of Metal-oxide Powders

As for metal-oxide powders, even a given material with the same chemical formula can be different if manufacturers are different. If the production lot is different, it has been thought that the characteristic is also different even for the same metal-oxide powder of the same manufacturer. Although it is possible to analyze powders by dissolving it in acid or base, it is not always the same as the original powder even if the solution is evaporated to dryness. This point is very different from organic compounds.

What has been conventionally evaluated as structural properties of metal-oxide powders is crystal phase and primary particle diameter by powder X-ray diffraction (XRD) pattern analysis, secondary particle diameter by size distribution analysis, and specific surface area (SSA) or pore distribution estimated from nitrogen adsorption measurement. We can know how much anatase and rutile is included in a particulate titania sample by XRD pattern analysis corresponding to elemental composition and NMR pattern analysis for organic molecules, however, it is not sufficient to identify a powder sample. For example, it is well known that numerous kinds of titanium(IV) oxide (titania) powders all assigned to anatase by XRD patterns have different properties

and reactivity (**Table 3-1** in *3.2*). Of course, metal-oxide powders consisting of only non-crystalline components cannot be absolutely identified by XRD measurements. Such a difference of identification between organic molecules and metal-oxide powders is attributable to the existence of both surface and bulk for powders. On the surface of solid materials, the periodicity of the crystal is broken, and there are characteristic structures, electronic states, vibrational states different from the bulk of the particles. Then, it is significant to analyze and evaluate surface of metal-oxide powders. Although SSA contains information on surface area, SSA is irrelevant to structural property of the surface and reflect only bulk size. Thus, conventional evaluation of metal-oxide powders has focused on only bulk composition and bulk size. Although some methods for analyzing surface property exist, microscopic information is obtained. For example, in surface observation with electron microscope and probe microscope, it is possible to see the surface state precisely, however, observation with an enormous number of fields is required for the whole sample surface. Thus, such a method is not suitable for overall average evaluation. In other words, a lack of sufficient analytical method that enables measurement of a property reflecting macroscopic surface structure has prevented characterization and thereby identification of metal-oxide powders. Thus, what is needed for identification of metal-oxide powders is a parameter that can be a fingerprint reflecting surface structural property.

In Chapter 2, energy-resolved density of electron traps (ERDT) was measured by newly developed method and the results were similar to previous reported ERDT patterns. Those electron traps seem to exist on the surface, thereby ERDT can contain information relating surface structural properties. By using new parameters reflecting both surface and bulk structures, identicalness/similarity/differentness of metal-oxide powders can be evaluated. Furthermore, those parameters can be decisive factors of performances of metal-oxide powders. In this chapter, identification and characterization by combination of ERDT with bulk structures and quantitatively evaluation method of degree of coincidence were discussed.

3.2. Experimental

3.2.1 Materials

Titania powders are the same as those described in *2.2.1*. For reproducibility test, FP-6 was taken from close and different positions in a same container. Structural properties of titania powders are shown in **Table 2-1**.

3.2.2 Reversed Double-beam Photoacoustic Spectroscopic Measurement

Experimental details are described in *2.2.2*.

3.2.3 X-ray Diffraction Pattern Analysis

Crystalline composition was determined through XRD measurements using Cu-Kα radiation in a Rigaku RINT 2500 equipped with a carbon monochromator. Metal-oxide powders and nickel oxide as an internal standard were mixed at the weight ratio of 8:2, respectively. Mix samples were packed in a glass sample holder of ca. 0.5-mm depth. Measurements were done of following conditions. Presence and absence of crystalline phase of anatase and rutile was confirmed by XRD pattern analysis.

3.2.4 Nitrogen Adsorption Measurement

Specific surface area of collected appropriate amount of metal-oxide powders of which surface area is so as to be between 2 m^2 and 10 m^2 was evaluated according to a Brunauer-Emmett-Teller equation with data of nitrogen adsorption isotherms at 77 K by using liquid nitrogen on Yuasa-Quantachrome NOVA 1200 e surface and pore size analyzer. Adsorption cross section of nitrogen, 0.162 nm^2, was used for calculation. Six data points in the relative pressure range between 0.05 and 0.3 were collected.

3.2.5 Activity Test of Heterogeneous Photocatalytic Reaction

Three representative photocatalytic reactions, (a) hydrogen (H_2) evolution from deaerated aqueous methanol, (b) carbon-dioxide (CO_2) evolution from aqueous acetic acid under aerobic conditions and (c) oxygen (O_2) evolution from aqueous silver fluoride, were conducted. Amount of 50 mg metal-oxide powders was suspended in 5.0 mL of an aqueous solution in a borosilicate glass tube (transparent for wavelength > 290 nm, 18 mm in inner diameter and 180 mm in length) containing (a) 50vol% of methanol aqueous solution with hydrogen hexachloroplatinate(IV) hexahydrate corresponding to 2wt% platinum loading on the metal-oxide powders, (b) 5vol% of acetic acid and (c) 50 mmol L^{-1} of silver fluoride aqueous solution. For reactions (a) and (c), after argon gas bubbling to remove O_2, every tube was sealed by a double-capped rubber septum and a Parafilm sheet after argon gas bubbling to remove O_2. The samples were irradiated by a 400-W high-pressure mercury arc (Eiko-sha) at 298 K with magnetic stirring (1000 rpm). Photocatalytic activities were calculated as the rate of (a) H_2, (b) CO_2, and (c) O_2 evolution by gas chromatography (Shimadzu GC-8A gas chromatograph equipped with a TCD and columns of molecular sieve 5A for H_2 and O_2 and Porapak Q for CO_2).

Table 2-1 Structural properties and photocatalytic-activity rank of titania powders.

supplier[a]	code[b]	composition[c] (%)		SSA[d]/	D^{e}/μmol	E_{CBB}[f]/eV	activity rank		
		anatase	rutile	$m^2\ g^{-1}$	g^{-1}		H_2	CO_2	O_2
CSJ	TIO-1	91	0	79	97	3.20	42	34	33
CSJ	TIO-2	91	0	17	32	3.14	48	37	28
CSJ	TIO-3	0	90	47	98	2.98	44	48	32
CSJ	TIO-4	72	23	53	129	3.06	6	2	16
CSJ	TIO-5	9	85	6	17	2.96	34	26	3
CSJ	TIO-6	0	78	102	152	3.03	41	36	49
CSJ	TIO-7	80	0	336	19	3.19	21	18	40
CSJ	TIO-8	80	0	308	119	3.18	17	23	45
CSJ	TIO-9	89	0	292	15	3.18	3	28	46
CSJ	TIO-10	86	0	322	22	3.19	19	19	34
CSJ	TIO-11	82	9	100	155	3.14	28	6	26
CSJ	TIO-12	73	0	359	56	3.17	14	24	35
CSJ	TIO-13	93	0	70	106	3.19	18	16	25
CSJ	TIO-14	69	0	331	114	3.20	9	22	44
CSJ	TIO-15	76	13	53	119	3.07	11	1	18
Aerosil	P25	82	15	58	114	3.06	16	8	14
Aerosil	VP-P90	84	7	106	155	3.16	8	7	22
Aldrich	634662	20	74	14	42	2.98	13	40	12
Aldrich	637254	89	0	211	32	3.16	29	10	39
Aldrich	637262	2	89	3	17	2.94	46	39	9
Fluka	(Fluka)	93	3	9	10	3.16	47	38	7
Hombikat	UV-100	81	0	334	16	3.16	23	14	38
ISK	CR-EL	1	94	8	23	2.97	7	42	4
ISK	ST-01	80	0	344	94	3.17	15	21	43
ISK	ST-21	87	0	67	116	3.17	38	15	36
ISK	ST-41	98	1	11	13	3.17	40	20	20
Kanto	(Kanto)	97	1	11	32	3.16	45	32	21
Merck	(Merck)	93	4	12	12	3.18	43	33	30
SDC	ST-F1	78	20	22	70	3.02	30	31	13
SDC	ST-F2	79	16	34	98	3.04	26	12	10
SDC	ST-F3	81	15	38	110	3.04	25	3	11
SDC	ST-F4	77	14	52	152	3.05	35	4	19
SDC	ST-F5	84	3	84	190	3.16	12	25	23
SDC	FP-6	83	8	104	154	3.15	33	9	24
SDC	ST-F10	4	93	14	55	2.98	5	45	5
SDC	ST-G1	0	97	7	45	2.97	2	46	2
SDC	ST-G2	3	95	4	29	2.95	1	43	6
Tayca	AMT-100	85	0	302	36	3.19	31	17	47
Tayca	AMT-600	93	0	55	65	3.18	39	30	29
Tayca	MT-150A	0	82	114	221	3.03	36	47	48
Tayca	ST-157	81	0	81	75	3.20	49	41	41
Tayca	TKP-101	75	0	315	59	3.21	37	29	42
Tayca	TKP-102	89	0	114	77	3.19	27	11	37
Titan	PC-101	89	0	332	15	3.19	20	13	31
Titan	PC-102	91	0	157	117	3.06	32	27	27
Toho	HT-0514	1	94	7	23	2.97	22	44	1
Toho	HT-2301	12	83	24	59	2.98	10	35	8
Toho	HT-431A	21	75	7	72	2.99	24	49	17
Wako	(Wako)	79	16	46	145	3.05	4	5	15

[a]CSJ: Catalysis Society of Japan, Aerosil: Nippon Aerosil, Aldrich: Sigma Aldrich, Fluka: Honeywell Fluka, ISK: Ishihara Sangyo, Kanto: Kanto Chemical, SDC: Showa Denko Ceramics, Titan: Titan Kogyo, Toho: Toho Titanium and Wako: Wako Pure Chemical Industries. [b]() show no code. [c]The rest corresponds to non-crystalline component. [d]Specific surface area. [e]Electron-trap density density. [f]Conduction-band bottom (CBB) position.

3.3 Results and Discussion

3.3.1 Structural Properties of Measured Parameters

Representative ERDT/CBB patterns for titania powders gotten out from **Fig. 2-14** are shown in **Fig. 3-1**. Figures in < > in **Figure 3-1** is total density of electron traps in the unit of μmol g^{-1} and SSA in the unit of m^2 g^{-1} and these are shown below sample names. Abbreviations "A" and "R" in the bottom row are anatase and rutile, respectively, and "a" and "r" are anatase and rutile in minor composition, respectively. Estimated CBB was ca. 3.2 eV and 3.0 eV for anatase and rutile, respectively, and CBB of samples containing both anatase and rutile shows middle values. The values corresponded to reported band gap energies of anatase [Tang 1993] and rutile [Minoura 1985]. It has been proposed that band gap energy can be controlled by mixing anatase-type and rutile-type titania powders based on the experimental results that a value of band gap of a mixed titania nanocrystal with rutile and anatase structure decreased continuously with the increase of rutile content [Toyoda 2003]. Thus, CBB seems to depend on crystalline phase, thereby CBB reflects crystalline composition.

It has been suggested that electron traps are located close to the surface since the nature of electron traps is influenced by the degree of protonation of colloidal titania particles [Kölle 1985]. Hence similar trend is supposed to be obtained for untreated titania powders. Relation between SSA and total density of electron traps is shown in

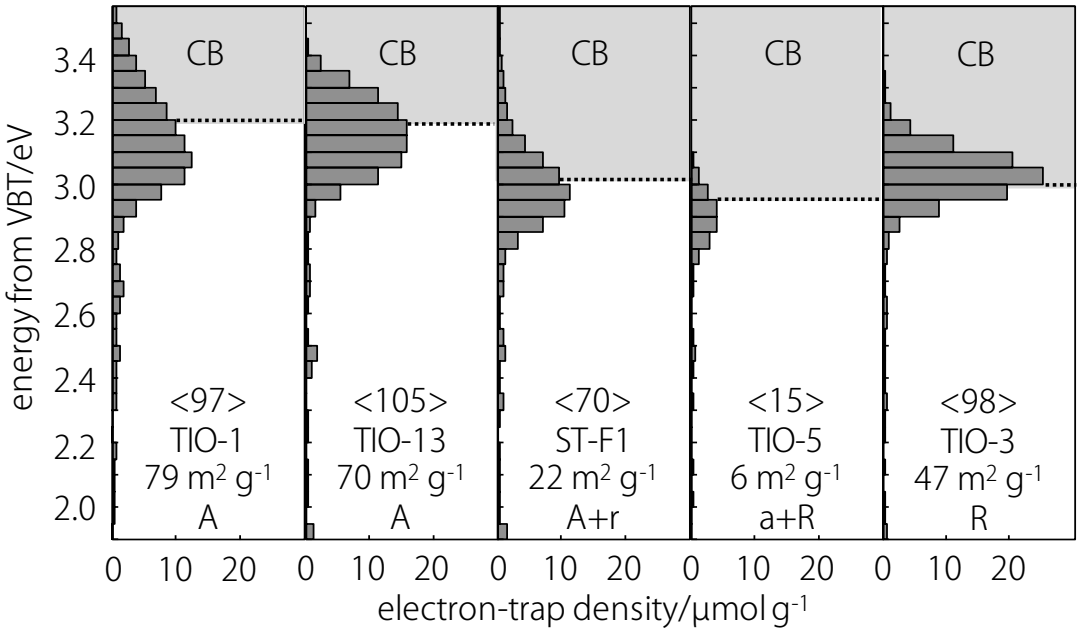

Fig. 3-1 Representative ERDT/CBB patterns for titania powders.

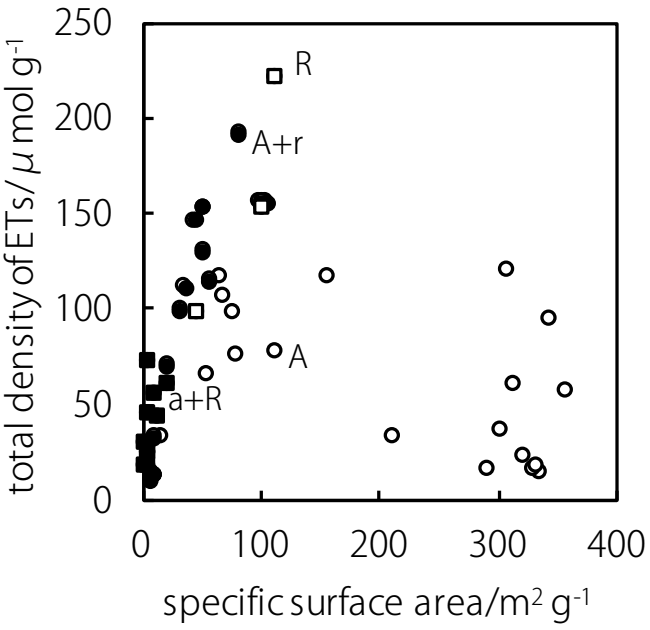

Fig. 3-2 Relation between specific surface area and total density of electron traps. Open circles, closed circles, closed squires, and open circles show anatase (A), mainly anatase (A+r), mainly rutile (a+R), and rutile (R) titania powders.

Fig. 3-2. Even though trend was different depending on crystalline phase, total density of electron traps tends to increase with increase in SSA especially below 120 $m^2 g^{-1}$. For anatase with high SSA, low values of total density of electron traps were due to large amount of surface adsorbed water and surface hydroxyl groups or low light intensity of continuous light might cause no linear relation between SSA and total density of electron traps. Even if SSA is close to 0 $m^2 g^{-1}$, total density of electron traps would not become 0 μmol g^{-1}. It indicates that a part of them also exists in bulk, but most electron traps are located on or close to the surface of the particles. Thus, total density of electron traps can reflect bulk size.

On the other hand, even if compared sample's properties are quite similar in crystalline composition and SSA, bulk structures (see ERDT/CBB patterns of TIO-1 and TIO-13 in **Fig. 3-1**), ERDT patterns seem to be clearly different. Therefore, ERDT may reflect surface electronic properties independently of crystalline composition and SSA. Thus, ERDT is possibly a sole comprehensive macroscopic parameter reflecting surface structure among surface-related parameters reported so far.

If the ERDT pattern reflects structural characteristics of the surface, ERDT pattern is expected to change greatly by surface treatment. If titania powders were treated by hydrogen fluoride, total density of electron traps decreased and those were treated by sodium hydrate after that, total density of electron traps increased and ERDT patterns became similar to untreated samples (**Fig. 3-3**). Therefore, fluoride can fill a

part of electron traps. Thus, electron traps can be decreased by surface treatment such as fluoride treatment.

Therefore, although a parameter reflecting bulk structure or microscopic surface structure has been conventionally evaluated by respective methods, ERDT/CBB patterns include both surface and bulk structures and metal-oxide powders can be identified without measuring crystalline composition and SSA.

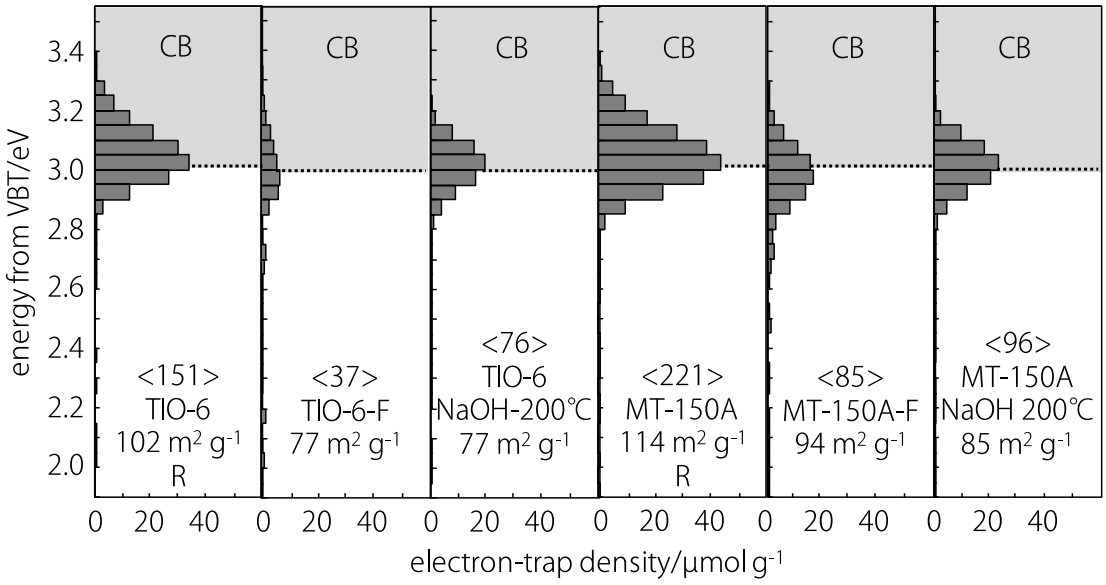

Fig. 3-3 ERDT/CBB patterns for titania powders with fluoride treatment.

3.3.2 Reproducibility Test and Calculation Method for Degree of Coincidence

To identify metal-oxide powders by ERDT/CBB patterns, reproducibility test of RDB-PAS and PAS measurements was conducted by using FP-6 taken from almost the same and close position in the bottle. The reason why the sample was taken from almost the same and close position was that ERDT/CBB patterns cannot be repeated since RDB-PAS is a breakdown measurement and there are no samples with constant composition. The results of three independent measurements are shown in **Fig. 3-4** (the three patterns from left side shown as same1, same2, and same3). All ERDT/CBB patterns for FP-6 seemed to be quite similar. It is very difficult to compare those patterns by only showing values of CBB and total density of electron traps, and bar graphs, thereby ERDT/CBB patterns were quantitatively evaluated by calculating each degree of coincidence for ERDT pattern (f) expressed as energy function from valence-band top (VBT) as ζ(a), total density of electron traps (D) obtained by integral of function f with energy (E) as ζ(b), and CBB energy (E_{CBB}) as ζ(c). For each degree of coincidence, following **eq. 3-1** to

eq. 3-3 were used. Here, $f(1)$ and $f(2)$ were determined by given two ERDT patterns to be $\int f(1)\,dE < \int f(2)dE$. Accompanied by determined $f(1)$ and $f(2)$, $D(1)$ ($=\int f(1)\,dE$) and $D(2)$ ($=\int f(2)dE$) were also defined. When ζ(a) becomes minus value, ζ(a) is regarded as 0.0001. Also $E_{CBB}(1)$ and $E_{CBB}(2)$ were determined to be $E_{CBB}(1) < E_{CBB}(2)$ independently of relationship between magnitude of f and D. In addition, α in **eq. 3-1** is determined using the least squares method so as to minimize $\left(f(1) - \alpha f(2)\right)^2$, thereby α is defined as $(\int f(1)f(2)dE / \int f(2)^2 dE)$.

$$\zeta(a) = 1 - \int |f(1) - \alpha f(2)|dE / \int f(1)dE \qquad \textbf{(eq. 3-1)}$$

$$\zeta(b) = D(1)/D(2) \qquad \textbf{(eq. 3-2)}$$

$$\zeta(c) = E_{CBB}(1)/E_{CBB}(2) \qquad \textbf{(eq. 3-3)}$$

Calculated values are shown in **Table 3-1**. By calculating standard deviation using ζ(a), ζ(b), and ζ(c) in **Table 3-1**, it is revealed that measurement deviation is the largest for ζ(b). Given the dependence on the sample conditions including packed amount and surface flatness for intensity of PA signal, total density of electron traps is predisposed to have relatively large error accompanied by fluctuation of PA signal. On the other hand, standard deviation of ζ(c) is the smallest. Thus, total degree of coincidence (ζ) is calculated by multiplying each degree of coincidence with weighting based on magnitude of standard deviation for descriptive purposes (**eq. 3-4**).

$$\zeta = \zeta(a) \times \zeta(b)^{\frac{1}{2}} \times \zeta(c)^2 \qquad \textbf{(eq. 3-4)}$$

Powders taken from close positions in the same bottle gave $\zeta > 0.89$ in three independent measurements. Thus, practically speaking, identicalness of samples can be concluded

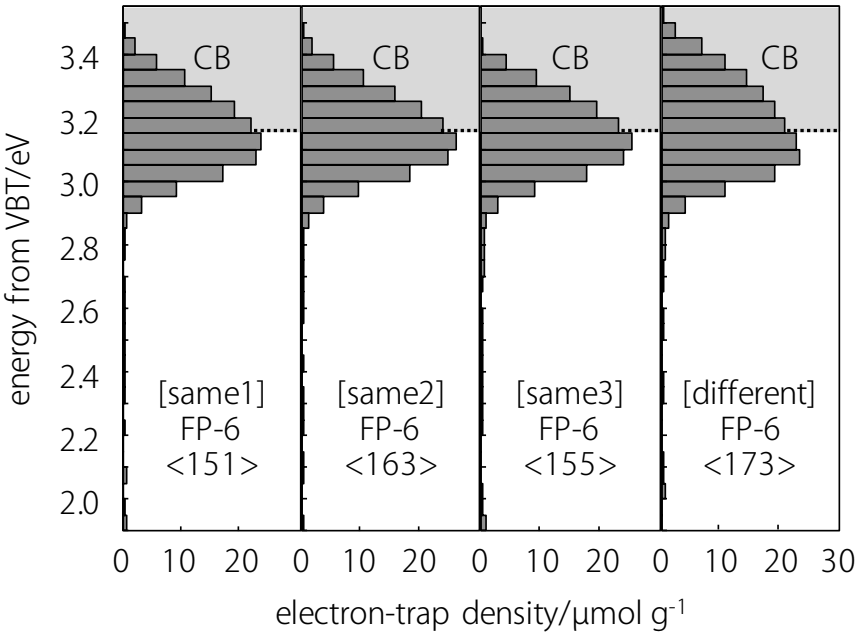

Fig. 3-4 Reproducibility test for ERDT/CBB measurements using FP-6 taken from a same container.

when ζ is equal to 0.9 or higher, however ζ shows less than 0.75 when a sample was taken from different position (shown as different). The lower ζ was attributable to lower ζ(a) compared to higher ζ(b) and ζ(c). Thus, surface structure of metal-oxide powders may have large difference (**Table 3-2**). These results indicate that metal-oxide powders have some difference in their surface/bulk properties even if they manufactured using the same regulated or fixed procedure, in other words, they may be heterogeneous in composition. Although this has been expected, this is the first example showing experimental evidence for such heterogeneity of metal-oxide powders. Therefore, metal-oxide powders can be identified by using ERDT/CBB pattern as a fingerprint like NMR patterns for organic molecules.

Table 3-2 Degrees of coincidence for ERDT/CBB patterns of a titania sample (FP-6).

pair	ζ(a)	ζ(b)	ζ(c)	ζ
same1/same2	0.927	0.929	0.999	0.891
same1/same3	0.930	0.949	0.998	0.902
same2/same3	0.905	0.978	0.999	0.893
same1/different	0.792	0.875	0.999	0.739
same2/different	0.772	0.942	0.998	0.746
same3/different	0.747	0.894	1.00	0.707

3.3.3 Degree of Coincidence among Titania Powders

Values of ζ for two pairs of titania powders which are different names even if manufacturing methods are the same were calculated (shown in addendum). Values of ζ for titania powders are summarized in *addendum*. Many titania pairs show ζ values less than 0.5. It seems to be natural since different samples are compared. However, there are titania pairs having $\zeta > 0.6$ suggesting similarities of structural properties of both surface and bulk. Top 29 ranked high ζ larger than 0.6 pairs of those titania samples are shown in **Table 3-3**.

Table 3-3 High-ζ (> 0.6) pairs of titania powders.

rank	sample pair		ζ [a]	ζ(a)[b]	ζ(b)[c]	ζ(c)[d]	ζ_{pc}(ave)[e]
1	ST-F3	P25	0.837	0.861	0.969	0.994	0.911
2	TIO-11	VP-P90	0.810	0.818	0.998	0.996	0.823
3	TIO-4	(Wako)	0.788	0.863	0.941	0.970	0.901
4	TIO-15	ST-F3	0.779	0.823	0.925	0.992	0.745
5	ST-F10	HT-2301	0.767	0.799	0.925	0.999	0.662
6	ST-F2	ST-F3	0.761	0.808	0.892	0.998	0.894
7	TIO-4	P25	0.760	0.810	0.939	0.999	0.884
8	TIO-4	TIO-15	0.757	0.792	0.924	0.998	0.887
9	TIO-8	ST-01	0.751	0.851	0.885	0.996	0.839
10	TIO-8	TIO-14	0.749	0.778	0.952	0.994	0.929
11	TIO-4	ST-F2	0.748	0.870	0.762	0.992	0.675
12	TIO-15	P25	0.744	0.764	0.955	0.998	0.796
13	ST-F2	P25	0.732	0.800	0.865	0.992	0.843
14	TIO-4	ST-F3	0.727	0.796	0.855	0.994	0.760
15	(Wako)	P25	0.723	0.844	0.884	0.969	0.864
16	TIO-15	ST-F2	0.713	0.801	0.825	0.990	0.667
17	TIO-14	ST-01	0.710	0.795	0.823	0.992	0.964
18	TIO-6	MT-150A	0.705	0.856	0.828	0.995	0.793
19	ST-F3	(Wako)	0.697	0.806	0.757	0.997	0.805
20	TIO-13	FP-6	0.684	0.847	0.827	0.976	0.748
21	ST-F2	(Wako)	0.680	0.835	0.675	0.996	0.729
22	TIO-15	(Wako)	0.674	0.753	0.818	0.994	0.799
23	ST-F1	ST-F2	0.666	0.799	0.711	0.994	0.811
24	ST-F4	VP-P90	0.657	0.710	0.980	0.967	0.740
25	ST-F5	VP-P90	0.638	0.708	0.814	0.999	0.811
26	TIO-11	FP-6	0.615	0.620	0.998	0.994	0.697
27	ST-F4	(Wako)	0.608	0.624	0.958	0.998	0.775
28	TIO-13	ST-157	0.603	0.724	0.705	0.996	0.278
29	ST-F4	P25	0.600	0.697	0.748	0.998	0.755

[a]Overall degree of coincidence. [b]Degree of coincidence of ERDT patterns. [c]Degree of coincidence of total density of electron traps. [d]Degree of coincidence of CBB energy. [e]Average degree of coincidence of photocatalytic activities in three photocatalytic reactions.

Here, TIO-4, TIO-8, TIO-11 are known to be P25, ST-01, and FP-6, respectively. Among those 12 pairs, only pairs of TIO-4/P25, TIO-8/ST-01, and TIO-11/FP-6 show higher values of ζ than those of the others. These data suggest that metal-oxide powders manufactured by same method give similar surface and bulk structures. However, either values of ζ in **Table 3-2** show lower than above mentioned those of ζ for FP-6 taken from the close position in the same bottle (ζ > 0.89). Even for a sample taken from the same bottle that means same number of lot, but taken from different position, it is also clear that ERDT/CBB patterns differ, giving ζ = ca. 0.7 in **Fig. 3-4**. Taking a look at **Table 3-2**, it is revealed that ζ(a) is lower than ζ(b) and ζ(c) and thereby even a powder sample

in the same bottle has a different surface property. Those trends that surface property has large difference are the same for each degree of coincidence for TIO-4/P25, TIO-8/ST-01, and TIO-11/FP-6 pairs. Above results suggests that even if titania powders have been manufactured at the same time with the same code name or by a certain routine with different lot number, their surface and bulk structures differ somewhat. Thus, heterogeneity of metal-oxide powders has been quantitatively demonstrated by calculating ζ. It is impossible to obtain these results by bulk structural properties such as conventionally evaluated crystalline composition, specific surface area, and particle size. However, taking a look at ζ values of TIO-4/P25, TIO-8/ST-01, and TIO-11/FP-6 pairs, it has been unveiled that samples that are known to be the same does not always show the highest ζ. For example, the highest ζ given by ST-F3/P25 pair. Also, TIO-12 and TIO-13 are known to be AMT-100 and AMT-600, however, ζ = 0.510 and 0.511, respectively, in other words, there are clearly difference in surface and bulk structures. Those evaluations cannot be achieved by judging only crystalline composition and specific surface area. Thus, it is suggested that an ERDT/CBB pattern reflecting surface and bulk structure, respectively, can be a fingerprint of metal-oxide powders for identification and characterization. In this way, metal-oxide powders that were said to be the same are actually different and cannot be said to be the same even if the labels are the same. This powder evaluation cannot be achieved except by this method. As above mentioned, it is basic to take energy position standard as VBT in ERDT measurement by RDB-PAS, therefore it is difficult to compare among samples with different VBT. However, there is no problem for using ERDT/CBB patterns to identify metal-oxide powders. If titania powders with high specific surface area were calcined at 393 K for 1 hour in vacuum condition or exposed to UV light, electron-trap density increased and ERDT became broad (**Fig. 3-5**). Surface adsorbed water or hydroxyl group, or organic compounds may be a partly removed by those treatments. In this sense, ERDT pattern may be affected by surface treatment because of its reflected surface structure. Thus, ERDT analysis can be useful to compare slight difference on surface change triggered by surface treatment. Identification using ERDT/CBB pattern is useful for not only titania powders but also other metal-oxide powders such as WO_3 and CeO_2 powders (**Fig. 2-16)**. Furthermore, ERDT patterns for niobium(V) oxide powders that

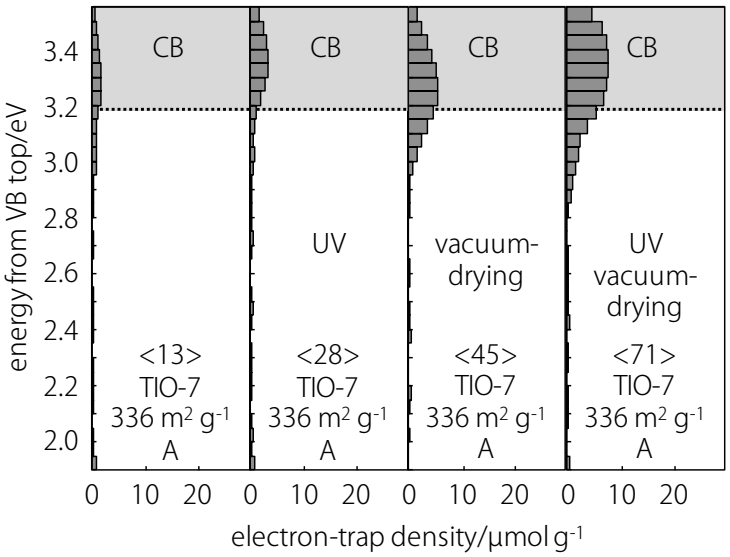

Fig. 3-5 Effect of pre-treatment for ERDT/CBB patterns.

contains only non-crystal component and zirconium(IV) oxide powders that have band gap lager than 3.55 eV could be observed. Although RDB-PAS measurement has been done for only metal oxides, ERDT/CBB-pattern analysis of metal-oxide powders can be applied broadly.

Metal-oxide powders have various applications such as catalysts, photocatalysts, sensors, and luminescence materials. These functionalities are governed not only by the bulk structure of the powder but also by the surface structure. Thus, it is expected that functionality can be predicted by ERDT/CBB pattern reflecting the surface structure, bulk size, and bulk composition. Titania is a metal oxide which is most widely used for fundamental research and applied research as a photocatalyst. If

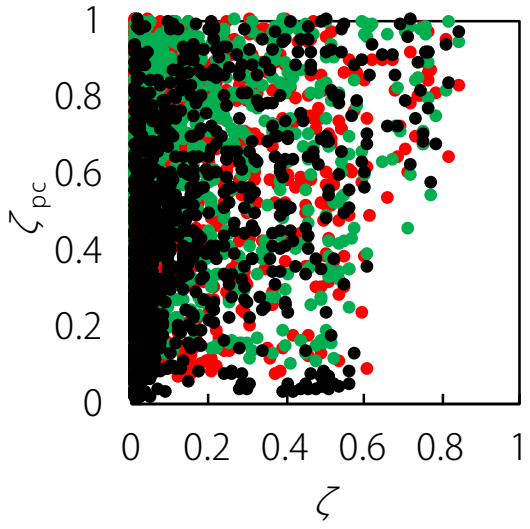

Fig. 3-6 Relation between ζ and ζ_{pc}.

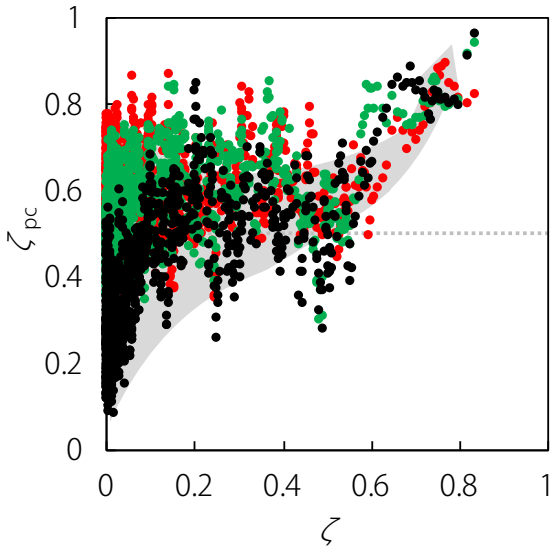

Fig. 3-7 Relation between ζ and ζ_{pc} replotted with non-weighted seven-point moving average.

the same samples are used for photocatalytic activity test, the activities should be similar values. For each combination of titanium oxide samples, degree of coincidence for photocatalytic activity ζ_{pc} (the ratio of low activity to high activity) in the three photocatalytic reaction systems, (1) dehydrogenation reaction of methanol under an argon atmosphere using a sample carrying platinum ($CH_3OH \rightarrow HCHO + H_2$), (2) oxidative decomposition reaction of acetic acid under air atmosphere ($CH_3COOH + 2O_2 \rightarrow 2CO_2 + 2H_2O$), and (3) the oxygen production reaction from the silver fluoride aqueous solution under argon atmosphere ($4Ag^+ + 2H_2O \rightarrow 4Ag + O_2 + 4H^+$) were calculated and shown in **Table 3-1**. If the values of ζ are high, values of ζ_{pc} also became higher values. Then, values of ζ_{pc} were plotted as a function of the degree of agreement ζ in **Fig. 3-6**. Scattering of data in the ζ range lower than ca. 0.6 in **Fig. 3-6** seems reasonable since those low-ζ sample pairs are different in their structures and thereby the ζ_{pc} values might be accidentally low or high. However, it is noticeable that low ζ_{pc} was not observed at $\zeta > 0.7$, indicating that sample pairs with similar bulk/surface structures showed similar photocatalytic activities. In the case of a combination of titanium oxide having high values of ζ, the values of ζ_{pc} were similar in **Table 3-2**. To further see the statistical trend, values of ζ and ζ_{pc} were replotted with noon-weighted seven-point moving average again in **Fig. 3-7**. It was shown that values of ζ_{pc} was increased almost linearly with values of ζ at > 0.6. In the lower ζ range, i.e., for the pairs of titania powders with different structures, values of ζ_{pc} can be high or low accidentally, while in the higher ζ range, a pair of titania powders with similar ERDT/CBB patterns may have high values of ζ_{pc}. This sounds consequent or no mystery, however it should be noted that each of

those titania samples was adequately identified by at least ERDT/CBB analysis with bulk/surface structures which determines the overall photocatalytic activity. Thus, it was shown that judgement of whether it is the same or not was going well.

The standard deviation (SD) of moving seven points as a function of ζ is shown in **Fig. 3-8**. As expected, SD values were also scattered in the low ζ range and decreased with ζ at > 0.6 to reach ca. 0.1 at $\zeta = 0.8$ in all three photocatalytic reaction systems, being consistent with the trend in ζ_{pc}. Only the O_2 system showed as SD maximum at ζ_{pc} ca. 0.5. A possible explanation of this unexpected behavior is that the photocatalytic activity for this system is regulated by a parameter that is not reflected in ERDT/CBB patterns. In other words, the O_2-system activity depends on a certain property not involved in ordinary bulk and/or structures. However, as shown in *3.3.4*, the top rankers of titania samples for the O_2 system exhibited characteristic ERDT/CBB patterns even if an important parameter for the activity is not reflected in the patterns.

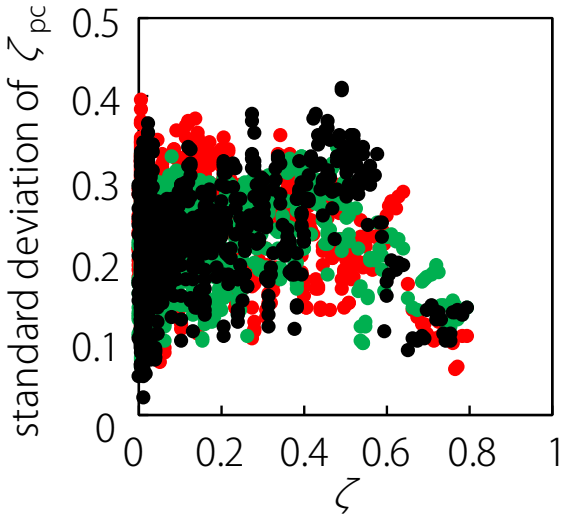

Fig. 3-8 Relation between ζ and standard deviation of ζ_{pc}.

3.3.4 Relation between Electron-trap Density and Photocatalytic Activity

Then, ERDT/CBB patterns were lined up based on the order of high photocatalytic activity based for each photocatalytic reaction as shown in **Fig. 3-9**. Although platinum loading may affect largely on photocatalytic activity to make observation difficult in ERDT/CBB patterns, for carbon dioxide and oxygen evolutions, similar ERDT/CBB patterns were observed at top ranked activities. It can be clearly seen that titania samples with high levels of activity exhibited similar ERDT/CBB patterns; patterns with high-density electron traps with a peak at ca 3.0 eV and low-density electron traps with a peak at ca. 2.9 eV were preferable for the CO_2 and O_2 systems,

respectively. Note that the similarities of neighboring ERDT/CBB patterns are not related to ζ_{pc}, since ζ_{pc} can be accidentally high if the neighboring pair exhibits low ζ, in other words, the observed pattern similarities are not a natural consequence. There seems to be proper structural properties for each reaction because of similar patterns observed in high-ranked photocatalytic activities, and ERDT/CBB patterns can reflect the effective structures. Thus, ERDT/CBB patterns can be a structural index not only for metal-oxide powders but also for each photocatalytic reaction.

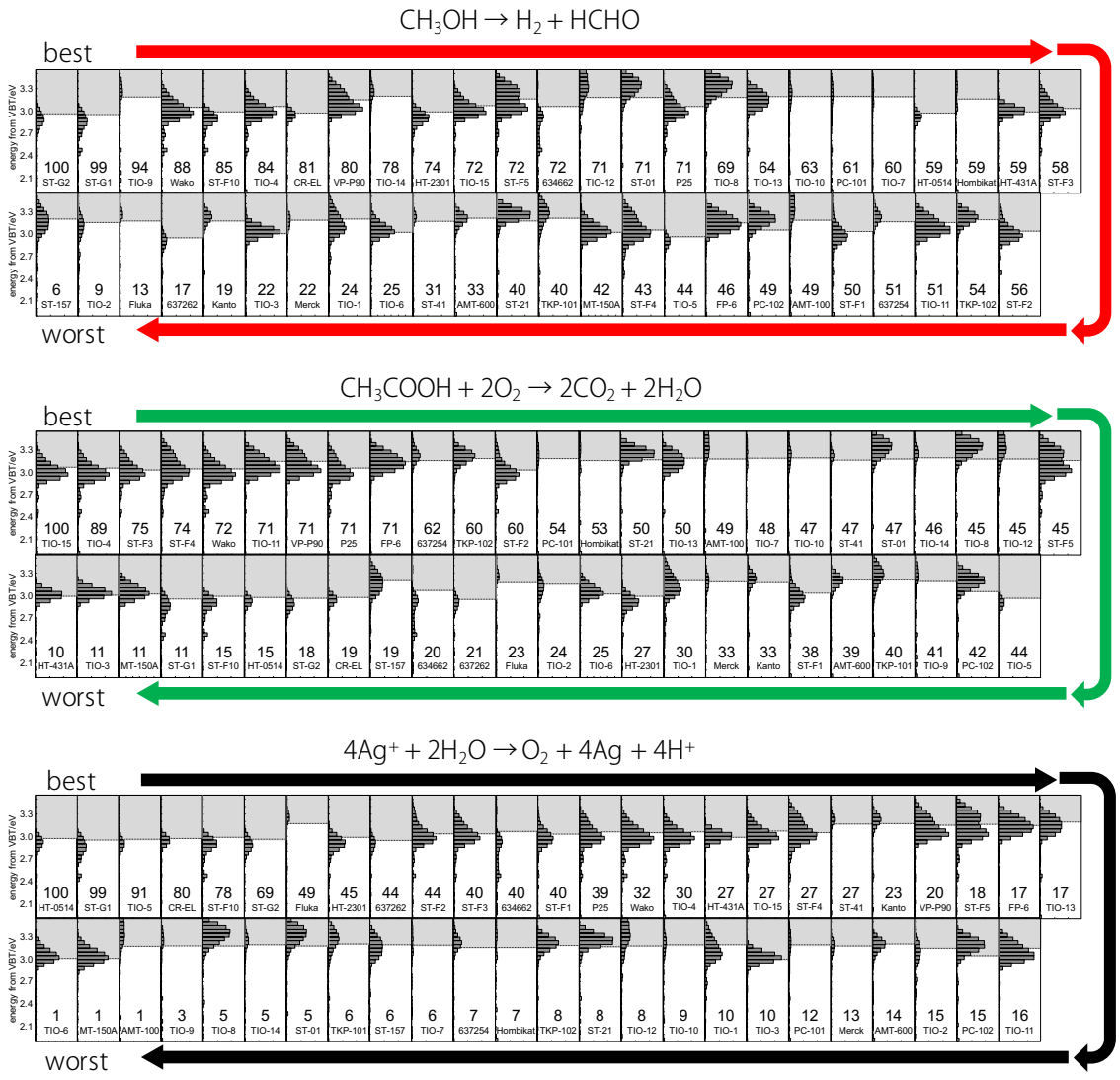

Fig. 3-9 ERDT/CBB patterns for titania powders arranged in descending order of photocatalytic activity.

3.4 Conclusions

In this chapter, it is suggested that an ERDT/CBB pattern can be a fingerprint of metal-oxide powders for identification and characterization. Although CBB and total density of electron traps tended to depend on crystal type and SSA of titania powders,

respectively, ERDT patterns were clearly different irrespective of crystal type and SSA. Thus, although CBB and total density of electron traps can reflect bulk composition and bulk size, ERDT may reflect surface electronic properties and can be possibly a sole comprehensive macroscopic parameter reflecting surface structure among surface-related parameters reported so far. Therefore, ERDT/CBB pattern may contain both surface and bulk structures that are elements required for identification. To evaluate ERDT/CBB patterns, reproducibility test was conducted by using a titania powder taken from almost the same position in the same container. Reproducibility was measured by calculating degree of coincidence in ERDT pattern matching (ζ(a)), total density of electron traps (ζ(b)), and CBB positions (ζ(c)), respectively. Based on standard deviation, degrees of coincidence (ζ) was calculated by multiplying by ζ(a), by $\zeta(b)^{1/2}$, and by $\zeta(c)^2$. Samples taken from almost the same position in the same container yielded $\zeta > 0.88$, however taking from another position even in the same container gave $\zeta < 0.75$. It is suggested that powder sample is homogeneous, and ERDT/CBB pattern can be a fingerprint for identifying and characterizing the metal-oxide powders. Actually, ζ for TIO-4/P25, TIO-11/FP-6, and TIO-8/ST-01, known as same samples respectively, were relatively high compared to a given pairs of titania powders and $\zeta <$ 0.8 that was lower than ζ acquired in reproducibility test. This identicalness was guaranteed by results that degree of coincidence for photocatalytic activities (ζ_{pc}) became similar if ζ was higher. Although plots of ζ and ζ_{pc} were scattered, ζ_{pc} showed more than 0.5 at $\zeta > 0.7$. If those values were replotted by non-weighted seven-point average, increase of ζ_{pc} with increase in ζ was observed regardless of H_2, CO_2, and O_2 evolution reaction system. Those ERDT/CBB patterns can be also functional fingerprint. When ERDT/CBB patterns were ranked from higher photocatalytic activities for each heterogeneous photocatalysis, top ranked ERDT/CBB patterns were similar. Thus, performance of electron transfer reaction using metal-oxide powders with electron traps can be predicted by measuring ERDT/CBB patterns. Therefore, a new concept of using ERDT/CBB patterns to identify and characterize metal-oxide powders were established.

3.5 References

Dunkel 2007 Dunkel, R.; Wu, X., Identification of organic molecules from a structure database using proton and carbon NMR analysis results, *J. Magn. Reson.*, **188**, 97–110 (2007).

Ikeda 2003 Ikeda, S.; Sugiyama, N.; Murakami, S.; Kominami, H.; Kera, Y.; Noguchi, H.; Uosaki, K.; Torimoto, T.; Ohtani, B., Quantitative analysis of defective sites in titanium(IV) oxide photocatalyst powders, *Phys. Chem. Chem. Phys.*, **5**, 778–783 (2003).

Kölle 1985 Kölle, U.; Moser, J.; Grätzel, M., Dynamics of Interfacial Charge-Transfer Reactions in Semiconductor Dispersions. Reduction of Cobaltoceniumdicarboxylate in Colloidal TiO_2, *Inorg. Chem.*, **24**, 2253–2258 (1985).

Minoura 1985 Minoura, H.; Nasu, M.; Takahashi, Y., Comparative Studies of Photoelectrochemical Behaviours of Rutile and Anatase Electrodes Prepared by OMCVD Technique, *Ber. Bunsenges. Phys. Chem.*, **89**, 1064–1069 (1985).

Tang 1993 Tang, H.; Berger, H.; Schmid, P. E.; Lévy, F.; Burri, G., Photoluminescence in TiO_2 anatase single crystals, *Solid State Commun.*, **87**, 847–850 (1993).

Toyoda 2003 Toyoda, T.; Tsuboya I., Apparent band-gap energies of mixed TiO_2 nanocrystals with anatase and rutile structures characterized with photoacoustic spectroscopy, *Rev. Sci. Instrum.*, **74**, 782–784 (2003).

Chapter 4

Evaluation of Apparent Valence-band Top Position by Simulation

4.1 Introduction

4.1.1 Band Structure of Metal Oxides

Bulk composition of titania has been classified as two mainly crystalline structures, anatase and rutile. It is well known that the bandgaps of anatase and rutile are ca. 3.2 eV [Tang 1993] and 3.0 eV [Minoura 1985], respectively. Quoted from a well-known report of Scaife [Scaife 1980], it has been said that energy of valence-band top (VBT) has no connection with the kinds of metals since the valence band consists of O 2p orbital and is almost constant at 2.94 V vs SHE based on relations between flat band potential and bandgaps. Thereby, CBB of anatase has been believed to be higher than that of rutile due to large bandgap of anatase. This is simplified estimation and there were exceptions of the relations, but estimation of CBB position has been done by electrochemical experiments to determine flat-band potential of anatase and rutile by Mott-Schottky plots [Kavan 1996]. Quoted from the report, the flat-band potential for anatase (101) and rutile (001) were -0.16 and +0.04 V vs SHE at pH = 0, respectively. This is consistent with estimation of CBB position by simplified calculation. However, since energy bands become wider when interaction among the atomic orbitals in the crystal is promoted and the density of rutile is higher than that of anatase, reconsideration of intrinsic band alignment within anatase and rutile has been proposed [Nosaka 2016]. It has been also reported that the flat-band potential for titania surfaces is almost equal to -0.06 V vs SHE at pH = 0 regardless of crystalline composition as long as the surface is not atomically flat [Tsuji 2014]. Strictly speaking, it is needed to measure VBT of respective metal-oxide powders.

4.1.2 Valence-band Top Position by Experimental and Theoretic Calculation

Recently, a new and different band alignment that VBT of rutile is lower than that of anatase has been proposed by X-ray photoelectron spectroscopy (XPS) and theoretical calculation [Scanlon 2013]. However, in XPS measurement, solid/solid interface can be involved [Zhang 2017], respective VBT energies of anatase and rutile cannot be measured, and a measurement should be conducted in a vacuum. Given above problems of XPS, photoelectron yield spectroscopy (PYS) can be a candidate for VBT

evaluation. In PYS, under monochromatic light irradiation, the amounts of photoelectrons emitted from a sample as a current and of photons of excited monochromatic light are measured, and ionization energy (ionization potential) from the threshold at which the yield changes is detected. Use of PYS enables ionization energy measurement under air, and ionization energy measurement by PYS has been applied to titania samples including powders and single crystal [Toyoda 2015]. However, although VBT estimated by PYS corresponds to the top of density of states (DOS), direct excitation of electrons from valence band to electron traps may occur from high DOS that is lower than VBT in RDB-PAS measurement since photoabsorption coefficient for direct excitation of electrons from valence band to electron traps. Energy difference of ERDT between RDB-PAS and photochemical method, that also enables ERDT measurement of metal-oxide powders by using pH-dependent electron transfer from electron traps to methylviologen with low energy resolution and narrow energy range compared to RDB-PAS, may be caused by the energy shift of ERDT. In other words, not only measurement of VBT by PYS but also of apparent VBT corresponding to high DOS that enables direct excitation of electrons to electron traps, are needed. In this study, apparent VBT positions of anatase and rutile powders were evaluated by ERDT/CBB pattern analysis.

4.2 Experimental

4.2.1 Materials

Titania powders from commercial sources and reference catalysts supplied by the Catalysis Society of Japan (JRC-TIO series) were used and the properties are shown in **Table 4-1**. A mixture of titania powders was given by grounding in agate motor for 10 minutes.

4.2.2 Reversed Double-beam Photoacoustic Spectroscopic Measurement

Experimental details are shown in *2.2.2*.

4.2.3 Photoelectron Yield Spectroscopic Measurement

Ionization energy of titania powders were measured by PYS in air with BIP-KV201 (Bunkoukeiki). Light of each wavelength was irradiated while applying voltage so that electrons are easily emitted to the sample, and the number of emitted electrons was calculated from the current. Ionization energy was estimated from threshold value of photoelectron yield spectrum that x-axis was photon energy and y-axis was one-third power of yield.

4.3 Results and Discussion

4.3.1 Valence-band Top Evaluation from Ionization Energy

The PY spectra of titania powders (TIO-2 and CR-EL) as a function of photon energy are shown in **Fig. 4-1**. Ionization energy (I_p) regarded as VBT position was acquired on the basis of the intersection of the tangent to the spectra with the baseline. Measured I_p values for TIO-2 and CR-EL were 7.53 eV and 7.28 eV, respectively, and I_p values for the others were shown in **Table 4-1**. As shown in **Table 4-1**, even if chemical formula is the same described as TiO_2, I_p values of titania powders were unveiled to be totally different. It seemed that I_p of rutile tended to be lower than that of anatase except for some powders, meaning VBT position of rutile is located higher than that of anatase. Values of I_p for anatase titania powders were similar to reported value of I_p for nanoparticulate anatase titania electrodes, 7.52 eV [Toyoda 2015]. Although these values of I_p for anatase titania powders were different from another reported value of an anatase titania powder, 7.25 eV [Fujisawa 2017], the value was calculated at range of photon energy less than 7.5 eV. From the view of the larger increase in yield of y-axis over 8 eV of photon energy, I_p which was obtained from PYS measurement with low energy region that photon energy is less than ca. 8 eV can be data with low reliability.

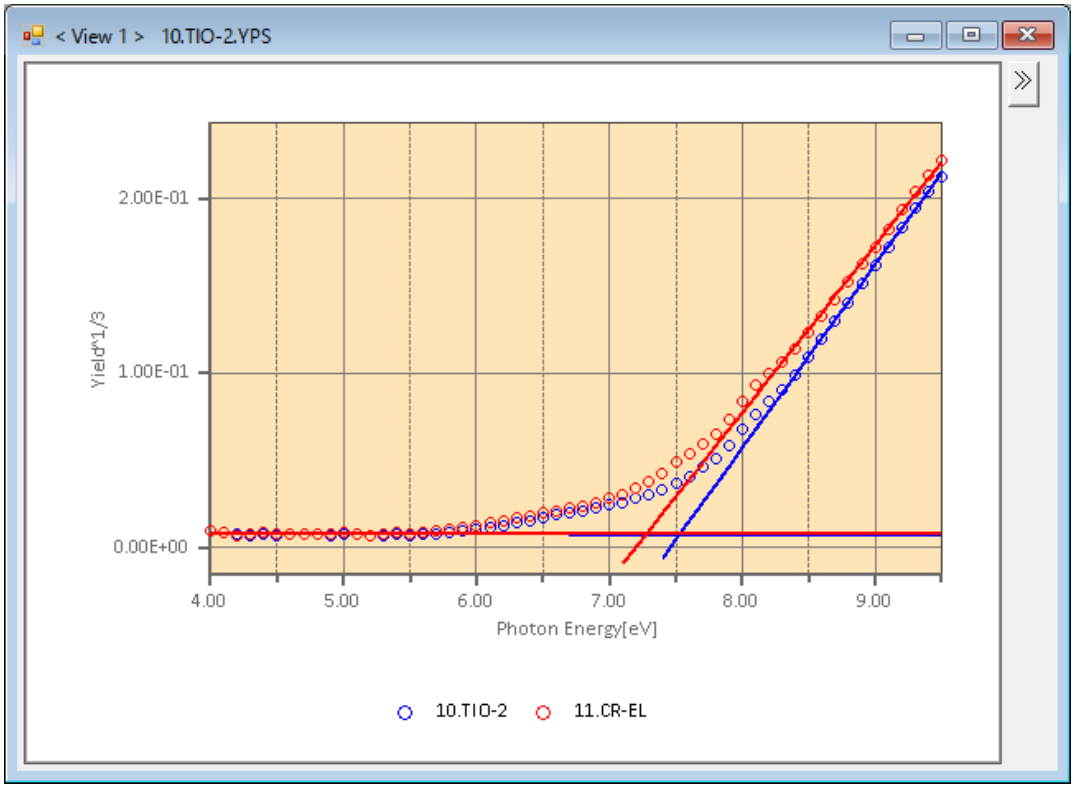

Fig. 4-1 Photoelectron yield (PY) spectra for TIO-2 and CR-EL.

Table 4-1 Structural properties, ionization energy difference, and apparent VBT energy difference of titania powders.

code	composition (%)		E_{CBB}/eV	I_p[a]/eV	ΔI_p[b]/eV	ΔE[c]/eV[b]	difference[d] /eV
	anatase	rutile					
TIO-1	91	0	3.20	7.88	-0.60	-0.19	0.41
TIO-2	91	0	3.14	7.53	-0.25	-0.22	0.03
TIO-3	0	90	2.98	7.19	0.09	-0.02	0.11
TIO-11	82	9	3.14	7.47	-0.19	-0.11	0.08
TIO-13	93	0	3.19	7.38	-0.10	-0.18	0.08
CR-EL	1	94	2.97	7.28	0	0	0
ST-21	87	0	3.17	7.35	-0.07	-0.26	0.19
(Kanto)	97	1	3.16	7.41	-0.13	-0.23	0.10
ST-G1	0	97	2.97	7.31	-0.03	0.04	0.07
FP-6	83	8	3.15	7.36	-0.08	-0.16	0.08
ST-F1	78	20	3.02	7.42	-0.14	-0.02	0.12
ST-F5	84	3	3.16	7.49	-0.21	-0.14	0.07
AMT-600	93	0	3.18	7.26	0.02	-0.19	0.21
HT-0514	1	94	2.97	7.39	-0.11	0.02	0.13

[a]Ionization energy, [b]energy difference of Ip based on CR-El, [c]energy difference VBT position measured by RDB-PAS based on CR-EL, [d]absolute value of difference between ΔI_p and ΔE.

4.3.2 Energy-resolved Density of Electron Traps for Mixed Samples

Electron traps are located not only within bandgap but also above CBB position regardless of crystalline phase and specific surface area as shown in **Fig. 2-15**. Possible factors are ERDT shift toward high energy direction due to direct excitation from high DOS located lower than the VBT because of fine absorption coefficient for electrons to be excited to electron traps, and difference in structural properties between surface on which electron traps may mainly be located and bulk in which donor levels of n-type semiconductor may exist. Another factor is determination of CBB position for titania powders having both anatase and rutile. Since it is impossible to prescribe CBB positions of anatase and rutile for titania powders having both crystalline phase, experimentally estimated CBB of mixed phase titania will be lower than that of anatase and higher than that of rutile. Thus, it is no wonder that electron traps exist over estimated CBB by PAS in mixed phase titania powders. Well then, titania powders formed by only anatase and by only rutile were mixed to compare with each original

titania powder. As a representative example, ERDT/CBB patterns of anatase-type TIO-2, rutile-type CR-EL, and the 50/50 mixture of TIO-2 and CR-EL (TIO-2+CR-EL) are shown in **Fig. 4-2**. Measured ERDT pattern was totally different from summation of 50/50 mixed ERDT of TIO-2 and CR-EL since photoabsorption of electrons in electron traps located over 3.1 eV could be hardly observed in spite of existence for electron traps until 3.45 eV in TIO-2. By confirming XRD pattern and specific surface area, mixed sample TIO-2+CR-EL contained almost a half ratio of anatase and rutile and had a half of specific surface area of sum amount for that of TIO-2 and CR-EL. Thus, mixed sample could be synthesized a certain homogeneity of both powders. One of the assumption of the result is difference in VBT position of each sample. If VBT of TIO-2 is located lower than that of CR-EL, electron traps originated from TIO-2 in higher energy level can be covered by electron traps of CR-EL that corresponds to energy of continuous light. From the point of I_p, it is consistent with the assumption because I_p of TIO-2 is higher than that of CR-EL. This phenomenon that no observation of ERDT pattern for mixture sample with anatase and rutile at high energy region derived from anatase titania, was observed when another pair of two powder sample was chosen. In this sense, results that VBT positions were different and trends of VBT positions for anatase and rutile, were corresponding to trends reported by XPS and actual data of PYS.

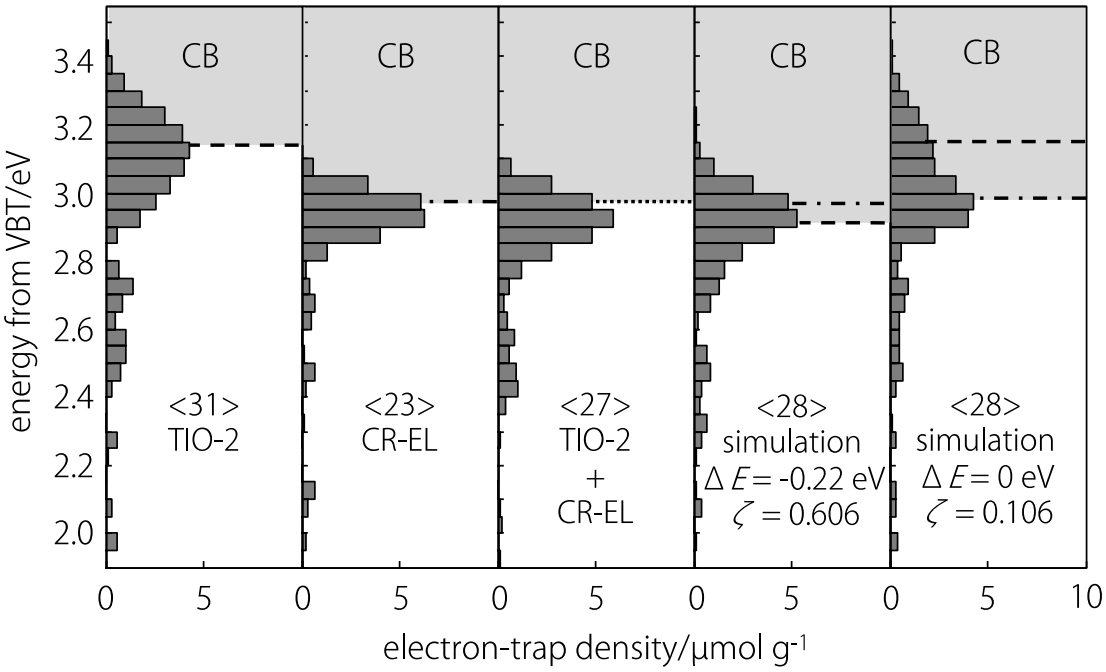

Fig. 4-2 Analysis of ERDT/CBB patterns for actual mixed and simulated samples.

4.3.3 Simulation of Energy-resolved Density of Electron Traps

If energy difference of VBT positions affect ERDT patterns of mixed sample, VBT energy difference can be estimated by obtaining the ERDT shift. In other words, ERDT patterns of mixed samples might consist of mixed ERDT patterns for two samples with different energy level from VBT. Therefore, comparison between actual ERDT pattern for mixed sample and simulated ERDT pattern which is combined by two ERDT patterns to maximize degree of coincidence (ζ) calculated by weighted product of degree of coincidence in (a) ERDT pattern, (b) total density of electron traps, and (c) CBB position ($\zeta = \zeta(a) \times \zeta(b)^{1/2} \times \zeta(c)^2$), can provide VBT energy difference. For example, ERDT/CBB pattern of TIO-2 was shifted toward lower energy side on 0.01 eV basis without shifting ERDT/CBB pattern of CR-EL (**Fig. 4-3**). By mixing those ERDT/CBB patterns at 50/50 ratio, the most similar ERDT pattern with actual ERDT pattern of TIO-2+CR-EL was simulated. From the simulation, 0.22 eV was determined to be energy difference of VBT positions between TIO-2 and CR-EL estimated by ERDT/CBB pattern (**Fig. 4-2**). Therefore, if a given standard sample is chosen, comparison of relative VBT by ERDT simulation can be achieved. As standard sample, CR-EL with low total density of electron traps and narrow distribution range was chosen and simulation was done. If simulation was done by shifting ERDT pattern for a given titania powder toward lower energy side, in other words, VBT position was lower than that of CR-EL, energy difference (ΔE) was shown as positive value. Those values of ΔE is shown in

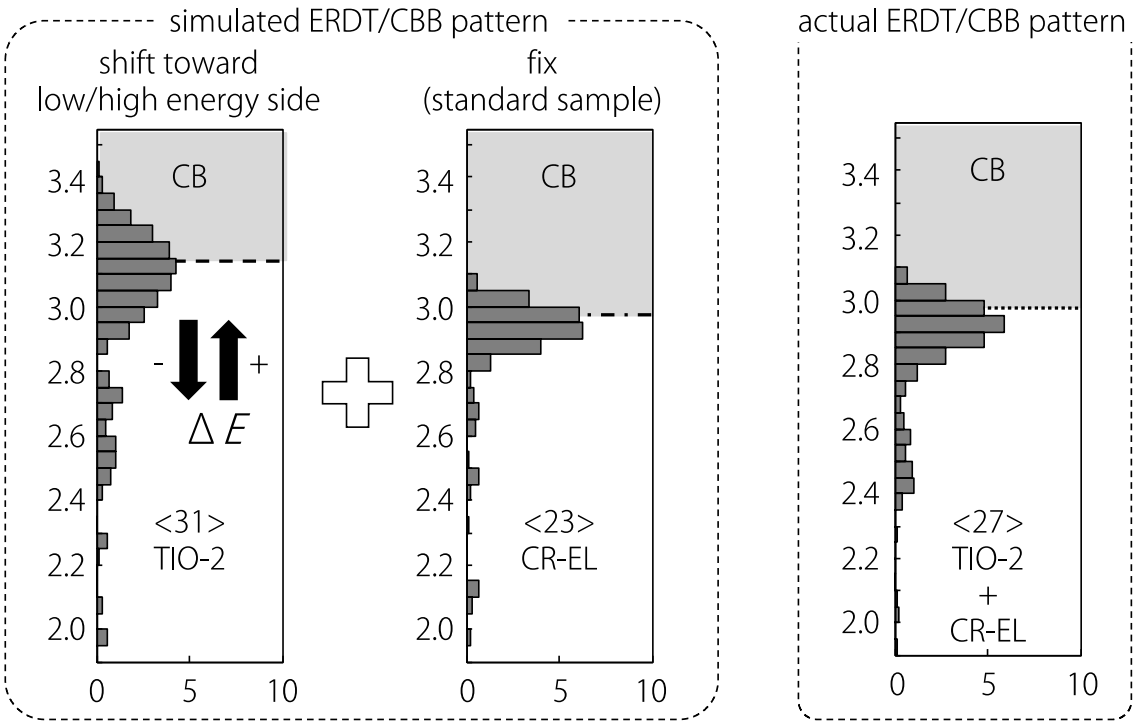

Fig. 4-3 Simulation analysis of ERTD/CBB patterns for VBT evaluation.

Table 4-1. Values of ΔE were small or negative for rutile-type titania powders indicated that possibility of VBT positions for rutile titania powders are higher than those of anatase titania.

4.3.4 Meaning of Energy Difference of Apparent Valence-band Top

As described in *4.3.1* and *4.3.3*, I_p and ΔE have been obtained. To compare results of VBT-position estimation by different methods, difference of I_p (ΔI_p) compared to I_p of CR-EL was also calculated by subtracting I_p of CR-EL from I_p of a given titania. Relations of ΔI_p and ΔE is shown in **Table 4-1** and **Fig. 4-4**. Absolute values of difference between ΔI_p and ΔE are not zero or negligible, in other words, values of ΔI_p and ΔE were clearly different. Therefore, what is measured by PYS and RDB-PAS should be elucidated. As previous report, I_p has been regarded as VBT position. The threshold of photoelectron emission, that is, the minimum energy necessary for electrons to jump out from the solid surface by UV irradiation, may be VBT for n-type oxide semiconductors. As described in *1.2.1*, metal oxides tend to lose oxygen and electrons remain when oxygen molecules are released from the two oxygen ions to create donor levels, but actually no absorption derived from such donor levels was observed for untreated metal-oxide powders by PAS measurement. Although there was a problem in measurement range of photon energy (till 6.2 eV), values of I_p of titanium-niobium oxides calcined in air or under hydrogen reduction have been reported [Ishihara 2015]. In the

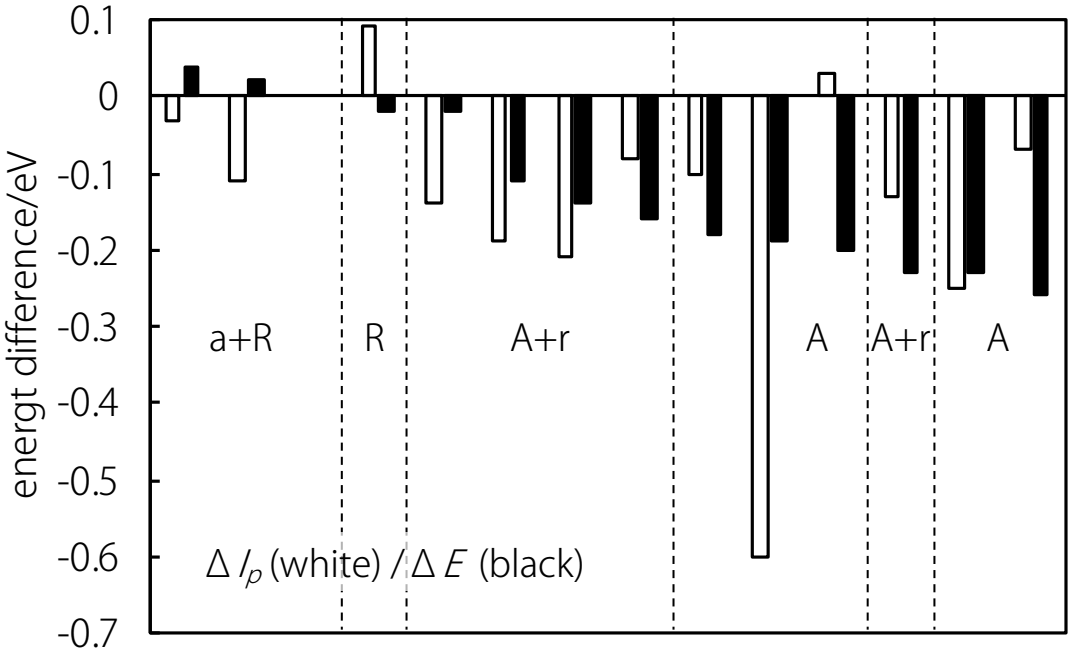

Fig. 4-4 Relation between ΔI_p (white bar) and ΔE (black bar).

report, values of I_p for reductive titanium-niobium oxides (minimum: 5.1 eV) are lower than those for the oxides calcined in air (ca. 5.8 eV) and only values of I_p for reductive titanium-niobium oxides decrease accompanied by increasing temperature. The oxides calcined under reductive condition has donor levels corresponding to trivalent titanium ions and those electrons might jump out by PYS measurement. Therefore, I_p for untreated metal-oxide powders may be derived from actual VBT position corresponding to the highest energy so that DOS become almost 0. On the other hand, as described in Chapter 2, RDB-PAS employs direct excitation from valence band to electron traps, and there may be a possibility that direct excitation occurs not from VBT but high DOS located anodic side compared to VBT. In this sense, apparent VBT from which it is enough for electrons in valence band to be excited directly to electron traps. Difference between ΔI_p and ΔE might arise from different meaning of VBT positions. Among values in **Table 4-1**, absolute values of difference between ΔI_p and ΔE for TIO-2 was relatively low. This means that energy level of direct excitation in valence band may be located close. Two kinds of ERDT patterns of titania powders, TIO-2 and CR-EL, have already measured by photochemical method [Ikeda 2003]. Although ERDT patterns seem to be similar between RDB-PAS and photochemical method, energy difference is observed. Difference of VBT and apparent VBT cannot be contained in photochemical method, thereby ERDT patterns obtained by RDB-PAS were adjusted with energy shift by calculating ζ(a) with ERDT acquired by photochemical method (**Fig. 4-5**). It seems that energy level in valence band where direct excitation occurs by RDB-PAS is 0.07 eV and 0. 10 eV lower than VBT of TIO-2 and CR-EL, respectively. This is consistent with relation of ΔI_p and ΔE. In other words, ΔE may correspond to energy difference of apparent VBT positions that are located lower than VBT and energy levels where direct excitation occur. Thus, although weak points of RDB-PAS are that ERDT patterns may not reflect energy difference from actual VBT and it is impossible to determine absolute CBB or VBT position, combination of photochemical method and PYS and analysis of ERDT/CBB patterns by ERDT/CBB pattern simulation lead to precise characterization of metal-oxide powders.

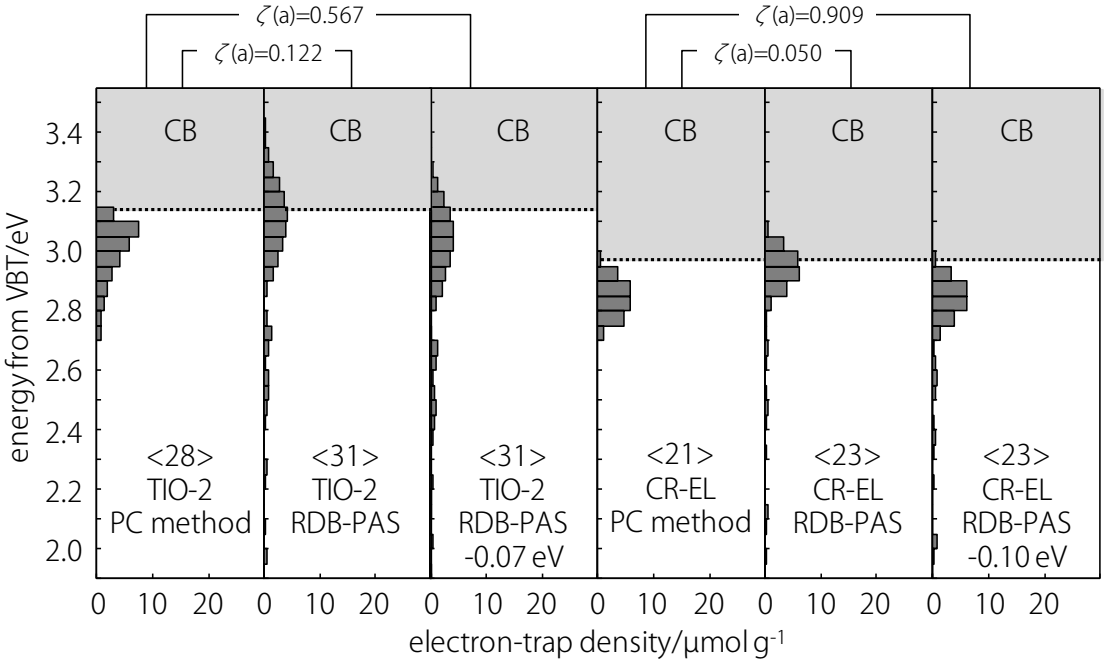

Fig. 4-5 Energy difference between RDB-PAS and photochemical method.

4.4 Conclusions

In this chapter, it was clarified that the apparent VBT corresponding to the high density of states (DOS) excited from valence band to electron traps can be evaluated by ERDT/CBB pattern analysis of RDB-PAS. The ERDT/CBB pattern of samples mixed with anatase and rutile at 50/50 was different from the 50/50 sum of the respective ERDT/CBB patterns. This was attributed to the fact that VBT positions differ considering from the principle of RDB-PAS utilizing direct excitation from valence band to electron traps. In other words, ζ between ERDT/CBB pattern of mixed sample and simulated ERDT/CBB pattern obtained by shifting one side of ERDT/CBB pattern by 0.01 eV in the direction of the energy axis and then mixing it at 50/50 with fixed ERDT/CBB pattern for the other. It is shown that the energy which becomes the maximum corresponds to the difference between VBT of both samples. It can reflect the apparent excitation from VBT as a factor in comparison with the photochemical method in Chapter 2 and the fact that the electron trap is observed on the higher energy side than CBB. Thus, weak point of RDB-PAS that it is impossible to obtain information on excitation energy level of valence band is conquered by ERDT/CBB pattern analysis with mixed sample and simulation.

4. 5 References

Fujisawa 2017 Fujisawa, J-i.; Eda, T.; Hanaya, M., Comparative study of conduction-band and valence-band edges of TiO_2, $SrTiO_3$, and $BaTiO_3$ by ionization potential measurements, **685**, 23–26 (2017).

Ikeda 2003 Ikeda, S.; Sugiyama, N.; Murakami, S.; Kominami, H.; Kera, Y.; Noguchi, H.; Uosaki, K.; Torimoto, T.; Ohtani, B., Quantitative analysis of defective sites in titanium(IV) oxide photocatalyst powders, *Phys. Chem. Chem. Phys.*, **5**, 778–783 (2003).

Ishihara 2015 Ishihara, A.; Tamura, Y.; Chisaka, M.; Ohgi, Y.; Kohno, Y.; Matsuzawa, K.; Mitsushima, S.; Ota, K., Titanium-Niobium Oxides as Non-Noble Metal Cathodes for Polymer Electrolyte Fuel Cells, *Catalysts*, **5**, 1289–1303 (2015).

Kavan 1996 Kavan, L.; Grätzel, M.; Gilbert, S. E.; Klemenz, C.; Scheel, J., Electrochemical and Photoelectrochemical Investigation of Single-Crystal Anatase, *J. Am. Chem. Soc.*, **118**, 6716–6723 (1996).

Minoura 1985 Minoura, H.; Nasu, M.; Takahashi, Y., Comparative Studies of Photoelectrochemical Behaviours of Rutile and Anatase Electrodes Prepared by OMCVD Technique, *Ber. Bunsenges. Phys. Chem.*, **89**, 1064–1069 (1985).

Nosaka 2016 Nosaka, Y.; Nosaka, A. Y., Reconsideratio, of Intrinsic Band Alignments within Anatase and Rutile TiO_2, *J. Phys. Chem. Lett.*, **7**, 431–434 (2016).

Scaife 1980 Scaife, D. E., Oxide Semiconductors in Photoelectrochemical Conversion of Solar Energy, *Solar Energy*, **25**, 41–54 (1980).

Scanlon 2013 Scanlon, D. O.; Dunnill, C. W.; Buckeridge, J.; Shevlin, S. A.; Logsdail, A. J.; Woodley, S. M.; Catlow, C. R. A.; Powell, M. J.; Palgrave, R. G.; Parkin, I. P.; Watson, G. W.; Keal, T. W.; Sherwood, P.; Walsh, A.; Sokol, A. A., Band alignment of rutile and anatase TiO_2, *Nat. Mater.*, **12**, 798–801 (2013).

Tang 1993 Tang, H.; Berger, H.; Schmid, P. E.; Lévy, F.; Burri, G., Photoluminescence in TiO_2 anatase single crystals, *Solid State Commun.*, **87**, 847–850 (1993).

Toyoda 2015 Toyoda, T.; Yindeesuk, W.; Okuno, T.; Akimoto, M.; Kamiyama, K.; Hayase, S.; Shen, Q., Electronic structures of two types of TiO_2 electrodes: inverse opal and nanoparticulate cases, *RSC Adv.*, **5**, 49623–49632 (2015).

Tsuji 2014 Tsuji E.; Fukui, K.; Imanishi, A, Influence of Surface Roughening of Rutile Single-Crystalline TiO_2 on Photocatalytic Activity for Oxygen Photoevolution from Water in Acidic and Alkaline Solutions, *J. Phys. Chem. C*, **118**, 5406–5413 (2014).

Zhang 2017 Zhang, D.; Yang, M.; Gao, H.; Dong, S., Translating XPS Measurement Procedure for Band Alignment into Reliable Ab Initio Calculation Method, *J. Phys. Chem. C*, **121**, 7139–7143 (2017).

Chapter 5

General Conclusions

5.1 Conclusions

Conventional methods for evaluating metal-oxide powders have been limited to analyze bulk structures such as crystalline composition, specific surface area, primary particle size, and secondary particle size. However, measurement of surface structure is needed since metal-oxide powders consist of surface and bulk. Although surface observation of metal-oxide powders by using electron microscope and probe microscope have been conducted, observation with enormous numbers of fields is necessary for evaluation by using such analytical techniques because of the microscopic measurements. In this study, a structural index reflecting surface of metal-oxide powders, energy-resolved density of electron traps (ERDT), has been suggested.

In Chapter 2, reversed double-beam photoacoustic spectroscopy (RDB-PAS) as a new measurement method of ERDT with higher energy resolution and wider energy range compared to a conventional method has been developed. Previously photoabsorption of electrons accumulated in electron traps of titanium(IV) oxide (titania) powders has been measured by PAS under ultraviolet continuous light irradiation, however electrons are accumulated in electron traps at random with such DB-PAS system because of band transition of electrons via conduction band. In this study, monochromatic light that has been used as modulated light is employed as continuous light to fill electron traps from deeper side to shallower side by electrons directly excited from valence band, and photoabsorption of such accumulated electrons is detected by wavelength-fixed modulated light. Comparing ERDT of various samples with those obtained by the conventional method, it was found out that basically good results can be obtained, and measurement time, measurable energy range and energy resolution are excellent in RDB-PAS measurement. It also shows that RDB-PAS can be applied to many kinds of metal-oxide powders other than titania which have not been measured so far.

In Chapter 3, it has been shown that an ERDT/CBB pattern consisting of ERDT pattern, total density of electron traps, and conduction-band bottom (CBB) position can be a fingerprint for identification and characterization of metal-oxide powders. As a result of examining a large number of titania powders, it has been suggested that CBB position, total density of electron traps, and ERDT pattern can reflect bulk composition shown by crystal form, bulk size shown by specific surface area, and surface structure,

respectively. From these three viewpoints, degree of coincidence (ζ) multiplied by degree of coincidence in ERDT pattern (ζ(a)), by that in total density of electron traps (ζ(b)), and by that in CBB position (ζ(c)), with weighting ($\zeta = \zeta(a) \times \zeta(b)^{1/2} \times \zeta(c)^2$) between two samples for ERDT/CBB patterns and as a result, it has been revealed that ζ was high when sampling from the same product, especially close proximity in the same container, and the higher of ζ, the more the performance such as photocatalytic activity tends to be equal. Therefore, an ERDT/CBB pattern can be a fingerprint for identification and characterization of metal-oxide powders. Furthermore, since ERDT/CBB patterns for titania powders with high photocatalytic activities were corresponding, ERDT/CBB patterns can be a functional fingerprint of metal-oxide powders.

In Chapter 4, it has been suggested that energy of valence-band top (VBT) positions with high density of states (DOS) can be evaluated by precisely analyzing ERDT/CBB patterns. Since ERDT/CBB patterns of samples obtained by mixing equal amounts of two crystalline types for samples of anatase and rutile could not be reproduced by adding each pattern, it is considered that the apparent VBT of two crystals are different, and estimation of the difference between the apparent VBT positions of both anatase and rutile was succeeded by optimization by simulation. Even in the same crystalline phase, new appearances such as apparent VBT differs depending on the samples were obtained. By applying this, it may be possible to estimate the VBT positions of metal-oxide samples by comparison with a standard sample.

In conclusion, electron traps which are located mainly on the surface of metal-oxide powders have been focused on, and it has been firstly suggested that ERDT can be a parameter reflecting the surface structure which is required for identification, ERDT/CBB pattern analysis by RDB-PAS as a macroscopic measurement method can be applied to various metal-oxide powders, and apparent VBT positions can be evaluated by ERDT/CBB pattern analysis. These results can not only propound a new concept on identification of solid powders but also permit identification and precise characterization of metal-oxide powders, which have been conventionally measured only for bulk structures and microscopic surface structures, by ERDT/CBB pattern as a structural index reflecting surface and bulk structures without using other methods. Furthermore, by discovering effective ERDT/CBB patterns for demonstrating various performances found in metal-oxide powders, it is expected that various application developments such as design guidelines for clarifying the structure-property correlation and preparing higher performance sample.

5.2 Future Aspects

It has been suggested that ERDT pattern reflects surface structure. However, detailed structural property of electron traps has not been elucidated. Respective ERDT pattern is intrinsic but it will be changed by treatment such as calcination, grinding, and doping. If ERDT pattern is able to be controlled, development and application of various field will be promoted. To elucidate the property of electron traps, observation of changes in ERDT pattern by treatment should be needed. Since ERDT/CBB pattern can be a functional fingerprint, effective ERDT/CBB patterns, in other words, proper surface and bulk structures of metal-oxide powders for electron transfer reactions such as perovskite solar cell can be also predicted. If now the fixed intermitted light, 625 nm of LED, is changed to LED sources with various wavelength, absorption spectrum of accumulated electrons at each energy can be obtained. Above research will enhance the application of ERDT/CBB pattern analysis toward various fields of materials science.

5.3 Original Papers Covering This Thesis

1) Nitta, A.; Takase, M.; Takashima, M.; Murakami, N.; Ohtani, B., A fingerprint of metal-oxide powders: Energy-resolved distribution of electron traps, *Chem. Commun.*, **52**, 12096–12099 (2016).
2) Nitta, A.; Takashima, M.; Takase, M.; Ohtani, B., Identification and characterization of titania photocatalyst powders using their energy-resolved density of electron traps as a fingerprint, *Catal. Today*, in press.
3) Nitta, A.; Takashima, M.; Murakami, N.; Takase, M.; Ohtani, B., Reversed double-beam photoacoustic spectroscopy of metal-oxide powders for estimation of their energy-resolved distribution of electron traps and electronic-band structure, *Electrochim. Acta*, **264**, 83–90 (2018).

Acknowledgment

This research work has been done from April 2015 to March 2018 in Ohtani Laboratory, Division of Environmental Materials Science, Graduate School of Environmental Science, Hokkaido University.

This research was accomplished with great leadership and encouragement from Prof. Bunsho Ohtani from Institute for Catalysis, Hokkaido University. He taught me what is research and I express my gratitude deeply to him.

I thank for peer review to Prof. Ichizo Yagi and Prof. Yuichi Kamiya from Graduate School of Environmental Science, Hokkaido University and Associated Prof. Mai Takase from Graduate School of Engineering, Muroran Institute of Technology.

Also, I would like to express my sincere gratitude to Associated Prof. Ewa Kowalska and Assistant Prof. Mai Takashima for giving me much advices and guidance in my research activities.

I also deeply appreciate professors from Division of Environmental Materials Science, Graduate School of Environmental Science, Hokkaido University who have supported students.

Thank technical staffs from Institute for Catalysis very deeply and gratefully for production, repair, and improvement of measurement equipment.

I would like to thank staffs of Bunkoukeiki Co.,Ltd. who lent me the equipment to measure ionization energy. I also express my sincere gratitude to Prof. Wojciech Macyk and Dr. Marcin Kobielusz for their help in spectroelectrochemical measurement and fruitful discussion.

This research has been financially supported by Ambitious Leader's Program fostering future leaders to open new frontiers in materials science from 2014. I express my gratitude here.

My bachelor supervisor Prof. Tomoaki Watanabe from Meiji University helped me to arise my interest in photocatalysis then I decided to study it regarding mechanism.

I would like to express my gratitude also to all the seniors, peers and juniors of Ohtani laboratory.

Finally, I appreciate my family’s supporting and understanding to study in the doctoral course.

Addendum

Table Degree of coincidence (ζ) for ERDT/CBB patterns of titania powders.

rank	sample 1	sample 2	ζ(a)	ζ(b)	ζ(c)	ζ
1	ST-F3	P25	0.861	0.969	0.994	0.837
2	TIO-11	VP-P90	0.818	0.998	0.996	0.810
3	TIO-4	Wako	0.863	0.941	0.970	0.788
4	TIO-15	ST-F3	0.823	0.925	0.992	0.779
5	ST-F10	HT-2301	0.799	0.925	0.999	0.767
6	ST-F2	ST-F3	0.808	0.892	0.998	0.761
7	TIO-4	P25	0.810	0.939	0.999	0.760
8	TIO-4	TIO-15	0.792	0.924	0.998	0.757
9	TIO-8	ST-01	0.851	0.885	0.996	0.751
10	TIO-8	TIO-14	0.778	0.952	0.994	0.749
11	TIO-4	ST-F2	0.870	0.762	0.992	0.748
12	TIO-15	P25	0.764	0.955	0.998	0.744
13	ST-F2	P25	0.800	0.865	0.992	0.732
14	TIO-4	ST-F3	0.796	0.855	0.994	0.727
15	Wako	P25	0.844	0.884	0.969	0.723
16	TIO-15	ST-F2	0.801	0.825	0.990	0.713
17	TIO-14	ST-01	0.795	0.823	0.992	0.710
18	TIO-6	MT-150A	0.856	0.828	0.995	0.705
19	ST-F3	Wako	0.806	0.757	0.997	0.697
20	TIO-13	FP-6	0.850	0.827	0.976	0.684
21	ST-F2	Wako	0.835	0.675	0.996	0.680
22	TIO-15	Wako	0.753	0.818	0.994	0.674
23	ST-F1	ST-F2	0.799	0.711	0.994	0.666
24	ST-F4	VP-P90	0.710	0.980	0.967	0.657
25	ST-F5	VP-P90	0.708	0.814	0.999	0.638
26	TIO-11	FP-6	0.620	0.998	0.994	0.615
27	ST-F4	Wako	0.624	0.958	0.998	0.608
28	TIO-13	ST-157	0.724	0.705	0.996	0.603
29	ST-F4	P25	0.697	0.748	0.998	0.600
30	ST-F3	ST-F4	0.709	0.725	0.996	0.598
31	TIO-1	TIO-13	0.628	0.920	0.997	0.598
32	TIO-11	ST-F4	0.641	0.978	0.971	0.598
33	VP-P90	FP-6	0.592	0.996	0.999	0.589
34	TIO-1	ST-157	0.671	0.766	1.000	0.587
35	ST-G1	ST-F10	0.642	0.821	0.995	0.576
36	TIO-3	TIO-6	0.728	0.648	0.986	0.570
37	TIO-13	PC-102	0.649	0.907	0.958	0.567
38	TIO-4	ST-F1	0.786	0.542	0.987	0.563
39	TIO-15	TIO-6	0.642	0.785	0.987	0.553
40	TKP-102	AMT-600	0.604	0.846	0.997	0.553
41	PC-102	TKP-102	0.738	0.663	0.959	0.552
42	TIO-11	TIO-6	0.604	0.976	0.962	0.552
43	TIO-1	VP-P90	0.706	0.628	0.986	0.543
44	637254	Kanto	0.547	0.985	1.000	0.543
45	ST-F1	ST-F3	0.691	0.634	0.993	0.543

46	TIO-11	ST-F5	0.601	0.816	0.995	0.537
47	ST-F4	ST-F5	0.643	0.798	0.967	0.537
48	ST-F1	P25	0.703	0.615	0.986	0.537
49	Wako	TIO-6	0.552	0.959	0.992	0.532
50	TIO-1	TIO-11	0.695	0.626	0.982	0.530
51	ST-157	TKP-102	0.545	0.964	0.995	0.530
52	CR-EL	HT-0514	0.535	0.982	0.998	0.527
53	ST-F1	Wako	0.761	0.480	0.990	0.517
54	HT-431A	TIO-3	0.607	0.731	0.996	0.514
55	TIO-15	MT-150A	0.714	0.538	0.989	0.513
56	PC-102	AMT-600	0.740	0.561	0.961	0.512
57	ST-F4	MT-150A	0.626	0.687	0.993	0.511
58	TIO-13	AMT-600	0.654	0.619	0.996	0.511
59	TIO-12	AMT-100	0.646	0.639	0.994	0.510
60	TIO-1	FP-6	0.657	0.630	0.985	0.506
61	VP-P90	TIO-6	0.554	0.978	0.958	0.503
62	TIO-15	ST-F1	0.676	0.587	0.984	0.502
63	TIO-1	ST-F5	0.721	0.511	0.987	0.501
64	ST-F3	TIO-6	0.594	0.726	0.995	0.501
65	TIO-4	ST-F4	0.543	0.849	0.998	0.499
66	TIO-7	TIO-10	0.537	0.862	1.000	0.498
67	TIO-12	TKP-101	0.519	0.959	0.989	0.497
68	ST-F2	TIO-3	0.514	0.999	0.982	0.495
69	TIO-5	637262	0.508	0.973	0.993	0.494
70	TIO-15	ST-F4	0.562	0.784	0.996	0.494
71	Wako	MT-150A	0.613	0.658	0.995	0.492
72	TIO-11	MT-150A	0.630	0.703	0.965	0.492
73	VP-P90	MT-150A	0.627	0.701	0.960	0.484
74	TIO-4	TIO-6	0.535	0.850	0.989	0.482
75	ST-21	TKP-102	0.594	0.667	0.995	0.480
76	ST-157	FP-6	0.713	0.483	0.984	0.480
77	ST-F1	HT-431A	0.495	0.972	0.992	0.480
78	ST-F2	ST-F4	0.601	0.647	0.994	0.477
79	TIO-15	TIO-3	0.545	0.826	0.972	0.469
80	ST-F3	MT-150A	0.667	0.498	0.997	0.469
81	TIO-12	ST-01	0.599	0.603	0.999	0.465
82	ST-G2	HT-2301	0.674	0.486	0.990	0.460
83	TIO-5	HT-0514	0.537	0.735	0.999	0.459
84	ST-G2	ST-F10	0.642	0.526	0.991	0.458
85	PC-102	FP-6	0.557	0.756	0.970	0.455
86	ST-F5	MT-150A	0.531	0.861	0.960	0.454
87	PC-102	ST-157	0.621	0.639	0.954	0.452
88	ST-F5	FP-6	0.504	0.811	0.998	0.452
89	ST-F4	FP-6	0.484	0.984	0.968	0.451
90	P25	TIO-6	0.533	0.749	0.989	0.450
91	TIO-13	TIO-11	0.562	0.681	0.985	0.450
92	ST-157	AMT-600	0.484	0.877	0.993	0.447
93	TIO-4	MT-150A	0.595	0.583	0.991	0.446

94	TKP-102	Kanto	0.698	0.414	0.992	0.442
95	ST-G1	HT-2301	0.512	0.759	0.994	0.441
96	TIO-3	MT-150A	0.684	0.445	0.983	0.441
97	TKP-101	TKP-102	0.508	0.761	0.995	0.439
98	TIO-5	ST-G2	0.570	0.582	0.997	0.432
99	P25	MT-150A	0.610	0.514	0.991	0.430
100	ST-01	TKP-101	0.553	0.629	0.990	0.429
101	TKP-102	637254	0.678	0.408	0.992	0.426
102	TIO-13	VP-P90	0.517	0.682	0.989	0.418
103	TIO-1	ST-F4	0.570	0.641	0.954	0.415
104	ST-F2	TIO-6	0.515	0.648	0.996	0.412
105	ST-G2	637262	0.534	0.599	0.996	0.409
106	TIO-11	P25	0.504	0.731	0.973	0.409
107	TIO-15	HT-431A	0.550	0.604	0.976	0.407
108	ST-F10	634662	0.465	0.762	0.999	0.405
109	TIO-13	TKP-102	0.474	0.731	0.999	0.405
110	ST-G1	ST-G2	0.505	0.640	0.996	0.400
111	ST-F4	TIO-6	0.408	0.999	0.991	0.400
112	ST-G2	HT-0514	0.452	0.792	0.996	0.399
113	TIO-7	AMT-100	0.548	0.524	1.000	0.397
114	TIO-11	Wako	0.430	0.937	0.970	0.392
115	TIO-1	PC-102	0.470	0.834	0.955	0.392
116	VP-P90	P25	0.487	0.733	0.969	0.391
117	ST-F3	TIO-3	0.430	0.893	0.980	0.391
118	ST-F1	TIO-3	0.475	0.711	0.988	0.391
119	TIO-14	TKP-101	0.545	0.517	0.998	0.390
120	TKP-101	AMT-100	0.503	0.613	0.995	0.390
121	ST-21	TKP-101	0.557	0.508	0.990	0.389
122	TIO-11	ST-F3	0.494	0.709	0.967	0.389
123	TIO-8	TIO-12	0.566	0.472	0.998	0.387
124	ST-F2	MT-150A	0.580	0.444	0.999	0.386
125	ST-157	TKP-101	0.432	0.789	1.000	0.384
126	ST-G1	634662	0.398	0.927	0.997	0.381
127	AMT-600	FP-6	0.593	0.424	0.992	0.379
128	ST-F3	VP-P90	0.485	0.710	0.963	0.379
129	HT-0514	HT-2301	0.618	0.385	0.994	0.379
130	TIO-11	TIO-15	0.454	0.766	0.975	0.378
131	ST-157	ST-F5	0.620	0.392	0.986	0.378
132	PC-102	ST-21	0.407	0.993	0.964	0.377
133	VP-P90	Wako	0.416	0.938	0.966	0.375
134	ST-01	ST-21	0.413	0.808	1.000	0.371
135	TIO-13	ST-F5	0.499	0.555	0.990	0.365
136	TIO-14	ST-21	0.372	0.982	0.992	0.363
137	TIO-12	TIO-14	0.524	0.496	0.991	0.363
138	ST-157	VP-P90	0.537	0.481	0.986	0.362
139	TIO-15	VP-P90	0.437	0.768	0.971	0.361
140	TIO-4	TIO-3	0.434	0.763	0.975	0.360
141	637262	HT-0514	0.421	0.756	0.992	0.360

142	ST-F10	HT-0514	0.557	0.416	0.995	0.356
143	TIO-7	TKP-101	0.634	0.321	0.995	0.356
144	TKP-101	AMT-600	0.380	0.900	0.992	0.355
145	TIO-8	TKP-101	0.508	0.493	0.991	0.351
146	ST-157	TIO-11	0.522	0.480	0.981	0.348
147	ST-F1	ST-F4	0.524	0.460	0.988	0.347
148	ST-21	ST-157	0.437	0.644	0.990	0.344
149	634662	HT-2301	0.404	0.704	0.997	0.337
150	TIO-1	P25	0.399	0.856	0.955	0.337
151	TIO-1	ST-F3	0.395	0.883	0.949	0.335
152	TIO-1	TIO-6	0.465	0.641	0.945	0.332
153	TIO-1	TIO-3	0.383	0.989	0.931	0.330
154	TIO-10	PC-101	0.391	0.703	1.000	0.327
155	ST-01	AMT-100	0.528	0.385	0.995	0.324
156	TIO-10	637254	0.391	0.694	0.993	0.321
157	ST-F2	HT-431A	0.381	0.731	0.986	0.317
158	TIO-5	ST-F10	0.577	0.306	0.994	0.316
159	TIO-8	ST-21	0.319	0.970	0.998	0.313
160	TIO-5	HT-2301	0.596	0.283	0.993	0.313
161	TIO-4	TIO-11	0.359	0.830	0.973	0.309
162	ST-F2	VP-P90	0.420	0.634	0.961	0.309
163	ST-F3	HT-431A	0.394	0.652	0.985	0.308
164	PC-102	TKP-101	0.476	0.505	0.954	0.308
165	TIO-11	ST-F2	0.415	0.633	0.966	0.307
166	TIO-7	637254	0.403	0.599	0.992	0.307
167	TIO-13	ST-21	0.325	0.913	0.994	0.307
168	ST-F5	P25	0.417	0.597	0.969	0.302
169	HT-431A	TIO-6	0.445	0.474	0.990	0.300
170	TIO-1	ST-F2	0.335	0.990	0.948	0.299
171	ST-F10	637262	0.547	0.315	0.987	0.299
172	TIO-4	HT-431A	0.417	0.558	0.979	0.298
173	TIO-7	PC-101	0.330	0.815	0.999	0.297
174	TIO-4	VP-P90	0.345	0.831	0.969	0.296
175	P25	TIO-3	0.334	0.865	0.974	0.295
176	TKP-101	637254	0.414	0.536	0.987	0.295
177	ST-F1	TIO-6	0.432	0.461	0.998	0.292
178	TIO-7	Kanto	0.381	0.590	0.992	0.288
179	TKP-102	FP-6	0.416	0.501	0.989	0.288
180	TIO-1	TIO-15	0.347	0.817	0.957	0.287
181	TIO-8	AMT-100	0.525	0.302	0.997	0.286
182	637254	AMT-600	0.416	0.482	0.995	0.286
183	637262	HT-2301	0.544	0.291	0.986	0.285
184	ST-F3	ST-F5	0.403	0.579	0.962	0.284
185	Wako	TIO-3	0.358	0.676	0.978	0.282
186	ST-F1	HT-2301	0.312	0.848	0.989	0.281
187	ST-F5	Wako	0.343	0.764	0.965	0.279
188	AMT-600	Kanto	0.403	0.489	0.995	0.279
189	FP-6	TIO-6	0.303	0.983	0.959	0.276

190	HT-431A	MT-150A	0.497	0.325	0.987	0.276
191	TIO-1	ST-21	0.307	0.840	0.990	0.276
192	TIO-7	TIO-12	0.482	0.335	0.994	0.276
193	ST-F1	MT-150A	0.491	0.316	0.995	0.273
194	Kanto	ST-41	0.433	0.400	0.998	0.273
195	PC-102	ST-F5	0.370	0.613	0.968	0.271
196	TIO-1	MT-150A	0.456	0.440	0.947	0.271
197	TIO-11	TIO-3	0.377	0.633	0.948	0.270
198	TIO-1	TIO-2	0.487	0.325	0.981	0.267
199	ST-21	637254	0.512	0.272	0.997	0.266
200	PC-102	637254	0.539	0.270	0.967	0.262
201	P25	FP-6	0.323	0.736	0.970	0.261
202	TIO-10	Kanto	0.318	0.684	0.993	0.259
203	PC-102	Kanto	0.521	0.275	0.967	0.255
204	CR-EL	HT-2301	0.410	0.392	0.996	0.255
205	FP-6	MT-150A	0.328	0.698	0.962	0.254
206	TIO-14	AMT-100	0.449	0.317	0.997	0.251
207	TIO-13	TKP-101	0.340	0.557	0.996	0.251
208	ST-F5	TIO-6	0.307	0.797	0.957	0.251
209	VP-P90	TIO-3	0.351	0.634	0.944	0.249
210	TIO-1	Wako	0.335	0.669	0.952	0.248
211	ST-157	ST-F4	0.385	0.491	0.953	0.245
212	TIO-5	CR-EL	0.289	0.721	0.997	0.244
213	TIO-1	TIO-4	0.306	0.755	0.955	0.243
214	PC-102	VP-P90	0.297	0.752	0.968	0.242
215	TIO-1	TKP-101	0.311	0.605	0.999	0.242
216	PC-102	TIO-11	0.294	0.751	0.973	0.241
217	TIO-15	ST-F5	0.323	0.625	0.970	0.241
218	TIO-13	ST-F4	0.313	0.696	0.957	0.239
219	ST-21	AMT-600	0.320	0.565	0.997	0.239
220	TIO-10	TKP-101	0.393	0.372	0.994	0.237
221	TIO-2	TIO-13	0.445	0.299	0.985	0.236
222	TIO-1	TKP-102	0.265	0.795	0.996	0.235
223	ST-F3	FP-6	0.297	0.714	0.964	0.233
224	ST-21	Kanto	0.446	0.276	0.997	0.233
225	Wako	FP-6	0.256	0.943	0.967	0.233
226	ST-F1	ST-F10	0.269	0.784	0.987	0.232
227	TIO-10	AMT-100	0.297	0.607	0.999	0.232
228	TIO-13	TIO-6	0.308	0.697	0.948	0.231
229	TIO-12	ST-21	0.332	0.487	0.999	0.231
230	ST-F2	ST-F5	0.348	0.516	0.961	0.231
231	TIO-1	AMT-600	0.284	0.672	0.993	0.230
232	TIO-2	TIO-11	0.495	0.203	1.000	0.223
233	P25	HT-431A	0.284	0.632	0.978	0.216
234	TIO-2	FP-6	0.477	0.205	0.997	0.214
235	ST-F4	TIO-3	0.277	0.647	0.976	0.212
236	TIO-7	Hombikat	0.233	0.847	0.993	0.211
237	TIO-10	ST-157	0.394	0.294	0.995	0.211

238	TIO-12	TKP-102	0.250	0.730	0.994	0.211
239	TIO-2	ST-157	0.336	0.424	0.981	0.211
240	TIO-12	AMT-600	0.228	0.863	0.997	0.211
241	TIO-1	ST-F1	0.277	0.718	0.942	0.209
242	TIO-7	ST-157	0.417	0.253	0.995	0.208
243	TIO-13	ST-F2	0.237	0.929	0.951	0.207
244	TIO-4	ST-F5	0.268	0.677	0.968	0.206
245	637254	AMT-100	0.224	0.874	0.992	0.206
246	TIO-2	AMT-600	0.303	0.483	0.988	0.206
247	ST-157	Kanto	0.321	0.429	0.987	0.205
248	ST-F10	CR-EL	0.316	0.424	0.997	0.204
249	TIO-7	ST-01	0.459	0.202	0.995	0.204
250	ST-F1	634662	0.270	0.597	0.986	0.203
251	TIO-4	HT-2301	0.313	0.460	0.976	0.202
252	Wako	HT-431A	0.298	0.494	0.982	0.202
253	TIO-12	ST-157	0.237	0.757	0.989	0.202
254	ST-G2	CR-EL	0.227	0.807	0.994	0.201
255	ST-157	637254	0.314	0.423	0.987	0.199
256	TIO-11	ST-F1	0.322	0.450	0.960	0.199
257	TKP-101	Kanto	0.274	0.544	0.987	0.197
258	ST-F1	VP-P90	0.319	0.451	0.956	0.196
259	ST-157	TIO-6	0.311	0.492	0.944	0.194
260	ST-F2	HT-2301	0.257	0.603	0.983	0.193
261	TIO-15	FP-6	0.232	0.771	0.972	0.193
262	ST-157	TIO-3	0.255	0.758	0.931	0.192
263	HT-2301	HT-431A	0.208	0.824	0.997	0.188
264	TIO-2	VP-P90	0.413	0.204	0.995	0.185
265	PC-102	P25	0.187	0.974	0.999	0.184
266	TIO-5	ST-G1	0.301	0.373	0.999	0.183
267	ST-F2	FP-6	0.247	0.637	0.963	0.183
268	637254	ST-41	0.288	0.406	0.998	0.183
269	AMT-600	TIO-11	0.286	0.421	0.989	0.181
270	TKP-101	FP-6	0.298	0.381	0.984	0.178
271	TIO-1	TIO-14	0.193	0.855	0.998	0.178
272	TIO-10	TKP-102	0.331	0.283	0.999	0.176
273	PC-102	ST-01	0.209	0.803	0.964	0.174
274	TKP-101	ST-F5	0.319	0.309	0.986	0.173
275	TIO-13	ST-F3	0.193	0.960	0.953	0.172
276	TKP-102	AMT-100	0.252	0.466	1.000	0.172
277	AMT-600	VP-P90	0.267	0.422	0.993	0.171
278	ST-157	ST-F3	0.230	0.677	0.949	0.171
279	TIO-7	TKP-102	0.345	0.244	1.000	0.171
280	TIO-1	TIO-7	0.226	0.598	0.986	0.170
281	Wako	HT-2301	0.277	0.407	0.979	0.169
282	TIO-13	MT-150A	0.270	0.478	0.950	0.169
283	TIO-7	TIO-8	0.426	0.158	0.997	0.168
284	TIO-12	PC-102	0.259	0.484	0.965	0.168
285	TIO-10	AMT-600	0.290	0.335	0.998	0.167

286	ST-157	P25	0.224	0.656	0.955	0.165
287	TKP-102	ST-F5	0.263	0.406	0.991	0.165
288	TIO-7	TIO-14	0.406	0.166	0.997	0.165
289	ST-G1	HT-0514	0.227	0.507	1.000	0.162
290	PC-102	ST-F4	0.185	0.768	0.999	0.162
291	TKP-102	ST-41	0.401	0.166	0.994	0.161
292	ST-G1	637262	0.264	0.383	0.992	0.161
293	CR-EL	637262	0.189	0.742	0.990	0.159
294	TIO-13	637254	0.296	0.298	0.991	0.159
295	TIO-13	P25	0.178	0.931	0.959	0.158
296	AMT-600	ST-F5	0.272	0.344	0.993	0.158
297	PC-101	TKP-101	0.312	0.261	0.994	0.158
298	TIO-4	ST-F10	0.254	0.425	0.974	0.157
299	TIO-13	TIO-15	0.180	0.888	0.961	0.157
300	ST-01	ST-157	0.179	0.796	0.990	0.157
301	TIO-1	TIO-7	0.359	0.194	0.995	0.157
302	TIO-14	TKP-102	0.191	0.680	0.997	0.156
303	ST-157	MT-150A	0.299	0.337	0.947	0.156
304	TIO-1	TIO-8	0.175	0.814	0.992	0.156
305	ST-157	TIO-15	0.214	0.626	0.957	0.156
306	PC-101	637254	0.226	0.488	0.993	0.155
307	ST-21	AMT-100	0.280	0.311	0.995	0.155
308	AMT-600	Merck	0.361	0.184	0.999	0.154
309	TIO-13	Kanto	0.286	0.303	0.991	0.154
310	TIO-4	FP-6	0.179	0.835	0.970	0.154
311	TIO-10	TIO-12	0.249	0.388	0.995	0.154
312	TIO-7	AMT-600	0.285	0.289	0.998	0.153
313	ST-01	TKP-102	0.167	0.826	0.995	0.150
314	PC-102	ST-F3	0.154	0.944	0.994	0.148
315	TIO-2	ST-F5	0.366	0.166	0.995	0.148
316	ST-157	ST-F2	0.188	0.759	0.948	0.147
317	ST-F2	ST-F10	0.204	0.558	0.982	0.147
318	TIO-2	ST-F4	0.341	0.208	0.972	0.147
319	TIO-7	ST-21	0.366	0.163	0.995	0.146
320	TIO-14	ST-157	0.181	0.655	0.998	0.146
321	TIO-10	TIO-13	0.317	0.207	0.998	0.144
322	ST-F1	ST-F5	0.258	0.367	0.955	0.143
323	TIO-10	PC-102	0.356	0.188	0.960	0.142
324	TIO-12	TIO-13	0.197	0.534	0.993	0.142
325	Hombikat	AMT-100	0.216	0.444	0.993	0.142
326	P25	HT-2301	0.206	0.521	0.975	0.141
327	Wako	ST-F10	0.240	0.377	0.978	0.141
328	ST-157	ST-F1	0.164	0.937	0.942	0.141
329	TIO-7	TIO-13	0.331	0.179	0.999	0.140
330	TKP-102	VP-P90	0.197	0.499	0.990	0.136
331	TKP-102	TIO-11	0.197	0.498	0.986	0.135
332	ST-157	AMT-100	0.195	0.484	0.995	0.135
333	PC-102	ST-F2	0.146	0.842	0.993	0.132

334	ST-F2	634662	0.210	0.425	0.981	0.131
335	TIO-7	PC-102	0.354	0.162	0.959	0.131
336	ST-F3	HT-2301	0.185	0.538	0.981	0.131
337	TIO-15	HT-2301	0.195	0.498	0.973	0.130
338	ST-F1	ST-G1	0.168	0.644	0.983	0.130
339	TIO-2	TIO-10	0.160	0.693	0.986	0.130
340	PC-101	ST-157	0.287	0.206	0.994	0.129
341	ST-F10	HT-431A	0.149	0.762	0.995	0.129
342	TIO-14	PC-102	0.142	0.976	0.956	0.128
343	TIO-1	TIO-10	0.273	0.225	0.995	0.128
344	ST-21	FP-6	0.149	0.751	0.994	0.127
345	TIO-8	TKP-102	0.159	0.647	0.996	0.127
346	TKP-101	VP-P90	0.211	0.380	0.985	0.126
347	TIO-8	PC-102	0.138	0.976	0.962	0.126
348	TIO-2	P25	0.251	0.278	0.974	0.125
349	TIO-2	ST-F3	0.250	0.287	0.968	0.125
350	AMT-100	AMT-600	0.169	0.551	0.998	0.125
351	TIO-7	ST-F5	0.401	0.099	0.991	0.124
352	TIO-12	637254	0.165	0.559	0.998	0.123
353	TIO-12	Hombikat	0.231	0.284	0.998	0.123
354	TIO-2	TIO-6	0.289	0.208	0.963	0.122
355	TIO-8	ST-157	0.155	0.624	0.992	0.120
356	ST-01	637254	0.205	0.337	0.997	0.118
357	TIO-13	ST-01	0.125	0.885	0.994	0.116
358	TIO-2	PC-102	0.233	0.271	0.973	0.115
359	TKP-101	TIO-11	0.193	0.379	0.981	0.114
360	AMT-600	ST-41	0.259	0.196	0.996	0.114
361	ST-157	TIO-4	0.164	0.579	0.955	0.114
362	ST-157	Wako	0.175	0.513	0.952	0.113
363	TIO-10	ST-21	0.262	0.189	0.996	0.113
364	TIO-13	ST-F1	0.155	0.661	0.946	0.113
365	TIO-12	FP-6	0.187	0.366	0.995	0.112
366	ST-21	Fluka	0.384	0.083	0.996	0.110
367	PC-101	Kanto	0.158	0.481	0.993	0.108
368	TIO-13	Wako	0.139	0.727	0.955	0.108
369	PC-102	TIO-6	0.124	0.769	0.989	0.107
370	P25	ST-F10	0.161	0.482	0.974	0.106
371	TIO-4	634662	0.197	0.324	0.973	0.106
372	TIO-2	Kanto	0.108	0.987	0.993	0.105
373	Wako	634662	0.206	0.287	0.976	0.105
374	TIO-12	ST-F5	0.195	0.297	0.997	0.105
375	TIO-14	637254	0.202	0.277	0.989	0.104
376	PC-102	AMT-100	0.200	0.309	0.959	0.102
377	TIO-10	Hombikat	0.121	0.731	0.993	0.102
378	TIO-2	TIO-3	0.200	0.321	0.949	0.102
379	TIO-7	FP-6	0.296	0.122	0.989	0.101
380	ST-F4	HT-431A	0.153	0.473	0.980	0.101
381	TIO-1	TIO-12	0.134	0.580	0.990	0.100

382	TIO-10	ST-F5	0.298	0.115	0.992	0.0994
383	TIO-13	TIO-4	0.119	0.820	0.959	0.0989
384	ST-F1	FP-6	0.160	0.453	0.957	0.0987
385	TIO-10	FP-6	0.267	0.142	0.990	0.0987
386	TIO-8	637254	0.192	0.264	0.996	0.0976
387	637254	FP-6	0.217	0.204	0.997	0.0975
388	ST-21	ST-F5	0.126	0.609	0.996	0.0975
389	ST-21	ST-41	0.293	0.111	0.999	0.0971
390	P25	634662	0.169	0.367	0.973	0.0967
391	PC-102	ST-41	0.313	0.110	0.965	0.0965
392	ST-F1	HT-0514	0.175	0.326	0.983	0.0963
393	Kanto	FP-6	0.210	0.207	0.997	0.0949
394	PC-101	AMT-100	0.146	0.427	0.999	0.0949
395	TIO-7	VP-P90	0.276	0.122	0.991	0.0947
396	TIO-2	Wako	0.198	0.217	1.007	0.0937
397	PC-101	AMT-600	0.193	0.235	0.998	0.0935
398	ST-F1	CR-EL	0.167	0.333	0.985	0.0935
399	TIO-2	MT-150A	0.264	0.143	0.965	0.0930
400	TIO-11	HT-431A	0.150	0.463	0.952	0.0925
401	TIO-10	ST-01	0.192	0.234	0.995	0.0922
402	TIO-15	ST-F10	0.142	0.460	0.972	0.0908
403	ST-F5	TIO-3	0.139	0.517	0.944	0.0891
404	TIO-7	TIO-11	0.262	0.122	0.986	0.0889
405	ST-F3	634662	0.151	0.379	0.979	0.0888
406	TIO-4	CR-EL	0.221	0.180	0.972	0.0886
407	ST-F3	ST-F10	0.130	0.497	0.980	0.0879
408	TIO-13	AMT-100	0.149	0.341	0.999	0.0869
409	TIO-2	ST-F2	0.163	0.322	0.966	0.0861
410	PC-101	TKP-102	0.193	0.199	0.999	0.0861
411	TIO-2	TIO-15	0.172	0.265	0.976	0.0846
412	634662	HT-431A	0.112	0.581	0.994	0.0846
413	Hombikat	TKP-101	0.161	0.272	0.987	0.0819
414	ST-01	FP-6	0.105	0.607	0.994	0.0810
415	TIO-1	637254	0.145	0.324	0.988	0.0805
416	TIO-2	TKP-102	0.129	0.408	0.986	0.0800
417	TIO-4	ST-G1	0.143	0.349	0.970	0.0797
418	PC-101	PC-102	0.236	0.132	0.960	0.0790
419	PC-102	MT-150A	0.110	0.528	0.992	0.0789
420	FP-6	TIO-3	0.109	0.637	0.945	0.0778
421	TIO-13	PC-101	0.202	0.146	0.998	0.0767
422	TIO-1	Kanto	0.137	0.329	0.987	0.0765
423	ST-157	ST-41	0.187	0.172	0.989	0.0759
424	TKP-101	ST-F4	0.134	0.388	0.953	0.0756
425	ST-21	P25	0.082	0.981	0.965	0.0752
426	TIO-7	ST-F4	0.229	0.124	0.958	0.0742
427	TIO-2	PC-101	0.109	0.487	0.987	0.0741
428	637254	ST-F5	0.182	0.166	0.999	0.0738
429	ST-157	Merck	0.185	0.162	0.994	0.0736

430	ST-21	ST-F2	0.0872	0.848	0.957	0.0735
431	ST-F2	CR-EL	0.157	0.237	0.979	0.0733
432	ST-F1	ST-G2	0.119	0.412	0.979	0.0733
433	TIO-8	TIO-10	0.170	0.183	0.997	0.0725
434	TIO-13	Merck	0.214	0.114	0.998	0.0719
435	TKP-101	ST-41	0.156	0.218	0.989	0.0712
436	Wako	ST-G1	0.134	0.309	0.973	0.0705
437	ST-F2	ST-G1	0.109	0.458	0.977	0.0703
438	TIO-1	PC-101	0.178	0.158	0.995	0.0701
439	VP-P90	HT-431A	0.113	0.463	0.948	0.0691
440	TIO-7	P25	0.183	0.166	0.960	0.0689
441	TIO-15	634662	0.123	0.351	0.971	0.0688
442	TIO-8	FP-6	0.0778	0.774	0.993	0.0675
443	AMT-100	ST-F5	0.158	0.190	0.991	0.0674
444	TIO-1	AMT-100	0.111	0.371	0.995	0.0668
445	ST-01	ST-F5	0.096	0.492	0.996	0.0665
446	TIO-12	PC-101	0.129	0.273	0.995	0.0665
447	TIO-4	ST-G2	0.151	0.223	0.966	0.0664
448	HT-2301	TIO-3	0.0854	0.602	0.999	0.0662
449	TIO-10	TIO-14	0.151	0.192	0.997	0.0660
450	637254	Fluka	0.119	0.306	0.999	0.0656
451	TKP-101	TIO-3	0.0966	0.599	0.934	0.0652
452	TIO-2	TIO-4	0.138	0.245	0.974	0.0648
453	Hombikat	ST-01	0.155	0.171	0.998	0.0639
454	TIO-7	ST-F3	0.168	0.171	0.954	0.0634
455	PC-102	TIO-15	0.0631	0.980	0.997	0.0621
456	PC-102	ST-F1	0.0822	0.599	0.987	0.0620
457	TIO-12	VP-P90	0.103	0.364	0.996	0.0617
458	PC-101	ST-F5	0.219	0.081	0.992	0.0613
459	PC-102	Merck	0.206	0.103	0.960	0.0612
460	TKP-101	TIO-6	0.110	0.388	0.944	0.0611
461	TIO-4	HT-0514	0.153	0.177	0.970	0.0607
462	TKP-101	P25	0.0905	0.518	0.955	0.0594
463	Fluka	Kanto	0.108	0.302	0.999	0.0593
464	TIO-7	ST-F2	0.149	0.192	0.952	0.0591
465	TIO-10	VP-P90	0.160	0.141	0.991	0.0590
466	AMT-600	ST-F4	0.0963	0.431	0.960	0.0583
467	AMT-100	FP-6	0.123	0.234	0.989	0.0580
468	TIO-7	ST-F1	0.124	0.270	0.947	0.0576
469	TIO-13	TIO-14	0.0595	0.929	0.998	0.0571
470	TIO-7	TIO-6	0.176	0.125	0.949	0.0560
471	TIO-2	HT-431A	0.0924	0.440	0.953	0.0556
472	AMT-600	TIO-6	0.0934	0.431	0.951	0.0555
473	TKP-101	ST-F3	0.0838	0.534	0.949	0.0552
474	TIO-7	TIO-3	0.144	0.192	0.935	0.0551
475	TIO-7	TIO-15	0.148	0.159	0.962	0.0544
476	Wako	CR-EL	0.143	0.160	0.975	0.0543
477	TIO-7	Wako	0.164	0.130	0.956	0.0542

478	PC-102	Wako	0.0606	0.802	0.997	0.0540
479	PC-101	ST-21	0.149	0.133	0.996	0.0538
480	TKP-101	ST-F1	0.0660	0.842	0.942	0.0537
481	TKP-102	ST-F4	0.0818	0.509	0.958	0.0536
482	TKP-101	TIO-15	0.0831	0.495	0.957	0.0535
483	Merck	ST-41	0.0546	0.940	0.995	0.0525
484	TIO-8	Hombikat	0.142	0.134	0.996	0.0517
485	Wako	ST-G2	0.123	0.198	0.969	0.0514
486	ST-G1	HT-431A	0.0651	0.626	0.991	0.0506
487	TKP-101	MT-150A	0.109	0.266	0.946	0.0506
488	TIO-10	TIO-11	0.138	0.141	0.987	0.0505
489	TIO-2	ST-F1	0.0813	0.452	0.961	0.0504
490	PC-101	FP-6	0.163	0.100	0.990	0.0504
491	CR-EL	HT-431A	0.0896	0.323	0.993	0.0502
492	ST-F5	Kanto	0.123	0.168	0.999	0.0502
493	TIO-7	TIO-4	0.142	0.147	0.960	0.0500
494	TKP-101	HT-431A	0.0632	0.819	0.934	0.0499
495	Merck	FP-6	0.181	0.078	0.990	0.0497
496	PC-102	TIO-4	0.0519	0.905	0.999	0.0493
497	P25	ST-G1	0.0832	0.396	0.969	0.0492
498	ST-21	ST-F3	0.0548	0.951	0.959	0.0491
499	TIO-7	HT-431A	0.108	0.263	0.939	0.0490
500	ST-F4	634662	0.0983	0.275	0.975	0.0489
501	TIO-13	ST-41	0.141	0.121	0.993	0.0483
502	ST-F2	ST-G2	0.0936	0.293	0.973	0.0480
503	TIO-12	TIO-11	0.0799	0.363	0.992	0.0474
504	TIO-7	MT-150A	0.176	0.085	0.951	0.0465
505	TKP-101	ST-F2	0.0663	0.599	0.947	0.0461
506	ST-G2	HT-431A	0.0746	0.401	0.987	0.0460
507	ST-G1	CR-EL	0.0632	0.516	0.998	0.0452
508	TIO-8	ST-F5	0.0555	0.628	0.994	0.0435
509	PC-101	ST-01	0.108	0.164	0.996	0.0433
510	TIO-10	ST-F4	0.124	0.144	0.958	0.0432
511	Hombikat	ST-157	0.0951	0.215	0.988	0.0430
512	TKP-101	Wako	0.0745	0.405	0.951	0.0429
513	TKP-102	ST-F1	0.0503	0.903	0.947	0.0428
514	ST-F2	HT-0514	0.0924	0.232	0.977	0.0425
515	TKP-101	TIO-4	0.0690	0.457	0.955	0.0425
516	TIO-9	TKP-101	0.0846	0.254	0.993	0.0420
517	TIO-1	Hombikat	0.106	0.165	0.988	0.0419
518	Hombikat	ST-F5	0.145	0.0841	0.998	0.0419
519	TKP-102	Fluka	0.120	0.125	0.991	0.0416
520	TIO-8	TIO-13	0.0441	0.885	0.995	0.0411
521	TIO-13	TIO-3	0.0487	0.930	0.934	0.0410
522	ST-F10	TIO-3	0.0545	0.557	1.000	0.0407
523	TKP-102	TIO-6	0.0625	0.510	0.935	0.0390
524	TKP-102	Merck	0.0981	0.156	0.999	0.0386
525	Fluka	ST-41	0.0444	0.753	0.997	0.0383

526	TKP-102	TIO-3	0.0485	0.787	0.935	0.0376
527	TIO-14	Hombikat	0.1020	0.141	0.990	0.0375
528	Wako	HT-0514	0.0998	0.157	0.973	0.0374
529	TKP-101	Fluka	0.0943	0.164	0.986	0.0372
530	TIO-15	ST-G1	0.0636	0.378	0.968	0.0366
531	TIO-9	PC-101	0.0360	0.970	0.999	0.0354
532	TIO-14	PC-101	0.0953	0.135	0.996	0.0348
533	TIO-14	Kanto	0.0642	0.281	0.989	0.0333
534	AMT-100	VP-P90	0.0696	0.233	0.990	0.0329
535	PC-101	ST-41	0.0348	0.833	0.995	0.0314
536	ST-G2	634662	0.0382	0.690	0.992	0.0313
537	ST-21	ST-F1	0.0438	0.603	0.952	0.0308
538	TKP-102	MT-150A	0.0573	0.350	0.951	0.0307
539	TIO-1	ST-01	0.0318	0.962	0.990	0.0306
540	634662	TIO-3	0.0470	0.424	0.998	0.0305
541	PC-101	Hombikat	0.0314	0.961	0.993	0.0303
542	ST-F3	ST-G1	0.0492	0.408	0.976	0.0299
543	TIO-12	ST-F4	0.0510	0.372	0.964	0.0289
544	TIO-15	CR-EL	0.0681	0.195	0.969	0.0283
545	TIO-14	Fluka	0.0989	0.085	0.989	0.0282
546	TIO-8	PC-101	0.0783	0.129	0.997	0.0279
547	P25	ST-G2	0.0595	0.253	0.965	0.0279
548	TIO-14	ST-F2	0.0332	0.863	0.950	0.0278
549	TIO-15	ST-G2	0.0604	0.242	0.964	0.0276
550	ST-F3	ST-G2	0.0566	0.261	0.972	0.0273
551	ST-41	FP-6	0.0950	0.083	0.995	0.0271
552	Hombikat	637254	0.0369	0.507	1.000	0.0263
553	HT-2301	MT-150A	0.0520	0.268	0.984	0.0261
554	Hombikat	VP-P90	0.0812	0.103	0.998	0.0260
555	AMT-100	TIO-11	0.0540	0.232	0.986	0.0253
556	TIO-14	FP-6	0.0297	0.737	0.986	0.0248
557	AMT-600	MT-150A	0.0496	0.296	0.954	0.0245
558	PC-101	VP-P90	0.0781	0.099	0.991	0.0242
559	TIO-8	ST-F2	0.0289	0.822	0.956	0.0239
560	ST-01	TIO-11	0.0304	0.603	0.991	0.0232
561	ST-01	VP-P90	0.0289	0.604	0.996	0.0223
562	TIO-14	ST-F5	0.0283	0.598	0.988	0.0213
563	TIO-12	Kanto	0.0280	0.567	0.998	0.0210
564	PC-101	ST-F4	0.0699	0.101	0.959	0.0204
565	HT-2301	TIO-6	0.0328	0.391	0.987	0.0200
566	TIO-7	CR-EL	0.0245	0.813	0.932	0.0192
567	TIO-11	Kanto	0.0426	0.206	0.994	0.0191
568	VP-P90	Kanto	0.0421	0.207	0.998	0.0190
569	HT-0514	HT-431A	0.0342	0.317	0.991	0.0189
570	ST-F3	CR-EL	0.0420	0.211	0.978	0.0185
571	TIO-7	634662	0.0301	0.453	0.934	0.0176
572	P25	CR-EL	0.0395	0.205	0.971	0.0169
573	TIO-12	TIO-6	0.0301	0.372	0.954	0.0168

574	637254	VP-P90	0.0369	0.203	0.998	0.0166
575	Merck	Kanto	0.0272	0.376	0.993	0.0165
576	AMT-100	ST-F4	0.0363	0.238	0.958	0.0162
577	TKP-102	ST-F3	0.0211	0.702	0.954	0.0161
578	PC-101	TIO-11	0.0524	0.099	0.987	0.0161
579	P25	HT-0514	0.0371	0.201	0.969	0.0156
580	634662	MT-150A	0.0369	0.189	0.981	0.0155
581	TIO-7	ST-41	0.0201	0.679	0.956	0.0151
582	TIO-8	ST-F1	0.0216	0.585	0.950	0.0149
583	TKP-102	TIO-15	0.0198	0.650	0.962	0.0147
584	ST-F1	TIO-5	0.0302	0.240	0.982	0.0143
585	ST-01	ST-F1	0.0181	0.746	0.952	0.0142
586	TIO-14	ST-F1	0.0202	0.614	0.944	0.0141
587	ST-01	Kanto	0.0235	0.342	0.997	0.0137
588	TIO-1	ST-41	0.0379	0.132	0.989	0.0135
589	TKP-102	ST-F2	0.0165	0.787	0.952	0.0133
590	ST-21	VP-P90	0.0145	0.747	0.995	0.0124
591	TKP-102	P25	0.0163	0.681	0.960	0.0123
592	Hombikat	FP-6	0.0377	0.104	0.997	0.0121
593	ST-F4	HT-2301	0.0200	0.390	0.977	0.0119
594	TIO-10	ST-41	0.0155	0.585	0.995	0.0118
595	ST-F10	MT-150A	0.0236	0.248	0.983	0.0113
596	TIO-8	Fluka	0.0391	0.081	0.995	0.0110
597	ST-01	Fluka	0.0332	0.103	0.997	0.0106
598	TKP-102	Wako	0.0155	0.532	0.956	0.0103
599	TIO-13	Hombikat	0.0269	0.151	0.991	0.0103
600	Hombikat	TIO-11	0.0298	0.103	0.994	0.00944
601	TIO-10	P25	0.0220	0.193	0.960	0.00890
602	ST-F5	ST-41	0.0325	0.067	0.997	0.00837
603	634662	TIO-6	0.0158	0.275	0.984	0.00804
604	TIO-8	Kanto	0.0151	0.268	0.996	0.00775
605	TIO-12	MT-150A	0.0167	0.255	0.957	0.00772
606	ST-01	TIO-6	0.0100	0.617	0.954	0.00714
607	ST-01	TIO-3	0.0082	0.952	0.940	0.00705
608	TIO-7	ST-F10	0.0137	0.345	0.935	0.00701
609	TIO-1	634662	0.0117	0.429	0.929	0.00661
610	TKP-101	HT-2301	0.0076	0.994	0.931	0.00654
611	637254	TIO-11	0.0136	0.203	0.994	0.00607
612	TIO-15	HT-0514	0.0141	0.192	0.968	0.00579
613	TKP-102	TIO-4	0.0079	0.600	0.959	0.00563
614	TIO-12	TIO-3	0.0081	0.574	0.941	0.00541
615	ST-F10	TIO-6	0.0079	0.361	0.985	0.00459
616	ST-F3	HT-0514	0.0096	0.207	0.976	0.00415
617	TIO-10	MT-150A	0.0136	0.099	0.952	0.00387
618	ST-01	MT-150A	0.00620	0.424	0.956	0.00369
619	AMT-600	TIO-3	0.00437	0.665	0.937	0.00313
620	AMT-100	TIO-6	0.00684	0.238	0.949	0.00300
621	TIO-10	TIO-6	0.00800	0.144	0.949	0.00274

622	TIO-2	ST-41	0.00422	0.406	0.992	0.00264
623	TIO-7	HT-2301	0.00451	0.319	0.936	0.00223
624	AMT-100	MT-150A	0.00543	0.163	0.951	0.00198
625	TIO-7	ST-G1	0.00304	0.420	0.931	0.00170
626	TIO-10	Wako	0.00452	0.151	0.957	0.00161
627	VP-P90	634662	0.00338	0.269	0.943	0.00156
628	TIO-7	HT-0514	0.00171	0.828	0.931	0.00135
629	AMT-600	ST-F3	0.00135	0.594	0.956	0.000953
630	ST-01	AMT-600	0.000912	0.699	0.997	0.000758
631	TIO-2	637254	0.000100	0.998	0.993	0.0000986
632	TIO-8	P25	0.000100	0.951	0.997	0.0000970
633	TIO-9	Hombikat	0.000100	0.933	0.994	0.0000955
634	TIO-8	TIO-15	0.000100	0.996	0.965	0.0000930
635	AMT-100	Kanto	0.000100	0.888	0.992	0.0000927
636	ST-21	TIO-15	0.000100	0.973	0.967	0.0000922
637	TIO-9	ST-41	0.000100	0.858	0.996	0.0000918
638	TIO-14	P25	0.000100	0.998	0.957	0.0000915
639	TIO-2	AMT-100	0.000100	0.876	0.986	0.0000909
640	TIO-14	TIO-15	0.000100	0.956	0.959	0.0000899
641	TIO-9	Merck	0.000100	0.807	1.000	0.0000898
642	ST-01	ST-F2	0.000100	0.953	0.957	0.0000895
643	TIO-8	TIO-4	0.000100	0.927	0.963	0.0000893
644	Hombikat	ST-41	0.000100	0.801	0.999	0.0000892
645	TIO-14	ST-F3	0.000100	0.968	0.951	0.0000890
646	TIO-7	TIO-9	0.000100	0.790	0.998	0.0000886
647	PC-101	Merck	0.000100	0.783	1.000	0.0000884
648	Merck	Fluka	0.000100	0.801	0.993	0.0000882
649	ST-21	TIO-4	0.000100	0.899	0.964	0.0000882
650	TIO-8	ST-F3	0.000100	0.922	0.957	0.0000879
651	PC-102	TIO-3	0.000100	0.843	0.975	0.0000873
652	AMT-600	ST-F1	0.000100	0.936	0.949	0.0000872
653	TIO-12	ST-F10	0.000100	0.970	0.940	0.0000871
654	TIO-8	VP-P90	0.000100	0.771	0.994	0.0000867
655	TIO-12	HT-2301	0.000100	0.953	0.942	0.0000866
656	TIO-14	TIO-4	0.000100	0.883	0.957	0.0000860
657	TIO-8	TIO-11	0.000100	0.769	0.990	0.0000859
658	Hombikat	Merck	0.000100	0.753	0.994	0.0000857
659	TIO-10	TIO-5	0.000100	0.765	0.990	0.0000857
660	Hombikat	TIO-5	0.000100	0.955	0.936	0.0000857
661	Hombikat	637262	0.000100	0.929	0.941	0.0000853
662	ST-157	HT-431A	0.000100	0.964	0.932	0.0000852
663	TKP-102	HT-431A	0.000100	0.929	0.939	0.0000850
664	TIO-10	HT-0514	0.000100	0.960	0.931	0.0000849
665	ST-21	TIO-11	0.000100	0.746	0.991	0.0000848
666	ST-01	ST-F3	0.000100	0.850	0.959	0.0000848
667	AMT-600	HT-431A	0.000100	0.911	0.941	0.0000846
668	ST-01	P25	0.000100	0.824	0.965	0.0000845
669	TIO-10	CR-EL	0.000100	0.942	0.933	0.0000845

670	TIO-2	ST-G2	0.000100	0.911	0.940	0.0000844
671	AMT-600	HT-2301	0.000100	0.906	0.938	0.0000838
672	TIO-14	VP-P90	0.000100	0.734	0.988	0.0000836
673	TIO-8	Wako	0.000100	0.821	0.960	0.0000835
674	TKP-101	ST-F10	0.000100	0.931	0.930	0.0000834
675	637254	ST-G2	0.000100	0.913	0.934	0.0000833
676	ST-01	TIO-15	0.000100	0.787	0.967	0.0000829
677	PC-101	TIO-5	0.000100	0.918	0.930	0.0000829
678	TIO-14	TIO-11	0.000100	0.733	0.983	0.0000828
679	Kanto	ST-G2	0.000100	0.899	0.934	0.0000827
680	ST-21	Wako	0.000100	0.796	0.961	0.0000824
681	TIO-9	TIO-10	0.000100	0.682	0.999	0.0000824
682	TIO-8	ST-F4	0.000100	0.787	0.961	0.0000820
683	TIO-9	TIO-5	0.000100	0.891	0.931	0.0000818
684	TIO-12	ST-F1	0.000100	0.808	0.952	0.0000815
685	ST-21	TIO-3	0.000100	0.849	0.940	0.0000814
686	TIO-7	TIO-5	0.000100	0.887	0.929	0.0000814
687	TIO-7	637262	0.000100	0.912	0.923	0.0000813
688	AMT-100	634662	0.000100	0.865	0.934	0.0000811
689	ST-21	ST-F4	0.000100	0.763	0.963	0.0000810
690	TIO-14	TIO-3	0.000100	0.864	0.933	0.0000808
691	PC-101	637262	0.000100	0.893	0.924	0.0000806
692	TIO-8	TIO-6	0.000100	0.788	0.952	0.0000805
693	TIO-14	Wako	0.000100	0.782	0.954	0.0000804
694	AMT-600	ST-F10	0.000100	0.837	0.937	0.0000803
695	TIO-8	TIO-3	0.000100	0.823	0.938	0.0000799
696	TIO-7	Merck	0.000100	0.638	0.999	0.0000797
697	TIO-9	637262	0.000100	0.866	0.924	0.0000795
698	ST-21	TIO-6	0.000100	0.764	0.954	0.0000795
699	TIO-9	Fluka	0.000100	0.647	0.993	0.0000793
700	ST-01	TIO-4	0.000100	0.726	0.965	0.0000793
701	TIO-12	HT-431A	0.000100	0.786	0.945	0.0000791
702	TIO-14	ST-F4	0.000100	0.749	0.955	0.0000790
703	ST-01	HT-431A	0.000100	0.767	0.944	0.0000781
704	TIO-2	634662	0.000100	0.757	0.947	0.0000781
705	PC-101	Fluka	0.000100	0.628	0.992	0.0000780
706	TIO-12	ST-G1	0.000100	0.797	0.935	0.0000780
707	Kanto	634662	0.000100	0.767	0.941	0.0000776
708	TIO-14	TIO-6	0.000100	0.750	0.946	0.0000776
709	AMT-100	ST-G1	0.000100	0.802	0.930	0.0000775
710	Hombikat	Fluka	0.000100	0.603	0.999	0.0000775
711	ST-157	HT-2301	0.000100	0.795	0.932	0.0000774
712	637254	634662	0.000100	0.756	0.941	0.0000770
713	TIO-2	CR-EL	0.000100	0.736	0.946	0.0000767
714	AMT-100	ST-G2	0.000100	0.798	0.927	0.0000767
715	TKP-102	HT-2301	0.000100	0.766	0.936	0.0000767
716	ST-41	TIO-5	0.000100	0.765	0.935	0.0000764
717	TIO-12	634662	0.000100	0.739	0.939	0.0000758

718	637254	CR-EL	0.000100	0.737	0.940	0.0000758
719	TIO-2	HT-0514	0.000100	0.722	0.944	0.0000757
720	TIO-10	637262	0.000100	0.787	0.923	0.0000756
721	PC-102	HT-431A	0.000100	0.616	0.979	0.0000752
722	Kanto	CR-EL	0.000100	0.726	0.940	0.0000752
723	TIO-1	HT-431A	0.000100	0.739	0.935	0.0000751
724	TIO-14	AMT-600	0.000100	0.575	0.995	0.0000750
725	TIO-10	ST-G2	0.000100	0.761	0.927	0.0000750
726	TKP-101	ST-G1	0.000100	0.764	0.926	0.0000749
727	637254	HT-0514	0.000100	0.723	0.938	0.0000748
728	TIO-2	ST-G1	0.000100	0.702	0.944	0.0000747
729	CR-EL	634662	0.000100	0.557	0.999	0.0000744
730	AMT-600	ST-F2	0.000100	0.666	0.955	0.0000743
731	ST-41	637262	0.000100	0.744	0.928	0.0000743
732	Kanto	HT-0514	0.000100	0.712	0.938	0.0000742
733	Kanto	ST-G1	0.000100	0.712	0.938	0.0000742
734	ST-157	ST-F10	0.000100	0.735	0.930	0.0000742
735	ST-01	Wako	0.000100	0.644	0.961	0.0000741
736	TIO-10	Merck	0.000100	0.550	0.999	0.0000741
737	TIO-8	AMT-600	0.000100	0.548	0.999	0.0000738
738	637254	ST-G1	0.000100	0.701	0.938	0.0000736
739	Hombikat	HT-0514	0.000100	0.702	0.937	0.0000736
740	TIO-2	TIO-12	0.000100	0.560	0.992	0.0000736
741	TKP-102	ST-F10	0.000100	0.708	0.935	0.0000735
742	634662	HT-0514	0.000100	0.547	0.997	0.0000734
743	Merck	TIO-5	0.000100	0.719	0.930	0.0000734
744	Hombikat	CR-EL	0.000100	0.689	0.939	0.0000732
745	ST-01	ST-F4	0.000100	0.616	0.963	0.0000728
746	TKP-101	634662	0.000100	0.709	0.929	0.0000726
747	TIO-13	HT-431A	0.000100	0.680	0.938	0.0000725
748	AMT-600	ST-G1	0.000100	0.688	0.933	0.0000721
749	Merck	637262	0.000100	0.699	0.924	0.0000714
750	PC-101	CR-EL	0.000100	0.662	0.936	0.0000712
751	PC-101	HT-0514	0.000100	0.675	0.931	0.0000712
752	AMT-100	ST-F10	0.000100	0.659	0.935	0.0000709
753	Hombikat	Kanto	0.000100	0.500	1.000	0.0000706
754	ST-01	HT-2301	0.000100	0.633	0.941	0.0000704
755	TIO-2	TKP-101	0.000100	0.537	0.981	0.0000704
756	TIO-7	Fluka	0.000100	0.511	0.992	0.0000703
757	TIO-9	HT-0514	0.000100	0.654	0.932	0.0000703
758	AMT-600	P25	0.000100	0.576	0.962	0.0000703
759	TIO-2	Hombikat	0.000100	0.507	0.993	0.0000702
760	ST-21	HT-431A	0.000100	0.620	0.944	0.0000701
761	AMT-600	634662	0.000100	0.638	0.936	0.0000700
762	TIO-9	CR-EL	0.000100	0.643	0.934	0.0000699
763	AMT-100	CR-EL	0.000100	0.644	0.932	0.0000698
764	TIO-14	HT-431A	0.000100	0.631	0.936	0.0000697
765	TIO-7	ST-G2	0.000100	0.656	0.927	0.0000696

766	TIO-12	ST-F2	0.000100	0.575	0.958	0.0000695
767	AMT-600	TIO-15	0.000100	0.550	0.964	0.0000689
768	TIO-8	HT-431A	0.000100	0.601	0.942	0.0000689
769	AMT-100	HT-0514	0.000100	0.632	0.930	0.0000688
770	AMT-100	HT-2301	0.000100	0.609	0.936	0.0000684
771	TIO-2	ST-F10	0.000100	0.577	0.948	0.0000683
772	TIO-9	637254	0.000100	0.473	0.994	0.0000680
773	PC-102	HT-2301	0.000100	0.508	0.976	0.0000679
774	Kanto	ST-F10	0.000100	0.585	0.942	0.0000679
775	TIO-1	HT-2301	0.000100	0.609	0.932	0.0000678
776	ST-01	ST-F10	0.000100	0.585	0.940	0.0000676
777	TIO-9	Kanto	0.000100	0.466	0.994	0.0000674
778	637254	ST-F10	0.000100	0.576	0.942	0.0000674
779	TIO-2	TIO-9	0.000100	0.473	0.987	0.0000670
780	TIO-8	MT-150A	0.000100	0.540	0.955	0.0000670
781	ST-G1	TIO-3	0.000100	0.458	0.995	0.0000670
782	Fluka	TIO-5	0.000100	0.576	0.937	0.0000667
783	ST-157	ST-G1	0.000100	0.603	0.926	0.0000666
784	ST-21	MT-150A	0.000100	0.524	0.956	0.0000662
785	TKP-102	ST-G1	0.000100	0.582	0.930	0.0000660
786	AMT-600	TIO-4	0.000100	0.508	0.962	0.0000659
787	TIO-12	ST-F3	0.000100	0.512	0.959	0.0000659
788	TIO-2	HT-2301	0.000100	0.533	0.950	0.0000659
789	TIO-12	P25	0.000100	0.497	0.966	0.0000657
790	ST-41	HT-0514	0.000100	0.562	0.936	0.0000657
791	Kanto	HT-2301	0.000100	0.540	0.944	0.0000654
792	TIO-13	HT-2301	0.000100	0.560	0.935	0.0000654
793	TIO-10	Fluka	0.000100	0.441	0.992	0.0000654
794	ST-41	CR-EL	0.000100	0.552	0.938	0.0000653
795	PC-102	ST-F10	0.000100	0.470	0.975	0.0000651
796	Hombikat	ST-G2	0.000100	0.556	0.934	0.0000650
797	TIO-1	ST-F10	0.000100	0.563	0.931	0.0000650
798	637254	HT-2301	0.000100	0.532	0.943	0.0000649
799	Fluka	637262	0.000100	0.560	0.931	0.0000648
800	TIO-2	TIO-5	0.000100	0.531	0.943	0.0000647
801	TIO-2	637262	0.000100	0.546	0.936	0.0000647
802	ST-157	634662	0.000100	0.560	0.929	0.0000646
803	TIO-14	MT-150A	0.000100	0.515	0.949	0.0000646
804	TIO-12	TIO-15	0.000100	0.474	0.967	0.0000644
805	AMT-100	ST-F1	0.000100	0.516	0.947	0.0000644
806	TIO-9	AMT-100	0.000100	0.414	0.998	0.0000641
807	TKP-102	634662	0.000100	0.540	0.934	0.0000640
808	637254	TIO-5	0.000100	0.531	0.937	0.0000639
809	637254	637262	0.000100	0.546	0.930	0.0000639
810	Kanto	TIO-5	0.000100	0.523	0.937	0.0000635
811	Kanto	637262	0.000100	0.538	0.930	0.0000635
812	TIO-10	634662	0.000100	0.525	0.934	0.0000632
813	Merck	HT-0514	0.000100	0.528	0.932	0.0000631

814	PC-101	ST-G2	0.000100	0.534	0.928	0.0000629
815	TIO-14	HT-2301	0.000100	0.521	0.934	0.0000629
816	TIO-5	634662	0.000100	0.402	0.995	0.0000628
817	634662	637262	0.000100	0.413	0.988	0.0000628
818	Merck	CR-EL	0.000100	0.519	0.934	0.0000628
819	TIO-13	ST-F10	0.000100	0.518	0.934	0.0000628
820	ST-21	HT-2301	0.000100	0.511	0.935	0.0000625
821	AMT-100	HT-431A	0.000100	0.502	0.939	0.0000625
822	TIO-8	HT-2301	0.000100	0.496	0.939	0.0000621
823	TIO-12	ST-G2	0.000100	0.510	0.932	0.0000621
824	TIO-9	ST-G2	0.000100	0.519	0.928	0.0000620
825	TIO-12	TIO-4	0.000100	0.438	0.965	0.0000617
826	ST-F1	Kanto	0.000100	0.458	0.954	0.0000616
827	AMT-600	Wako	0.000100	0.450	0.959	0.0000616
828	FP-6	HT-431A	0.000100	0.466	0.949	0.0000615
829	637254	ST-F1	0.000100	0.451	0.954	0.0000612
830	637254	Merck	0.000100	0.382	0.993	0.0000610
831	ST-21	ST-F10	0.000100	0.473	0.939	0.0000607
832	ST-01	ST-G1	0.000100	0.481	0.935	0.0000607
833	TIO-10	ST-G1	0.000100	0.487	0.931	0.0000605
834	TIO-2	Merck	0.000100	0.381	0.987	0.0000602
835	Kanto	HT-431A	0.000100	0.446	0.946	0.0000598
836	TIO-8	ST-F10	0.000100	0.458	0.938	0.0000596
837	TKP-101	ST-G2	0.000100	0.489	0.922	0.0000594
838	637254	HT-431A	0.000100	0.439	0.946	0.0000593
839	TIO-14	ST-F10	0.000100	0.481	0.924	0.0000592
840	AMT-100	ST-41	0.000100	0.355	0.994	0.0000589
841	AMT-100	TIO-5	0.000100	0.465	0.929	0.0000589
842	AMT-100	637262	0.000100	0.478	0.923	0.0000588
843	ST-01	634662	0.000100	0.446	0.939	0.0000588
844	PC-102	ST-G1	0.000100	0.386	0.970	0.0000585
845	TIO-1	ST-G1	0.000100	0.462	0.926	0.0000583
846	ST-41	ST-G2	0.000100	0.445	0.932	0.0000580
847	AMT-100	Merck	0.000100	0.334	0.999	0.0000576
848	TIO-12	Wako	0.000100	0.388	0.962	0.0000576
849	Fluka	HT-0514	0.000100	0.423	0.938	0.0000573
850	AMT-600	ST-G2	0.000100	0.440	0.929	0.0000572
851	ST-F4	ST-F10	0.000100	0.361	0.976	0.0000572
852	TIO-2	ST-01	0.000100	0.337	0.991	0.0000570
853	Fluka	CR-EL	0.000100	0.416	0.940	0.0000570
854	PC-102	634662	0.000100	0.358	0.972	0.0000565
855	TIO-12	CR-EL	0.000100	0.412	0.938	0.0000564
856	TIO-13	ST-G1	0.000100	0.426	0.929	0.0000564
857	Merck	ST-G2	0.000100	0.419	0.928	0.0000557
858	TIO-12	HT-0514	0.000100	0.404	0.936	0.0000557
859	TIO-11	HT-2301	0.000100	0.381	0.949	0.0000556
860	FP-6	HT-2301	0.000100	0.384	0.946	0.0000555
861	TIO-10	ST-F10	0.000100	0.400	0.935	0.0000553

862	VP-P90	HT-2301	0.000100	0.382	0.945	0.0000552
863	ST-F5	HT-431A	0.000100	0.377	0.948	0.0000552
864	AMT-100	ST-F2	0.000100	0.367	0.952	0.0000549
865	Hombikat	634662	0.000100	0.384	0.941	0.0000548
866	TIO-13	634662	0.000100	0.395	0.933	0.0000546
867	TIO-2	Fluka	0.000100	0.306	0.994	0.0000546
868	ST-21	ST-G1	0.000100	0.388	0.935	0.0000545
869	TIO-14	ST-G1	0.000100	0.395	0.928	0.0000541
870	TKP-101	CR-EL	0.000100	0.395	0.927	0.0000540
871	TIO-8	ST-G1	0.000100	0.377	0.934	0.0000535
872	TIO-11	ST-F10	0.000100	0.353	0.948	0.0000534
873	TKP-101	HT-0514	0.000100	0.388	0.926	0.0000533
874	TIO-10	HT-2301	0.000100	0.370	0.937	0.0000533
875	FP-6	ST-F10	0.000100	0.355	0.945	0.0000532
876	ST-G2	TIO-3	0.000100	0.293	0.991	0.0000531
877	PC-101	634662	0.000100	0.369	0.935	0.0000530
878	AMT-100	TIO-3	0.000100	0.367	0.935	0.0000530
879	VP-P90	ST-F10	0.000100	0.353	0.944	0.0000530
880	ST-157	ST-G2	0.000100	0.386	0.922	0.0000528
881	ST-21	634662	0.000100	0.360	0.938	0.0000528
882	ST-F2	Kanto	0.000100	0.326	0.960	0.0000526
883	TIO-14	634662	0.000100	0.367	0.931	0.0000525
884	Hombikat	ST-G1	0.000100	0.356	0.937	0.0000524
885	ST-G1	TIO-6	0.000100	0.297	0.981	0.0000524
886	TKP-102	ST-G2	0.000100	0.372	0.927	0.0000524
887	TIO-9	634662	0.000100	0.358	0.935	0.0000523
888	637254	ST-F2	0.000100	0.321	0.960	0.0000522
889	AMT-600	CR-EL	0.000100	0.355	0.935	0.0000521
890	AMT-100	ST-F3	0.000100	0.328	0.954	0.0000521
891	AMT-100	P25	0.000100	0.318	0.960	0.0000519
892	TIO-8	634662	0.000100	0.349	0.937	0.0000519
893	AMT-600	HT-0514	0.000100	0.349	0.933	0.0000514
894	ST-F4	ST-G1	0.000100	0.296	0.971	0.0000514
895	TIO-2	ST-21	0.000100	0.273	0.991	0.0000512
896	TIO-9	TIO-12	0.000100	0.265	0.996	0.0000510
897	AMT-100	TIO-15	0.000100	0.303	0.962	0.0000509
898	TIO-2	TIO-14	0.000100	0.278	0.983	0.0000509
899	AMT-100	Fluka	0.000100	0.268	0.991	0.0000509
900	PC-101	ST-G1	0.000100	0.342	0.931	0.0000507
901	Kanto	TIO-3	0.000100	0.326	0.943	0.0000507
902	Fluka	ST-G2	0.000100	0.335	0.935	0.0000506
903	TIO-2	TIO-8	0.000100	0.264	0.989	0.0000503
904	637254	TIO-3	0.000100	0.321	0.942	0.0000503
905	TIO-10	ST-F1	0.000100	0.313	0.947	0.0000502
906	TIO-9	ST-G1	0.000100	0.332	0.932	0.0000500
907	ST-F3	Kanto	0.000100	0.291	0.961	0.0000498
908	ST-F5	HT-2301	0.000100	0.311	0.945	0.0000498
909	Kanto	P25	0.000100	0.282	0.967	0.0000497

910	637254	ST-F3	0.000100	0.286	0.961	0.0000494
911	637254	P25	0.000100	0.278	0.967	0.0000493
912	Hombikat	AMT-600	0.000100	0.245	0.995	0.0000490
913	ST-41	634662	0.000100	0.307	0.939	0.0000489
914	TIO-10	HT-431A	0.000100	0.305	0.940	0.0000487
915	TIO-15	Kanto	0.000100	0.269	0.969	0.0000487
916	AMT-100	TIO-4	0.000100	0.280	0.960	0.0000487
917	637254	TIO-15	0.000100	0.265	0.969	0.0000484
918	CR-EL	TIO-3	0.000100	0.236	0.997	0.0000483
919	ST-01	ST-G2	0.000100	0.307	0.932	0.0000481
920	ST-157	CR-EL	0.000100	0.312	0.928	0.0000481
921	Hombikat	ST-F10	0.000100	0.292	0.942	0.0000479
922	TIO-11	ST-G1	0.000100	0.290	0.944	0.0000479
923	FP-6	ST-G1	0.000100	0.292	0.941	0.0000478
924	ST-F5	ST-F10	0.000100	0.288	0.943	0.0000477
925	TIO-9	AMT-600	0.000100	0.228	0.999	0.0000477
926	HT-0514	TIO-3	0.000100	0.232	0.995	0.0000477
927	TIO-12	ST-41	0.000100	0.227	1.000	0.0000476
928	TKP-102	CR-EL	0.000100	0.300	0.932	0.0000476
929	TIO-12	TIO-5	0.000100	0.297	0.935	0.0000476
930	TIO-12	637262	0.000100	0.305	0.928	0.0000476
931	VP-P90	ST-G1	0.000100	0.290	0.939	0.0000475
932	ST-157	HT-0514	0.000100	0.306	0.926	0.0000474
933	TIO-5	HT-431A	0.000100	0.233	0.990	0.0000473
934	637262	HT-431A	0.000100	0.240	0.983	0.0000473
935	ST-F1	637262	0.000100	0.247	0.975	0.0000472
936	TKP-102	HT-0514	0.000100	0.295	0.930	0.0000470
937	Merck	634662	0.000100	0.289	0.935	0.0000470
938	ST-41	ST-G1	0.000100	0.285	0.936	0.0000468
939	TIO-4	Kanto	0.000100	0.248	0.967	0.0000466
940	TIO-11	634662	0.000100	0.269	0.947	0.0000465
941	PC-101	ST-F10	0.000100	0.281	0.936	0.0000464
942	PC-102	ST-G2	0.000100	0.247	0.966	0.0000464
943	FP-6	634662	0.000100	0.270	0.944	0.0000463
944	TIO-1	ST-G2	0.000100	0.296	0.922	0.0000463
945	637254	TIO-4	0.000100	0.245	0.967	0.0000463
946	Hombikat	HT-2301	0.000100	0.270	0.943	0.0000462
947	TIO-12	Merck	0.000100	0.213	0.995	0.0000458
948	TIO-9	ST-F10	0.000100	0.273	0.936	0.0000458
949	TKP-101	TIO-5	0.000100	0.285	0.924	0.0000456
950	TKP-101	637262	0.000100	0.293	0.918	0.0000456
951	AMT-100	Wako	0.000100	0.248	0.956	0.0000455
952	TIO-13	ST-G2	0.000100	0.272	0.929	0.0000451
953	Merck	ST-G1	0.000100	0.268	0.932	0.0000449
954	Hombikat	TKP-102	0.000100	0.207	0.992	0.0000448
955	PC-101	HT-2301	0.000100	0.260	0.937	0.0000447
956	TKP-101	Merck	0.000100	0.205	0.993	0.0000447
957	TIO-9	ST-157	0.000100	0.200	0.994	0.0000442

958	TIO-9	HT-2301	0.000100	0.252	0.938	0.0000441
959	AMT-600	TIO-5	0.000100	0.256	0.932	0.0000439
960	AMT-600	637262	0.000100	0.263	0.925	0.0000439
961	TIO-9	TKP-102	0.000100	0.193	0.998	0.0000438
962	ST-01	CR-EL	0.000100	0.248	0.937	0.0000438
963	Kanto	Wako	0.000100	0.220	0.964	0.0000436
964	Hombikat	ST-F1	0.000100	0.229	0.954	0.0000435
965	637254	Wako	0.000100	0.217	0.964	0.0000433
966	ST-21	ST-G2	0.000100	0.248	0.931	0.0000432
967	ST-G1	MT-150A	0.000100	0.204	0.978	0.0000432
968	TIO-14	ST-G2	0.000100	0.253	0.924	0.0000430
969	ST-F5	ST-G1	0.000100	0.236	0.939	0.0000429
970	TIO-10	ST-F2	0.000100	0.223	0.953	0.0000429
971	ST-F4	Kanto	0.000100	0.211	0.966	0.0000428
972	ST-41	ST-F10	0.000100	0.234	0.940	0.0000428
973	Fluka	634662	0.000100	0.231	0.942	0.0000427
974	637254	ST-F4	0.000100	0.208	0.965	0.0000425
975	ST-01	HT-0514	0.000100	0.244	0.928	0.0000425
976	TIO-8	ST-G2	0.000100	0.241	0.930	0.0000424
977	Hombikat	HT-431A	0.000100	0.223	0.946	0.0000422
978	PC-102	CR-EL	0.000100	0.199	0.972	0.0000422
979	PC-101	ST-F1	0.000100	0.220	0.948	0.0000421
980	TIO-1	CR-EL	0.000100	0.239	0.928	0.0000421
981	Kanto	TIO-6	0.000100	0.211	0.956	0.0000420
982	637254	TIO-6	0.000100	0.208	0.956	0.0000417
983	PC-102	HT-0514	0.000100	0.196	0.970	0.0000416
984	TIO-9	ST-F1	0.000100	0.214	0.948	0.0000416
985	ST-F5	634662	0.000100	0.219	0.942	0.0000416
986	ST-G2	TIO-6	0.000100	0.190	0.977	0.0000416
987	TIO-1	HT-0514	0.000100	0.234	0.926	0.0000415
988	TIO-10	TIO-3	0.000100	0.223	0.936	0.0000413
989	ST-41	HT-2301	0.000100	0.216	0.942	0.0000413
990	TIO-12	Fluka	0.000100	0.171	0.997	0.0000411
991	Merck	ST-F10	0.000100	0.220	0.936	0.0000411
992	PC-101	HT-431A	0.000100	0.214	0.940	0.0000409
993	Fluka	ST-G1	0.000100	0.215	0.938	0.0000408
994	TIO-5	TIO-3	0.000100	0.170	0.994	0.0000408
995	637262	TIO-3	0.000100	0.175	0.987	0.0000408
996	ST-F4	ST-G2	0.000100	0.190	0.967	0.0000407
997	TIO-13	CR-EL	0.000100	0.220	0.931	0.0000407
998	TIO-10	ST-F3	0.000100	0.199	0.954	0.0000406
999	ST-157	TIO-5	0.000100	0.225	0.925	0.0000406
1000	ST-157	637262	0.000100	0.231	0.918	0.0000405
1001	TIO-9	HT-431A	0.000100	0.208	0.941	0.0000403
1002	TKP-102	TIO-5	0.000100	0.217	0.929	0.0000402
1003	TKP-102	637262	0.000100	0.223	0.923	0.0000402
1004	TIO-13	HT-0514	0.000100	0.216	0.929	0.0000401
1005	TIO-10	TIO-15	0.000100	0.184	0.962	0.0000397

1006	TIO-9	ST-01	0.000100	0.159	0.996	0.0000396
1007	Merck	HT-2301	0.000100	0.203	0.937	0.0000396
1008	ST-F2	TIO-5	0.000100	0.171	0.976	0.0000393
1009	ST-F2	637262	0.000100	0.175	0.969	0.0000393
1010	ST-21	CR-EL	0.000100	0.201	0.937	0.0000393
1011	TIO-14	CR-EL	0.000100	0.204	0.930	0.0000391
1012	ST-F1	ST-41	0.000100	0.183	0.952	0.0000389
1013	ST-21	HT-0514	0.000100	0.197	0.935	0.0000388
1014	TIO-1	TIO-9	0.000100	0.153	0.994	0.0000387
1015	TIO-8	CR-EL	0.000100	0.194	0.936	0.0000386
1016	TIO-14	HT-0514	0.000100	0.200	0.928	0.0000385
1017	TIO-8	HT-0514	0.000100	0.191	0.934	0.0000381
1018	TIO-11	ST-G2	0.000100	0.185	0.940	0.0000380
1019	TIO-10	TIO-4	0.000100	0.170	0.960	0.0000380
1020	AMT-600	Fluka	0.000100	0.148	0.994	0.0000380
1021	FP-6	ST-G2	0.000100	0.187	0.937	0.0000379
1022	CR-EL	TIO-6	0.000100	0.153	0.983	0.0000378
1023	VP-P90	ST-G2	0.000100	0.186	0.936	0.0000377
1024	ST-41	HT-431A	0.000100	0.178	0.945	0.0000377
1025	TIO-9	TIO-13	0.000100	0.141	0.997	0.0000374
1026	ST-F1	Merck	0.000100	0.172	0.948	0.0000373
1027	Fluka	ST-F10	0.000100	0.176	0.943	0.0000373
1028	HT-0514	TIO-6	0.000100	0.150	0.981	0.0000373
1029	Hombikat	ST-F2	0.000100	0.163	0.959	0.0000371
1030	ST-F4	CR-EL	0.000100	0.153	0.973	0.0000371
1031	ST-F3	TIO-5	0.000100	0.152	0.974	0.0000370
1032	ST-F3	637262	0.000100	0.156	0.967	0.0000370
1033	Hombikat	ST-21	0.000100	0.138	0.998	0.0000370
1034	ST-01	ST-41	0.000100	0.137	0.999	0.0000369
1035	ST-01	TIO-5	0.000100	0.179	0.934	0.0000369
1036	ST-01	637262	0.000100	0.184	0.928	0.0000369
1037	ST-F4	HT-0514	0.000100	0.150	0.971	0.0000366
1038	Merck	HT-431A	0.000100	0.168	0.940	0.0000362
1039	P25	TIO-5	0.000100	0.148	0.968	0.0000360
1040	P25	637262	0.000100	0.152	0.961	0.0000360
1041	Fluka	HT-2301	0.000100	0.163	0.944	0.0000360
1042	PC-101	ST-F2	0.000100	0.157	0.953	0.0000359
1043	TIO-9	TIO-14	0.000100	0.131	0.996	0.0000359
1044	Hombikat	TIO-3	0.000100	0.163	0.942	0.0000358
1045	TIO-9	ST-21	0.000100	0.129	0.997	0.0000357
1046	ST-01	Merck	0.000100	0.129	0.996	0.0000356
1047	PC-102	TIO-5	0.000100	0.144	0.969	0.0000356
1048	PC-102	637262	0.000100	0.148	0.962	0.0000356
1049	TIO-1	TIO-5	0.000100	0.172	0.925	0.0000355
1050	TIO-1	637262	0.000100	0.177	0.919	0.0000355
1051	TIO-9	ST-F2	0.000100	0.152	0.954	0.0000355
1052	TIO-8	TIO-9	0.000100	0.125	0.998	0.0000352
1053	Hombikat	ST-F3	0.000100	0.145	0.961	0.0000352

1054	Hombikat	P25	0.000100	0.141	0.967	0.0000351
1055	ST-157	Fluka	0.000100	0.129	0.987	0.0000350
1056	TIO-15	TIO-5	0.000100	0.141	0.966	0.0000350
1057	TIO-15	637262	0.000100	0.145	0.959	0.0000350
1058	Kanto	MT-150A	0.000100	0.145	0.959	0.0000350
1059	TIO-1	Merck	0.000100	0.124	0.994	0.0000348
1060	PC-101	TIO-3	0.000100	0.156	0.936	0.0000347
1061	PC-102	Hombikat	0.000100	0.137	0.966	0.0000346
1062	TIO-11	CR-EL	0.000100	0.150	0.945	0.0000346
1063	637254	MT-150A	0.000100	0.143	0.956	0.0000345
1064	FP-6	CR-EL	0.000100	0.151	0.943	0.0000345
1065	Hombikat	TIO-15	0.000100	0.134	0.969	0.0000344
1066	VP-P90	CR-EL	0.000100	0.150	0.941	0.0000343
1067	TIO-13	TIO-5	0.000100	0.159	0.928	0.0000343
1068	TIO-13	637262	0.000100	0.163	0.922	0.0000343
1069	ST-G2	MT-150A	0.000100	0.130	0.974	0.0000342
1070	TIO-9	TIO-3	0.000100	0.152	0.937	0.0000342
1071	TIO-11	HT-0514	0.000100	0.147	0.944	0.0000341
1072	PC-101	ST-F3	0.000100	0.140	0.955	0.0000341
1073	FP-6	HT-0514	0.000100	0.148	0.941	0.0000340
1074	ST-F5	ST-G2	0.000100	0.151	0.935	0.0000340
1075	PC-101	P25	0.000100	0.135	0.961	0.0000340
1076	ST-F1	Fluka	0.000100	0.138	0.955	0.0000339
1077	VP-P90	HT-0514	0.000100	0.147	0.939	0.0000339
1078	TIO-4	TIO-5	0.000100	0.130	0.968	0.0000338
1079	TIO-4	637262	0.000100	0.134	0.962	0.0000338
1080	TIO-9	ST-F3	0.000100	0.136	0.955	0.0000336
1081	TIO-9	P25	0.000100	0.131	0.961	0.0000335
1082	PC-101	TIO-15	0.000100	0.129	0.963	0.0000333
1083	ST-21	TIO-5	0.000100	0.145	0.934	0.0000332
1084	ST-21	637262	0.000100	0.149	0.927	0.0000332
1085	ST-F2	ST-41	0.000100	0.130	0.958	0.0000331
1086	TIO-9	PC-102	0.000100	0.128	0.961	0.0000330
1087	TIO-14	ST-41	0.000100	0.113	0.991	0.0000330
1088	TIO-14	TIO-5	0.000100	0.147	0.927	0.0000330
1089	TIO-14	637262	0.000100	0.151	0.920	0.0000329
1090	Hombikat	TIO-4	0.000100	0.124	0.967	0.0000329
1091	Fluka	HT-431A	0.000100	0.134	0.947	0.0000329
1092	TIO-9	TIO-15	0.000100	0.125	0.963	0.0000329
1093	TIO-8	ST-41	0.000100	0.107	0.997	0.0000326
1094	TIO-8	TIO-5	0.000100	0.140	0.932	0.0000326
1095	TIO-8	637262	0.000100	0.144	0.926	0.0000326
1096	TIO-14	Merck	0.000100	0.106	0.996	0.0000323
1097	Wako	TIO-5	0.000100	0.115	0.972	0.0000321
1098	Wako	637262	0.000100	0.118	0.965	0.0000320
1099	ST-21	Merck	0.000100	0.104	0.996	0.0000320
1100	ST-41	TIO-3	0.000100	0.130	0.941	0.0000320
1101	TIO-5	TIO-6	0.000100	0.111	0.979	0.0000319

1102	637262	TIO-6	0.000100	0.114	0.972	0.0000319
1103	PC-101	TIO-4	0.000100	0.119	0.960	0.0000319
1104	ST-F2	Merck	0.000100	0.123	0.953	0.0000318
1105	TIO-8	Merck	0.000100	0.101	0.998	0.0000316
1106	TIO-9	TIO-4	0.000100	0.116	0.961	0.0000314
1107	ST-F3	ST-41	0.000100	0.116	0.960	0.0000314
1108	ST-41	P25	0.000100	0.113	0.966	0.0000313
1109	ST-F4	TIO-5	0.000100	0.110	0.970	0.0000313
1110	ST-F4	637262	0.000100	0.113	0.963	0.0000313
1111	CR-EL	MT-150A	0.000100	0.105	0.980	0.0000311
1112	ST-F5	CR-EL	0.000100	0.122	0.941	0.0000309
1113	Hombikat	Wako	0.000100	0.110	0.963	0.0000308
1114	HT-0514	MT-150A	0.000100	0.103	0.978	0.0000307
1115	TIO-15	ST-41	0.000100	0.108	0.967	0.0000307
1116	Merck	TIO-3	0.000100	0.123	0.936	0.0000307
1117	TIO-1	Fluka	0.000100	0.099	0.987	0.0000307
1118	TIO-9	VP-P90	0.000100	0.096	0.992	0.0000305
1119	ST-F5	HT-0514	0.000100	0.120	0.939	0.0000305
1120	TIO-9	TIO-11	0.000100	0.0961	0.988	0.0000303
1121	Hombikat	ST-F4	0.000100	0.105	0.965	0.0000302
1122	ST-F3	Merck	0.000100	0.109	0.955	0.0000302
1123	Merck	P25	0.000100	0.106	0.961	0.0000301
1124	PC-101	Wako	0.000100	0.106	0.957	0.0000298
1125	Hombikat	TIO-6	0.000100	0.106	0.956	0.0000297
1126	TIO-13	Fluka	0.000100	0.0913	0.990	0.0000296
1127	TIO-15	Merck	0.000100	0.101	0.963	0.0000295
1128	TIO-9	Wako	0.000100	0.103	0.958	0.0000294
1129	TIO-4	ST-41	0.000100	0.0994	0.965	0.0000294
1130	TIO-11	TIO-5	0.000100	0.108	0.942	0.0000292
1131	TIO-11	637262	0.000100	0.111	0.936	0.0000292
1132	FP-6	TIO-5	0.000100	0.109	0.939	0.0000291
1133	FP-6	637262	0.000100	0.112	0.933	0.0000291
1134	VP-P90	TIO-5	0.000100	0.108	0.938	0.0000289
1135	VP-P90	637262	0.000100	0.111	0.932	0.0000289
1136	ST-F2	Fluka	0.000100	0.0983	0.960	0.0000289
1137	TIO-9	ST-F4	0.000100	0.0983	0.960	0.0000289
1138	TIO-9	FP-6	0.000100	0.0967	0.961	0.0000288
1139	PC-101	TIO-6	0.000100	0.101	0.950	0.0000287
1140	VP-P90	ST-41	0.000100	0.0827	0.996	0.0000285
1141	TIO-9	TIO-6	0.000100	0.0984	0.950	0.0000283
1142	TIO-11	ST-41	0.000100	0.0825	0.992	0.0000283
1143	TIO-4	Merck	0.000100	0.0935	0.961	0.0000282
1144	Fluka	TIO-3	0.000100	0.0982	0.943	0.0000279
1145	TIO-9	ST-F5	0.000100	0.0784	0.993	0.0000276
1146	Wako	ST-41	0.000100	0.0881	0.962	0.0000275
1147	VP-P90	Merck	0.000100	0.0777	0.992	0.0000274
1148	ST-F3	Fluka	0.000100	0.0877	0.962	0.0000274
1149	Fluka	P25	0.000100	0.0850	0.968	0.0000273

1150	TIO-11	Merck	0.000100	0.0776	0.987	0.0000272
1151	ST-F4	ST-41	0.000100	0.0844	0.964	0.0000270
1152	PC-102	Fluka	0.000100	0.0828	0.967	0.0000269
1153	TIO-15	Fluka	0.000100	0.0811	0.970	0.0000268
1154	ST-41	TIO-6	0.000100	0.0845	0.955	0.0000265
1155	Merck	Wako	0.000100	0.0828	0.958	0.0000264
1156	TIO-5	MT-150A	0.000100	0.0758	0.977	0.0000263
1157	637262	MT-150A	0.000100	0.0780	0.970	0.0000263
1158	ST-F5	TIO-5	0.000100	0.0881	0.938	0.0000261
1159	ST-F5	637262	0.000100	0.0905	0.931	0.0000261
1160	ST-F4	Merck	0.000100	0.0793	0.959	0.0000259
1161	TIO-4	Fluka	0.000100	0.0749	0.968	0.0000256
1162	Merck	TIO-6	0.000100	0.0795	0.950	0.0000254
1163	VP-P90	Fluka	0.000100	0.0623	0.999	0.0000249
1164	Fluka	FP-6	0.000100	0.0626	0.998	0.0000249
1165	ST-F5	Merck	0.000100	0.0633	0.992	0.0000248
1166	Hombikat	MT-150A	0.000100	0.0724	0.958	0.0000247
1167	TIO-11	Fluka	0.000100	0.0622	0.995	0.0000247
1168	Fluka	Wako	0.000100	0.0664	0.964	0.0000240
1169	PC-101	MT-150A	0.000100	0.0696	0.952	0.0000239
1170	TIO-9	MT-150A	0.000100	0.0675	0.953	0.0000236
1171	ST-F4	Fluka	0.000100	0.0636	0.966	0.0000235
1172	Fluka	TIO-6	0.000100	0.0637	0.957	0.0000231
1173	ST-F5	Fluka	0.000100	0.0507	1.000	0.0000225
1174	ST-41	MT-150A	0.000100	0.0580	0.957	0.0000221
1175	Merck	MT-150A	0.000100	0.0545	0.953	0.0000212
1176	Fluka	MT-150A	0.000100	0.0437	0.959	0.0000192